INAUGURAL-DISSERTATION

zur
Erlangung der Doktorwürde
der
Naturwissenschaftlich-Mathematischen
Gesamtfakultät
der
Ruprecht-Karls-Universität
Heidelberg

vorgelegt von
Dirk Ollech (M. Sc.)
aus Bützow

TAG DER MÜNDLICHEN PRÜFUNG:
29. MÄRZ 2019

OPTOCHEMICAL CONTROL OF ADHESION PROTEIN COMPLEXES IN LIVING CELLS

Gutachter:

Prof. Dr. Joachim P. Spatz
Prof. (apl.) Dr. Reiner Dahint

ABSTRACT

Cell adhesion is essential for the formation and functional integrity of tissues and organs in multicellular organisms. In vertebrates, the epithelium is a specialized tissue that maintains a protective barrier around organs. Epithelial cells are attached to the extracellular matrix and form tight connections with each other *via* E-cadherin mediated multiprotein complexes called adherens junctions (AJs).

In this thesis, I present a method for light-induced dissociation of dimerizer-mediated AJs. This is the first optochemical tool which allows to control the formation and disassembly of adhesion complexes inside living cells with high spatiotemporal precision. The applied dimerizers are bifunctional small molecules that combine ligands of self-labeling protein tags like Halo and SNAP tag, *via* a photocleavable linker. These synthetic molecules induce dimeric complexes of proteins expressed as fusion constructs with the respective self-labelling tag inside living cells. The complexes are efficiently disassembled by cleaving the dimerizers with light.

To utilize photocleavable dimerizers in the context of cell adhesion, I first established a covalent-covalent binding dimerizer to ensure mechanical stability against mechanical forces acting on the induced protein complexes. I showed the potential to control the formation of adhesions complexes via retention, recruitment and complementation approaches for different target proteins. For example, I replaced the catenin binding sites on E-cadherin with a Halo tag and coexpressed them with SNAP-tagged α-catenin that was deficient of the β-catenin binding site. The dimerizer-mediated E-cadherin-α-catenin complexes could restore the epithelial phenotype of human epidermoid carcinoma cells (A431 cells) when induced in α-catenin KOs, but not in E-cadherin deficient A431D cells. I could show that the lack of AJ formation in A431D cells is associated with the failure of recruiting β-catenin. In α-catenin KOs -catenin was indirectly recruited to the dimerizer-mediated E-cadherin-α-catenin complex *via* lateral clustering with endogenous E-cadherin. This in turn led to the formation of AJ complexes, which are the coupling points for the contractile actomyosin network between epithelial cells. Moreover, the α-catenin KO phenotype could be restored upon light induced dissociation of the dimerizer-mediated AJs *via* exposure to near UV light. When using a 405 nm laser to cleave the dimerizers, I was able to target the AJs between two adjacent cells with subcellular precision or to create patterns of deactivated cell-cell adhesion in epithelial monolayers. Furthermore, I could prove the mechanical functionality of the reconstituted AJs by performing a correlation analysis of collective monolayer migration and traction force microscopy.

Herein, I demonstrated the application of photocleavable dimerizers to study the cellular response to AJ assembly and disassembly at different scales of space and time. Photocleavable dimerizers present several advantages for applications in living cells. Since the protein-protein interaction depends on external addition of the dimerizers and can be reliably abrogated by breaking the molecule, the setup offers two binary switches for the formation of AJ complexes, virtually without any basal activity. Furthermore, the system is bioorthogonal and light is a trigger that allows to dissociate the protein complexes at subcellular and subsecond resolution. The possibility to combine it with specialized imaging techniques like traction force microscopy renders it a powerful tool to study the mechanobiology of AJs and its contribution to processes in epithelial cell layers like cellular jamming and unjamming, collective migration and stress propagation. This new method will help to gain new insights in the dynamic regulation of cell adhesion in fundamental pathophysiological processes like embryonal development, wound healing or cancer metastasis.

ZUSAMMENFASSUNG

Zelladhäsion ist essentiell für die Herausbildung und funktionale Integrität von Geweben und Organen in multizellulären Organismen. In Wirbeltieren ist das Epithel ein spezialisiertes Gewebe, dass eine schützende Barriere um die Organe bildet. Die Epithelzellen sind einerseits mit der extrazelluären Matrix verbunden und bilden andererseits über E-cadherin vermittelte enge Verknüpfungen miteinander, sogenannte Adherens Junctions (AJs).

In dieser Doktorarbeit präsentiere ich eine Methode zur lichtinduzierten Auflösung von Dimerizer vermittelten AJs. Dies ist das erste optochemische Werkzeug, dass die Kontrolle über die Bildung und Degradation von Adhäsionskomplexen in lebenden Zellen mit hoher raumzeitlicher Präzision ermöglicht. Die verwendeten Dimerizer sind bifunktionelle kleine Moleküle, in denen die Liganden für sogenannte selbstmarkierende Protein-Tags (z.B. Halo-Tag und SNAP-Tag) über eine photospaltbare Gruppe miteinander kombiniert wurden. Diese synthetischen Moleküle induzieren in lebenden Zellen dimere Komplexe von Proteinen, welche als Fusionskonstrukte mit dem jeweiligen selbstmarkierenden Protein-Tag exprimiert werden. Die Komplexe können durch Spaltung des Dimerizers mit Licht effizient getrennt werden.

Für die Anwendung von photospaltbaren Dimerizern im Kontext der Zelladhäsion habe ich zunächst einen kovalent-kovalent bindenden Dimerizer etabliert, mit dem die Stabilität der indizierten Proteinkomplexe gegenüber Spannungen- und Zugkräften gewährleistet wird. Das Potential verschiedener Zielproteine für die Herausbildung von Adhäsionskomplexen über konzeptionelle Ansätze zur Zurückhaltung, Rekrutierung und Vervollständigung von Adhäsionsproteinen zu kontrollieren wurde evaluiert. Beispielsweise habe ich die Cateninbindestellen von E-Cadherin mit einem Halo-Tag ersetzt und diese Proteine mit einem SNAP-Tag fusionierten α-Catenin ohne β-Cateninbindestellen koexprimiert. Die dimerizervermittelten E-Cadherin-α-Catenin-Komplexe konnten den ursprünglichen epithelialen Phänotyp von humanen Epidermoidkarzinomzellen (A431 Zellen) wiederherstellen, wenn sie in α-Catenin knock-out (KO) Zellen induziert wurden, aber nicht in E-Cadherin defizienten A431D Zellen. Ich konnte zeigen, dass das Scheitern der Bildung von AJs in A431D Zellen mit der ausbleibenden Rekrutierung von β-Catenin assoziiert ist. In α-Catenin KO Zellen wurde β-Catenin indirekt über endogenes E-Cadherin rekrutiert, welches sich zusammen mit den dimerizervermittelten E-Cadherin-α-Catenin-Komplexen durch laterale Interaktionen anhäuft. Dies wiederum führte zur Bildung von AJ Komplexen, welche die Verknüpfungspunkte für das kontrakti-

le Aktin-Myosin-Netzwerk in Epithelzellen bilden. Darüber hinaus konnte durch die lichtinduzierte Zersetzung der dimerizervermittelten AJs nach Bestrahlung mit langwelligem UV-Licht der α-Catenin KO Phänotyp wiederhergestellt werden. Durch Verwendung eines 405 nm Lasers zur Spaltung der Dimerizer, konnte ich AJs zwischen zwei aneinandergrenzenden Zellen mit subzellulärer Präzision anvisieren oder Muster von deaktivierten Zell-Zell-Kontakten in epithelialen Monolagen erzeugen. Des Weiteren konnte ich die mechanische Funktionalität der rekonstituierten AJs mittels Durchführung von Korrelationsanalysen der kollektiven Migration von Zellmonolagen und Zugkraft Mikroskopie Messungen (Englisch: traction force microscopy), nachweisen.

In dieser Arbeit habe ich die Anwendung photospaltbarer Dimerizer zur Untersuchung der zellulären Reaktionen auf die Herausbildung und Zersetzung von AJs in verschiedenen räumlichen und zeitlichen Größenordnungen demonstriert. Photospaltbare Dimerizer haben mehrere Vorteile für die Anwendung in lebenden Zellen. Weil die Protein-Protein Interaktion von der externen Zugabe des Dimerizers abhängt und zuverlässig durch die Spaltung des Moleküls aufgehoben werden kann, bietet diese Methode zwei binäre Schalter für die Herausbildung von AJs, praktisch ohne Basalaktivität. Des Weiteren ist das System bioorthogonal und Licht als Stimulus erlaubt die Auflösung der Proteinkomplexe mit subzellulärer Auflösung in Bruchteilen von Sekunden. Die Möglichkeit zur Kombination mit spezialisierten Mikroskopiemethoden wie der Zugkraft Mikroskopie macht es zu einem leistungsfähigen Instrument zur Untersuchung der Mechanobiologie von AJs und deren Auswirkungen auf Vorgänge in epithelialen Zellschichten wie zelluläre Verdichtungsprozesse, kollektive Zellmigration oder die zellulären Übertragemechanismen von mechanischen Spannungen. Diese neue Methode wird dabei helfen, neue Erkenntnisse über die dynamische Regulation der Zelladhäsion in fundamentalen pathophysiologischen Prozessen wie der Embryonalentwicklung, der Wundheilung oder der Metastasierung von Krebs zu erlangen.

Mötst di nich argern,
Hett keinen Wiert,
Mötst di blot wunnern,
Wat all passiert.
Mötst ümmer denken,
De Lüd sünd nich klook,
Jeder hett Grappen,
Du hest se ok.

Mötst di nich argern,
Hett keinen Sinn,
Ward di blot schaden
Un bringt di nix in,
Ward an di fräten
As Qualm un Rook.
Is't nahst vergäten,
Büst grad so klook.

Mötst di nich argern,
Is Unrecht di dahn,
Haug mal up'n Disch
Un glieck is't vergahn.
Kort is dien Leben
Un lang' büst du dod,
Minsch, blot nich argern,
Ne, lachen deit good!

— Rudolf Tarnow

ACKNOWLEDGMENTS

This work would not have been possible without the support and contributions from some people. First of all, I would like to thank Joachim P. Spatz for being my first supervisor and giving me the opportunity to work on my PhD thesis in his group. Thank you for your generous support and patience and the inspiring interdisciplinary working environment. I am thankful to Rainer Dahint who kindly agreed on being the second examiner of this thesis. Moreover, I would like to thank E. Ada Cavalcanti-Adam for her supervision and granting the great trust to let me work on this project with great independency, not only during the time of her sabbatical. I would like to extend my gratitude to Ulrich Schwarz for supporting this work not only as a member of my thesis advisory committee, but also for helpful discussions and explanations about cellular mechanosensing and force measurements. I am extremely grateful to Richard Wombacher not only for supervision of the chemical synthesis part of this project and generous access to his chemistry labs. Besides your valuable contributions as a collaboration partner and member of my thesis advisory committee, you have been a great mentor and motivator.

Furthermore, I would like to thank the members of the Wombacher lab for their support on the synthesis work, especially Heiko Rudy for the HR-MS/MS analysis and Tobias Timmermann for NMR measurements. I acknowledge material support from various people. Carsten Schultz provided the SNAPf template plasmid and the EcGFP-α(280-906) plasmid was a gift from Sergey M. Troyanovsky. The A431D cells were kindly provided by René-Marc Mège and the A431 α-catenin KO were generated and provided by Takuya Kato. I appreciate the help of Monika Langlotz, Birgit Koch and Carmen Sahm for FACS sorting. I would like to thank Carmen additionally for general technical support and her effort to keep the cell culture in a good shape. I feel much obliged to Dimitri Probst for providing the pyTFM software for PIV and TFM data analysis and to Tamal Das for the algorithm for velocity correlation analysis. I also cherish the helpful discussions I had on these topics with Jacopo Di Russo, Medhavi Vishwakarma and Carlos Pérez-González. Special thanks to Sarah Kaspar for her MatLab crash course.

I would like to express my great thankfulness to all the students I was supervising during the past years. In particular, I would like to thank Sandra Diebel, Basant Birajee and Fatima Noureddine for working on the optogenetic tools for cell adhesion that we tested as alternatives to the opto-cemical dimerizer approach. Clara Grundmann did initial tests with the Ha-pl-BG dimerizer and Lena Thärichen tested the migration analysis with MDCK cells. Nino Baldok contributed

to a great extend in setting up the extracellular E-cadherin complementation and Anne Weiß was a great help for the preparation of processed EC12 proteins for the final live cell experiments. Last but not least, I would like to say special thanks to Tim Pflästerer who contributed a lot to the analysis of A431 mutant cells and the dimerizer mediated adherens junctions. Thank you also for being the helping hand in the lab during the writing phase of this thesis to keep the progression in the ongoing work.

My heartiest gratitude goes to all my colleagues and office mates who made working in the Spatz group a pleasuring experience. First of all, I want to thank Rebecca Medda for her enduring guidance and being the agony column for scientific and personal problems. I am happy I had the companion of my PhD colleagues Tina Wiegand, Julia Ricken, Volker Martin and Chiara Zambarda. Going through the process of graduation together we had a (mostly) great time. Most exceptionally I want to thank Chiara for sharing not only the ups and downs of my PhD work, but becoming the support and anchor point for my future life.

Many thanks also to my friends in Heidelberg and further away, who brought me up in the moments of doubt and were a supporting column of my everyday life. After ten years in Heidelberg I am grateful to have some people from the time before, that I can rely on if I need a place to escape, but also to the people that transitioned from fellow bachelor students into friends that I am confident will last beyond this time of academic education. Nevertheless, I will miss the MoBi lunch and pubquiz.

Finally, I would like to thank my family for believing in me and supporting me on my way into a scientific career. In the end, I guess the hard times you had in pronouncing names of dinosaurs and other prehistoric creatures seeded the spirit for new explorations and discoveries, although I shifted my focus from dead bones to living cells.

CONTENTS

Part I

INTRODUCTION

1 OPTOCHEMICAL TOOLS FOR BIOLOGY

1.1 LIGHT IS A TRIGGER WITH MANY ADVANTAGES

Biological processes inside a living cell are dynamically regulated with high spatial precision. Synthetic chemistry offers access to a plethora of small molecules that can specifically interact with biological systems for visualization (e.g. fluorescent labelling)[1–3], manipulation (enzyme inhibitors)[1, 4] and analysis (e.g. crosslinking to identify interaction partners in mass spectrometry analysis)[5]. In this so called field of chemical biology synthetic molecules that change their activity on a biological system *via* exposure to light are summarized under the term optochemical tool.

Light as a stimulus to trigger biological effect has multiple advantages as it can be applied dynamically with precise regulation in timing, location and intensity. In modest intensities light is regarded as non-invasive and non-cytotoxic and it is highly bioorthogonal for most applications in cell biology except for cellular systems that do contain light responsive proteins like e.g. photoreceptor cells in the retina.

The molecules ability to change its bioactivity upon light irradiation is generally facilitated *via* a reversible conformational change (e.g. *cis-trans* isomerization of azobenzene) or photo labile groups in functional positions of the molecule. In the later case, installation of a photo labile group at a position that is important for the activity and binding of the molecule is defined as photo-caging, while integration in a structural scaffold creates a photo cleavable linker and leads to disintegration of the molecule after irradiation. Among the growing variety of photo labile groups that were extensively reviewed in Brieke *et al.*[6], those based on nitrophenyl- and coumarinyl- moieties (figure 1.1) that can be removed with near UV-violet light (λ=350-405 nm) or violet-blue light (λ=400-460 nm), respectively, are still the most widely used.

1.2 PHOTOCAGING OF SMALL MOLECULES AND PROTEINS

Photocaging of small molecules is the most common used optochemical tool and was first realized for cAMP by Engels and Schlaeger [7] and for ATP by Hoffmann and coworkers [8] (figure 1.2 a). The toolbox of photocaged second messenger molecules and neurotransmitters (e.g. glutamate, GABA, inositol, Ca^{2+}) was constantly enlarged and applied since after and was extensively reviewed in [6, 9]. Al-

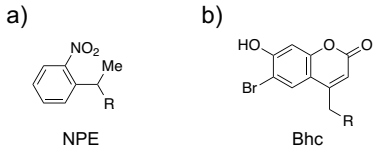

Figure 1.1: **Photo labile caging groups.**
a) Most nitrophenyl based caging groups like NPE are stable under ambient light, but can be cleaved with near UV light (λ=350-405 nm). b) Coumatin based caging groups like Bhc can be cleaved with visible blue light of longer wavelengths (λ=400-460 nm). R denotes the residue coupling site. NPE: 1-(2-nitrophenyl)ethyl; Bhc: 6-bromo-7-hydroxycoumarin-4-ylmethyl.

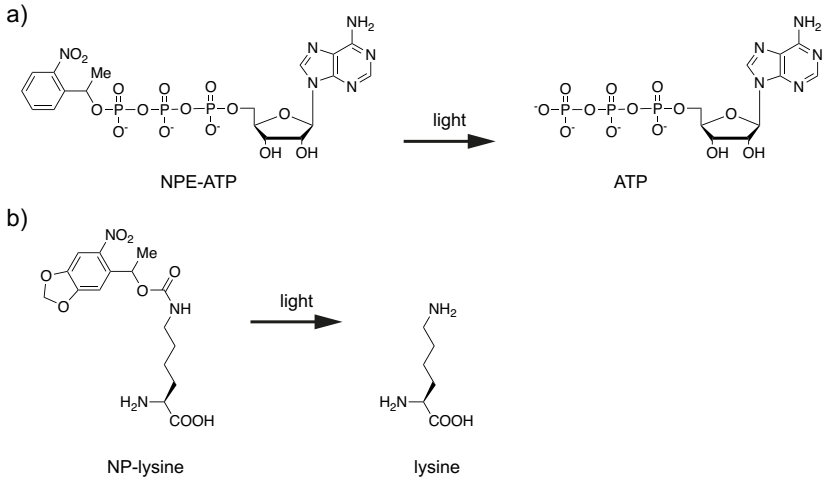

Figure 1.2: **Photocaged small molecules can be used to control protein activity.**
a) The bulky photocaging group prevents NPE-ATP from entering the reactive binding pocket of ATP dependent enzymes. Energy providing ATP hydrolysis can occur only after uncaging with light. [9] b) Photocaged unnatural amino acids like NP-lysine can be used to control enzymatic activity by blocking their reactive binding pocket. The activity turns in directly after the caging group is released[10].

though being easily accessible for chemical modifications photocaged small molecules sufferer from several limitations. First of all they offer only a single switch for activation or deactivation. Secondly, the general approach to use photocaged small molecules is limited to proteins that offer binding sites for the non-caged analogon. Finally, many second messenger molecules are recognized by multiple downstream effector proteins and therefore bear the risk of inducing cellular reactions activated by other proteins then the one under investigation.

Another approach is to install the photocaging group directly at the protein of interest at an amino acid that is essential for activating phosphorylation, ATP or ligand binding. This can be done by direct chemical modification of purified proteins *in vitro* [11, 12] or

the ligation of purified proteins with photocaged peptides that were generated in solid phase synthesis [13]. Applications in living cells however is fairly limited, because the modified proteins need to be delivered into the cells *via* microinjection or patch clamp dialysis due to limited cell permeability. A way to generate photocaged proteins inside living cells is the incorporation of photocaged unatural amino acids (UAA) *via* stop codon suppression as first demonstrated by Mendel *et al.* [14]. Reactive tyrosin, lysin, serin and cystein residues have been blocked by nitrobenzyl or coumarin caging groups (figure 1.2 b). UAA mutagenesis has been used to induce light controlled nuclear localization of proteins and to create light activated kinases, proteases, DNA recombinases . These and further applications have been reviewed recently [15]. Incorporation of photocaged UAA is highly specific, because it affects solely the modified protein. Nevertheless, its applicability in mammalian cells is still hampered by limited efficiency due to the need of extensive genetic modifications like introduction of the amber stop codon mutation in the target protein, expression of a complementary suppressor tRNA and an engineered amino-acyl tRNA synthetase that can load the tRNA with the UAA [16].

1.3 REVERSIBLE SWITCHING OF BIOACTIVE COMPOUNDS

Reversible photoswitching between "on" and "off" state can be achieved with moieties that undergo steric changes *via cis-trans* isomeric reactions of double bonds like azobenzene, stilbene or hemithioindigo or they change their conformational flexibility *via* unimolecular pericyclic reactions as in the case of spiropyran, diarrylethene or fulgide. Among these potential photoswitches only azobenzene based molecules have proofen to be capable of inducing functional changes under live cell conditions, while the others suffer from low solubility or impaired switching behavior in aqueous solutions, the need for shorter UV wavelength or instabilities under standard synthesis conditions [6]. A big advantage of azobenzenes is that the UV light induced isomerization from *trans* to *cis* is very stable, but can be reversed selectively with visible light (figure 1.3 a). Isostere of azobenzene are frequently found structural motifs in drugs that are small molecule inhibitors or activators. Exchange of theses motifs with photoswitchable azobenzene (termed "azologization") often yields comparable efficiency to the original compound, but light induced isomerization abrogates its activity. Another approach called "azoextension", adds an azobenzene group to a known structure (figure 1.3 b). The pioneering work of the Trauner lab in this so called field of photopharmacology has been extensively reviewed by Broichhagen *et al.* [17]. Furthermore azobenzenes can be used as light reactive linker between a ligand and a reactive moiety that conjugates the photoswitchable teth-

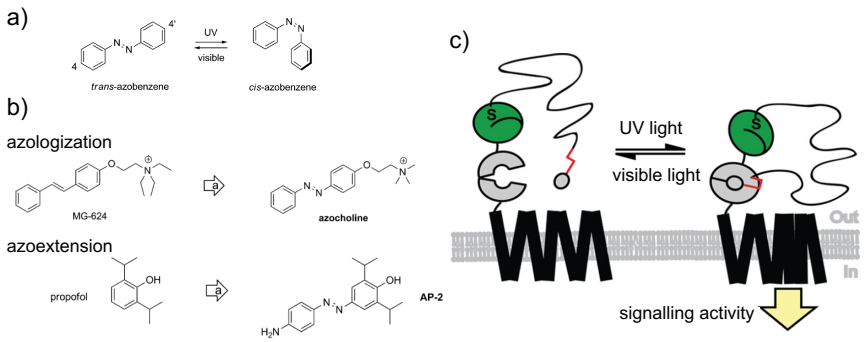

Figure 1.3: **cis-trans isomerization of azobenzene modified ligands can switch receptor activity.**
a) cis-trans isomerization of azobenzene can actively be switched in both directions with differen wavelenths. b) Azologisation and azoextensions are two concepts to turn known drugs into photoswitchable compounds. c) Photoswitchable orthogonal remotely tethered ligand (PORTL) can be fused to transmembrane receptors like G-protein coupled receptors or receptor tyrosin kinases to make their activity dependent on light. a,b) Adapted from [17]. c) Adapted from[19]

ered ligand (PTL) to its target protein [18]. More recently, this concept has been expanded by photoswitchable orthogonal remotely tethered ligand (PORTL) (figure 1.3 c)[19] and photoswitchable bioorthogonal ligand tethering (photo-BOLT) [20] that both increase the specificity of biconjugation using either the self-labelling protein SNAP tag (see also subsection 1.4.2) or the incorporation of UAA that can bind the ligand in a copper free click reaction.

Despite their immense relevance for controlling the activity of a large number of proteins the application of photocaging or photoswitchable groups is limited to target proteins with known small molecule ligands or single key regulatory reactive amino acid residues. To control proteins that are activated e.g. *via* complex phosphorylation patterns or conformational changes upon protein binding *via* large protein-protein interaction sites another concept is necessary, that will be explained in the next section.

1.4 PHOTOREACTIVE CHEMICAL INDUCERS OF DIMERIZATION

Many processes inside living cells are facilitated *via* dynamic spatiotemporal sorting of proteins and other reactive agents. Although this concept of compartmentalization is most obviously manifested in membrane enclosed organelles, biological activity can be regulated *via* local increase of protein concentration at non-enclosed subcellular compartments by e.g. recruitment to the plasma membrane or protein clustering. This can increase the availability of diffusible agents or the chance for activating phospohorylations e.g. by locally increased concentration of synthetases or kinases, but is particularly relevant

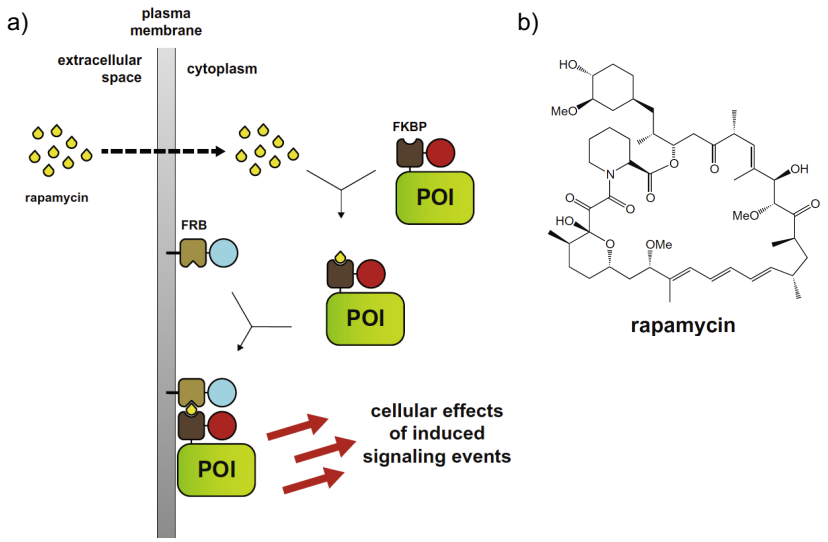

Figure 1.4: **Protein activity can be regulated by chemical induced dimerization.**
a) Chemical indicers of dimerization (CIDs) like rapamycin can be used to recruit a target protein to its place of action via dimerization with a localization domain. b) Molecular structure of rapamycin.
Adapted from [22]

for proteins that are active only in a multiprotein cluster *via* direct protein-protein interaction[21, 22].

Small molecules that induce the direct interaction between two proteins are called chemical inducers of dimerization (CID) or dimerizer in short. Dimerizer that facilitate binding between proteins of the same kind are called homodomerizer, whereas dimerizer which bring two different proteins together are referred to as heterodimerizer. Especially heterodimerizer can control protein activity e.g. by induced binding to a localization domain (figure a). A general concept is functional knock down by sequestration at cellular compartments distant from their place of action or activation by recruitment to their target site or direct induced interaction with an activating agent[22–26].

Since Schreiber a Crabtree introduced the first dimerizers based on rapamycin more than 20 years ago [27] the toolbox has been enlarged constantly with various protein binding small molecules [5, 21, 22]. They have been used in a broad spectrum of live cell applications ranging from induced gene expression (including pharmacological screenings in 3-hybrid systems in yeast [28, 29] and mammalian cells [30]), activation of split kinases [31] and T-cell receptors [27, 32], protein degradation [33–35], regulation of vesicle transport [36, 37] and to induce the formation of ruffles and protrusions [38, 39] of the plasma membrane, to name just a few. The vast variety of (non-photoreactive) dimerizers and their application have been reviewed in great detail recently [5, 21, 22, 40, 41].

Most dimerizer are cell permeable and can be applied to the cell *via* the culture medium. Therefore they offer a decent degree of temporal control, although the the onset rate can be limited by low diffusion rates through the plasma membrane. Furthermore, they are lacking the possibility for spatially defined activation. A great potential lies in the integration of photoreactive moieties in the chemical structures of CIDs.

1.4.1 *Photocaged derivatives of natural dimerizer*

1.4.1.1 *Rapamycin - a bacterial macrolide*

The most widely used dimerizer is rapamycin, a macrolide naturally produced by the bacterium *Streptomyces hygroscopicus.* Rapamycin induces the formation of a ternary complex *via* binding to FKBP12 (FK506-binding protein) and the FRB (FKBP-rapamycin binding) domain of mTOR (mammalian target of rapamycin) with high affinity (Kd = 12 nM for FKBP-rapamycin-FRB) [42]. The relatively small proteins FKBP12 (12 kDa) and FRB (11 kDa) can be fused to a large variety of target proteins as reviewed in [22].

Reasonably, photoreactive derivatives of rapamycin have been used to improve the spatiotemporal performance of protein dimerization. Extracellularly trapped caged rapamycin-avidin conjugate (cRb-A) was applied to recruit the Rac activator Tiam1 to the plasma membrane, leading to ruffle formation at defined subcellular regions [43]. The first intracellularly unchangeable dimerizer pRap (figure 1.5 a) was used to restore activity of focal adhesion kinase (FAK) again leading to ruffle formation with single cell precision [44]. Despite being a photo-cleavable rapamycin dimer that could be used for reversibe homodimerization of FKBP, dRap was used to activate split TEV protease and split Cre recombinase in HEK293T cells upon rapamycin release after irradiation [45]. The photo-cleavable FKBP-homodimerizer PhAP expanded the application to study endosomal dispersion by deactivating dynein light chain LC8, a motorprotein that transports intracellular vesicles along microtubule, *via* dimer formation [46].

Besides its broad pharmacological application as antifungal, antiproliferative and immunosuppressive drug, the physiological activity of rapamycin on the mTOR pathway limits its usability to study long term activations in mammalian cells [47].

1.4.1.2 *Absicic acid and gibberellic acid - growth hormones in plants*

In contrast to rapamycin, the phytohormones absicic acid (ABA) and gibberellic acid (GA_3) have no known activity in mammalian cells. ABA (figure 1.5 b) binds to PYL protein (pyrabactin resistance 1-like protein) and the complex is then bound by ABI (ABA insensitive 1). Crebtree and coworkers have reduced the protein to their minimal

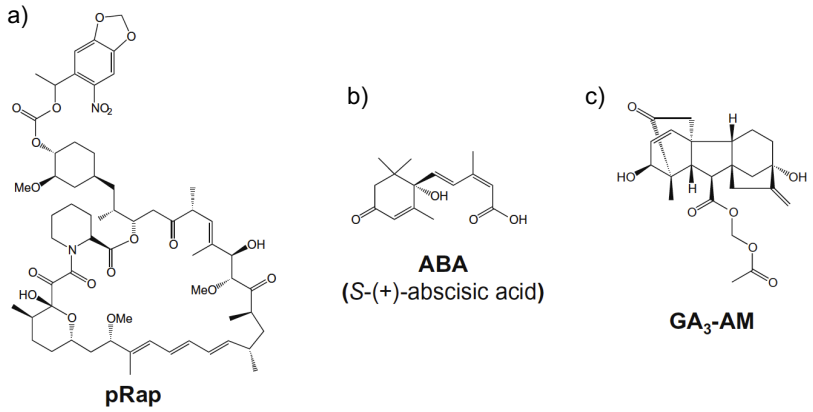

Figure 1.5: **Natural dimerizer can be decorated with caging groups.** a) Rapamycin can be turned into the photoactivatable dimerizer pRap via ligation of a photocleavable caging group at an exposed hydroxy residue[44]. b) Also the carboxylic acid residue in ABA can be decorated with a caging group[48]. c) The carboxylic acid residue of $GA_3$is decorated with an acetoxymethyl ester to increase cell permeability or can be used to install a photocleavable caging group[49]. AM: acetoxymethyl. Adapted from [22].

domains necessary to bind ABA (PYL_{cs}: 19.5 kDa, ABI_{cs}: 32.8 kDa) which can be used to target proteins of interest [50]. Analogously, the gibberellin metabolite GA_3induced conformational changes upon binding to its receptor GID1 (gibberellin insensitive dwarf1) and the resulting complex recruits the GAI (gibberellin insensitive). Despite the large GID1 domain (38.6 kDa) Inoue and colleagues optimized the system by reducing GAI to its first 92 amino acids ($GAI_{1\text{-}92}$, 10.1 kDa) and improving the cell permeability of $GA_3$by esterfication of its carboxylic acid with an acetoxymethyl group (GA_3-AM) (figure 1.5 c) [51]. Both dimerizer have been shown to work orthogonal to rapamycin, which offers the possibility of multiplexed dimerization [50, 51].

The photoactivatable derivatives PA-ABA [48] and PA-GA_3[49] have been synthesized by installation of a photocleavable nitrobenzyl group at the the respective free carbocylic acid. For GA_3Schelke et al presented also two new caging groups for photoactivation with two photon laser irradiation [49]. The proof-of-concept studies demonstrated the potential of these new photoreactive dimerizers *via* rapid translocation of fluorescent target proteins to subcellular compartments upon dimerization with distinct localization domains. Furthermore PA-ABA was shown to be applicable for known concepts of induced gene expression and ruffle formation [48].

1.4.2 *Synthetic photoreactive dimerizer based on self-labelling protein tags*

Self-labelling protein tags have been developed for fluorescent labelling of proteins inside living cells *via* binding of small molecule ligands that can be decorated with synthetic fluorophores. The combination of these ligands *via* a flexible linker of appropriate length leads to another class of small molecule dimerizer. The combination of two different ligands creates hetero bifunctional dimerizer that can be used in experiments analogous to those described for natural dimerizer systems (see section 1.4.1). A big advantage is the modular architecture of these dimerizer that can be easily exchanged or supplemented with functional moieties. Furthermore, self-labelling protein tags are a well established tool for live cell labelling experiments and many fusion proteins that are potential targets for a dimerization approach are already on hand.

The most widely used self-labelling tags that have been also applied in the context of protein dimerization are SNAP tag, Halo tag and TMP tag. The SNAP tag is based on the DNA repair enzyme human O^6-alkylguanine-DNA alkyltransferase (hAGT) that has been modified to react selectively with benzylguanine (BG) derivatives instead of the endogenous O^6-methylguanine-DNA substrate and to transfer the alkyl group of BG covalently and irreversibly to a reactive cystein residue[52] (figure 1.6 a). Furthermore Johnsson and coworkers reduced the size of the protein tag to 20 kDa [2] and improved its binding kinetics to 5.2×10^3 M^{-1} s^{-1}. Since the Halo tag (33 kDa) originates from a promiscous dehalogenase (DhaA), an enzyme that removes halides from aliphatic carbohydrates in bacteria of the genus *Rhodococcus,* it has no cross-reactive substrate in mammalian cells. Mutation of a catalytically active histidine into phenylalanine stabilizes the covalent transfer of the aliphatic hydrocarbon moiety to a reactive aspartate. The apparent second-order rate constant for a tetramethylrhodamin ligand (Ha-TMR) was measured to be 2.7×10^6 M^{-1} s^{-1} [3] (figure 1.6 b). In contrast to SNAP and Halo tag, the DHFR tag binds its preferred substrate trimetoprim (TMP) non-covalently with a dissociation constant of 32 ± 3 nM [53] (figure 1.6 c). The DHFR tag is based on the dihydrofolate reductase (DHFR) from *E. coli* which is binding TMP with much higher affinity (K_I = 1 nM) than mammalian DHFR (K_I = 4 µM) [54], therefore enabling fluorescent labelling with minimal background in living cells [53].

The first dimerizer based on self-labelling protein tags was presented by Erhart *et al. via* combining the chloroalkyl ligands for Halo tag (Ha) with the SNAP tag ligand BG [55]. In that work they could show how the length of the linker and incorporation of moieties that increase cell permeability can improve the efficiency and onset rates for dimerization of SNAP and Halo tagged GFP fusion proteins in-

side living cells. The same group also presented the first photo cleavable dimerizer by incorporating a photolabil dimethoxynitrobenzyl (DMNP) moiety in the linker between the Halo tag and the SNAP tag ligand (Ha-pl-BG) (figure 1.6 d). When cells coexpressing for example a Halo tagged giantin fusion protein that is localized at the Golgi apparatus and a cytosolic SNAP tagged teal fluorescent protein (SNAP-mTFP1) were treated with the Ha-pl-BG dimerizer the SNAP-mTFP1 protein could be sequestered at the Golgi vesicles and could be released with subcelluar precision upon irradiation with a near UV lasers [56].

The first photoactivatable dimerizer based in on self-labelling protein tags was developed in a collaborative work by the groups of Chanoweth and Lampson. They combined a DMNP photocaged TMP (pcTMP) with the halo ligand Ha (pcTMP-Ha) and could show the light induced recruitment of cytosolic mCherry-DHFR to various subcellular compartments depending on the localization domain the coexpressed Halo tag was fuesed to [57]. Because the dimerizer binds Halo tagged proteins directly after addition to the cells, but DHFR tag binding is blocked by the caging group, it was also possible to recruit the cytosolic protein to a single centromer targeted by 405 nm laser irradiation without recruition to non-targeted centromers in the same cell. Thus, the pcTMP-Ha dimerizer allows tight spatial control over the formation of protein-protein complexes. Additionally, due to the non-covalent binding between TMP and DHFR tag, the dimerizer could be outcompeted by an excess of free TMP, which gives the possibility to reverse the dimerization process although without spatial control [57]. In a follow up publication Zhang *et al.* enlarged the toolbox of photoreactive dimerizers with a coumarine caged pcTMP-Ha that can be activated with much lower light intensities and a photocleavable derivative TMP-pl-Ha [58]. Taking advantage of the spatiotemporally precise release of Mad1 (a methaphase-anaphase transition checkpoint protein) that had been recruited to methaphase kinetochores *via* TMP-pl-Ha, they showed that a small fraction of bound Mad1 is sufficient to halt cells in methaphase. Furthermore, precisely activated dimerization between the constitutive kinetochore protein SPC25 and the constitutively active motor domain of kinesin-1 K560 or CENP-E (kinesin-7) proofed findings from *in vitro* studies in live cell experiments [58].

Most recently, photoactivatable and photocleavable functionalization of DHFR-Halo tag dimerizers have been combined by decorating the TMP ligand of TMP-pl-Ha dimerizers with a coumarinyl caging group. These molecules allow two switches with high spatiotemporal control by inducing dimerization after removing the more sensitive coumarinyl group with light of $\lambda \sim 450$ nm wavelenght and dissociation of the protein complexes upon irradiation with light of $\lambda \leq 405$ nm wavelenght [59, 60].

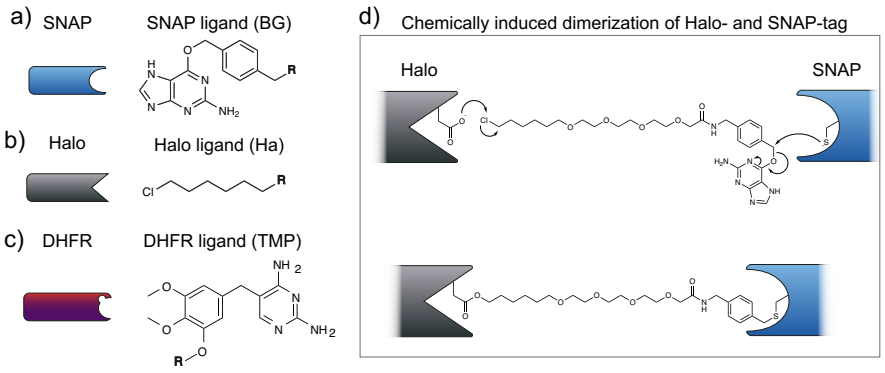

Figure 1.6: **The combination of ligands for self-labelling protein tags via flexible linker leads to a new class of synthetic dimerizers.**
a) SNAP-, b) Halo- and c) DHFR-tag and their ligands. d) Chemically induced dimerization of Halo- and SNAP-tag. BG: benzylguanin, TMP: trimethoprim

1.5 OPTOGENETICS - THE 'CHEMISTRY-FREE' PHOTOSWITCHING TOOLBOX

Optogenetics applies light reactive proteins that undergo dramatic sterical rearrangements under illumination that switches their biological activity between an "on" and an "off" state. For a long time optogenetics was mainly restricted to the light gated cation channels called channelrhodopsins that can be used to create action potentials in neurons upon illumination and have found a plethora of applications in neuroscience [61]. During the past years a variety of so called cellular or non-neuronal optogentic tools were developed and readily applied in living cells and animals[6, 62–64], but are beyond the scope of this work. However, the most widely used optogenetic tools and the basic concepts of how they are used to control cellular activities will be presented briefly, because of the great overlap with optochemical tools.

The LOV domain (figure 1.7 a) consists of a β-sheet core, that contains a flavin mononucleotid (FMN) chromophor, and a terminal α-helix. In the dark, the α-helix is attached to the β-sheet, but under blue light excitation the FMN binds to a rective cystein residue in the β-sheet and induced conformational changes that leads to unwinding of the α-helix[65] (figure 1.7b). Small peptides with signalling, binding or localization activity can be fused to the α-helix. The peptides are masked by the protein core in the dark, but readily exposed under illumination and thereby induce signalling events, dimerization with binding partners or translocation into another cellular compartment[24, 66, 67]. Alternatively, the LOV domain can be fused directly to the active side of an effector protein where it is sterically blocking interactions of the effector protein in the dark but not in the lit state [66]. The approach of controlled presentation of peptide motifs or

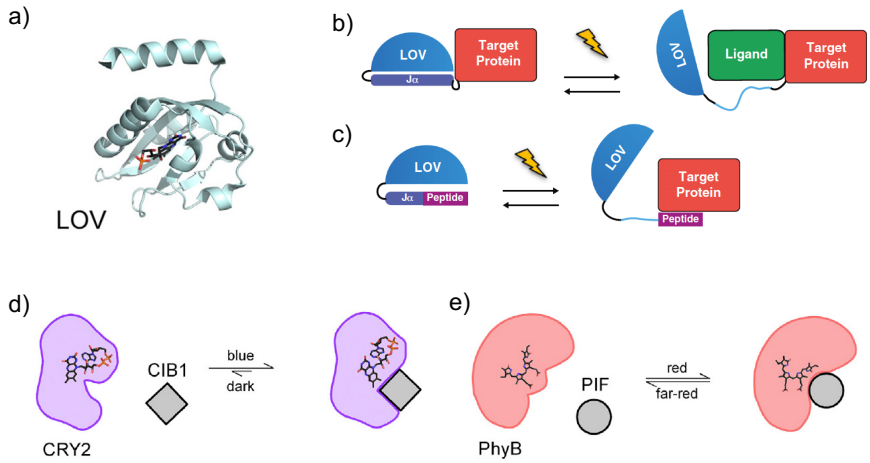

Figure 1.7: **Optogenetic tools can control protein activity.**
a) Crystal structure of the LOV domain with FMN cofactor. b) The love domain can be fused directly to its target protein or c) carry an activating peptide in the Jαhelix. d) CRY2 and CIBN dimerize under blue light. e) PhyB dimerization with PIF is switchable with red and far red light. Figure adapted from a,d,e) from [63], and b,c) [74].

blocking of reactive sites offers possibilities for various applications, but this high flexibility comes at a cost. Many LOV domain based tools show a substantial dark state activity that can be suppressed only *via* introduction of point mutations that have to be tested in tedious screenings and usually reduce also the activity of the lit state[24, 67, 68] . Thus, protein activity is rather switched between a "low" and a "high" rather then an "on" and an "off" state.

The cryptochrome CRY2 forms a heterodimer with the N-terminal fragment of the transcription factor CIB1 (CIBN) (figure 1.7c). Like the LOV domain they incorporate a FMN chromophore and are switchable with blue light.[69, 70] Similarly phytochrome B (PhyB) binds the phytochrome interaction factor 3 (PIF3) to form a heterodimeric complex. In contrast to LOV domains and cryptochromes, PhyB reacts to red light and dimerization is switched "on" with 650-670 nm light and whereas light of 700-750 nm wavelength induces the "off" state (figure 1.7d). Phytochrome photoswitching depends on a tetrapyrrole chromophore like phycocyanobilin (PCB), that has to be supplied externally in mammalian systems [71]. Obviously analogous to chemical dimerizes cryptochromes and phytochromes can be used to induce protein-protein interaction of fusion constructs and therefore can control protein activity by dimerization with effector proteins or *via* translocation to or away from their place of action.[61–63, 72, 73]

More recently the optogenetic tool box was complemented with the photocleabale fluorescent protein PhoCl. Excitation of the amino acid based chromophore leads to photoconversion and cleaves the protein backbone. This leads to a loss of fluorescence and the release of a short N-terminal fragment from the β-barrel core [75] PhoCl can act

as a photocleavable linker in a fusion protein construct, but for efficient photocleavage irradiation with near UV light for several minutes was necessary [75], which bears high risk for phototoxicity in live cell experiments.

The biggest advantage of all optogenetic tools except PhoCl is that they are reversible switchable and depend on relatively low doses of visible light, which reduces the risk of phototoxic side effects. Besides PhyB they do not depend on the external addition of molecules, which means they can be constantly renewed by the cells protein expression machinery. On the other side, to maintain long term effects switchable optogenetic systems depend on constant illumination. Furthermore, the broad absorption of visible light requires careful experimental precautions to prevent exposure to ambient light. The blue light absorbing LOV domain and cryptochromes prevent imaging of many of the most common fluorescent proteins from the blue to the green-yellow emission range (e.g. CFP, GFP, venus, etc.) [64].

To conclude, optogenetic tools are enlarging the tool box to control protein activity with light. Since most optogenetic proteins are activated with visible light they can in principle be used together with optochemical tools that react to light of $\lambda \leq 405$ nm wavelength but are stable under light of longer wavelengths. This spectral multiplexing would offer the chance to control complex dynamic systems with more precision then what is possible today.

2 EPITHELIAL CELL ADHESION AND MIGRATION

A cell is the smallest living unit and is confined by the plasma membrane, which contains the cytoplasma and highly specialized compartments. The subcellular compartments are called organelles and can be enclosed by membranes like the nucleus, mitochondria or the endoplasmatic reticulum (ER) or multiprotein complexes within the cytosol like ribosomes or proteasomes. In muticellular organisms cells are organized in tissues and organs that orchestrate the activity of the containing cells to facilitate complex biological processes that define life. In animals organs are outlined by the epithelium, which builds a tightly connected border to hold the inner tissues of the organ together and shields them from external cues to maintain its functional integrity. To form this sealed layer, epithelial cells need adhesive properties and rigidifying structures, but also need to be able undego dynamic rearrangements to allow processes like the formation of organs during embryonal development or wound healing in case of damage[76–78].

2.1 THE CYTOSKELETON DEFINES THE SHAPE OF CELLS

The rigidifying structures in eucaryotic cells are built out of filamentous protein structures that are summarized as the cytoskeleton in analogy to the bone skeleton of vertebrates. The main components of the cytoskeleton are actin filaments (also called microfilaments), intermediate filaments and microtubules (figure 2.1a).[79] Actin filaments are built out of globular actin (G-actin) monomers, that form a helical polymer of 8 nm in diameter with a double strand shape in an ATP and Mg^{2+} dependent polymerization[81]. Polymerization and depolymerization of G-actin happens at both ends of the actin filament (figure 2.1b), while polymerization is kinetically favored at the barbed end and slower at the point end , because ATP loaded G-actin hydrolyses the ATP to ADP soon after incorporation into the filament and ADP bound G-actin has a lower affinity to each other. This means, when the concentration of free G-actin is high enough and can constantly exchange ADP with ATP actin filaments are growing in both directions, but with different polymerization rate until the G-actin concentration reaches a critical level. In this steady state actin filaments are growing at the barbed end (therefore also called plus end) in the same rate as they are schrinking at the point end (also called minus end), which leads to a constant treadmilling of subunits in the filament under consumption of ATP[80]. Actin filaments can

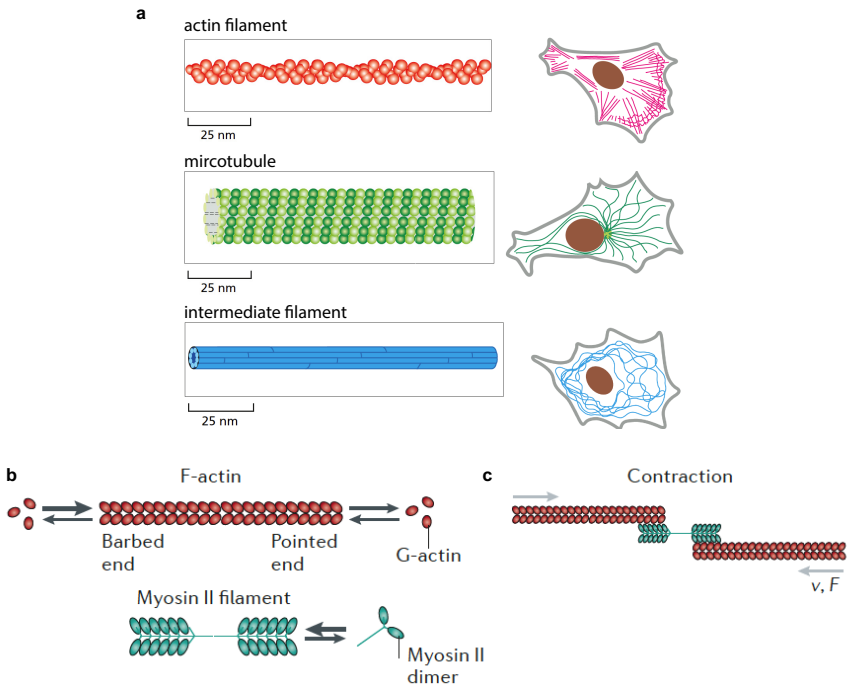

Figure 2.1: **Actin filaments, microtubuli and intermediate filaments are the main structural components of the cytoskeleton.**
a) The molecular architecture leads to distinct shapes of the cytoskeletal networks. b) Actin and myosin are forming filaments via polymerisation. c) Interaction of F-actin and myosin II fibres leads to contractility. Figure adapted from a) , b,c)[80].

be crosslinked into linear bundles, planar networks or 3D gels *via* a plethora of actin binding proteins and thereby build a skeletal framework[81].

Myosins are a family of motor proteins that form dimers which can bind and move along filamentous actin (F-actin). While most members of the myosin family are responsible for transporting vesicles along the actin fibers, myosin II dimers assemble into bipolar filaments[82]. Since myosin II binds F-actin in a defined orientation and moves towards the barbed end, myosin filaments can shift actin filaments towards each other leading to a contraction. Therefore, in the analogy to the bone skeleton, the contractile actomyosin network could be considered the muscles of the cell.

Microtubules (figure 2.1a) are tube like polymers consisting of two globular proteins α- and β-tubulin, that preassemble in heterodimers. The tubulin heterodimer polymerizes into protofilaments. A parallel bundle of 13 protofilaments forms the hollow cylindrical shape of microtubule with a diameter of 25 nm[81]. Like actin, the tubulin dimers polymerize and depolymerize at both ends of the polymer in with different kinetics driven by the energy from GTP hydrolysis. Microtubules are usually attached to an organelle in the center of the cells called centromer from which they sprout into the periphery of the cells. Their shape makes them less flexible then e.g. actin filaments. Therefore, they can act like stabilizing columns and additionally function as highways for vesicle trafficking mediated by processive motor-proteins like kinesins and dyneins that walk along the protofilaments[79, 81].

Unlike microtubules and actin filaments, intermediate filaments (figure 2.1a) are made out of various elongated monomers, which form parallel coiled-coil dimers, that assemble into bipolar tetramers. These tetramers can interconnect with each other to form fibers of 10 nm diameter which contain 8 tetramers (i.e. 32 coiled-coil dimers)[81]. The composition of the filaments is strongly dependent on the cell type and can change during differentiation or cancer formation. In epithelial cells intermediate filaments can span across the whole cell from one intercellular connection to another, thus supporting the mechanical connection of the whole epithelium[83].

2.2 CELL ADHESION STRUCTURES - A GRIP ON THE OUTSIDE WORLD

To allow the formation of a continuous and tight cellular tissue like the epithelium, the cytoskeleton needs to be anchored to stabilize the shape and structure of the cells. As shown in figure 2.2 polarized epithelial cells are interconnected *via* intermediate filaments that are linked to desmosomes. Desmosomes are multiprotein complexes, that contain the transmembrane cadherin-family proteins desmoglein

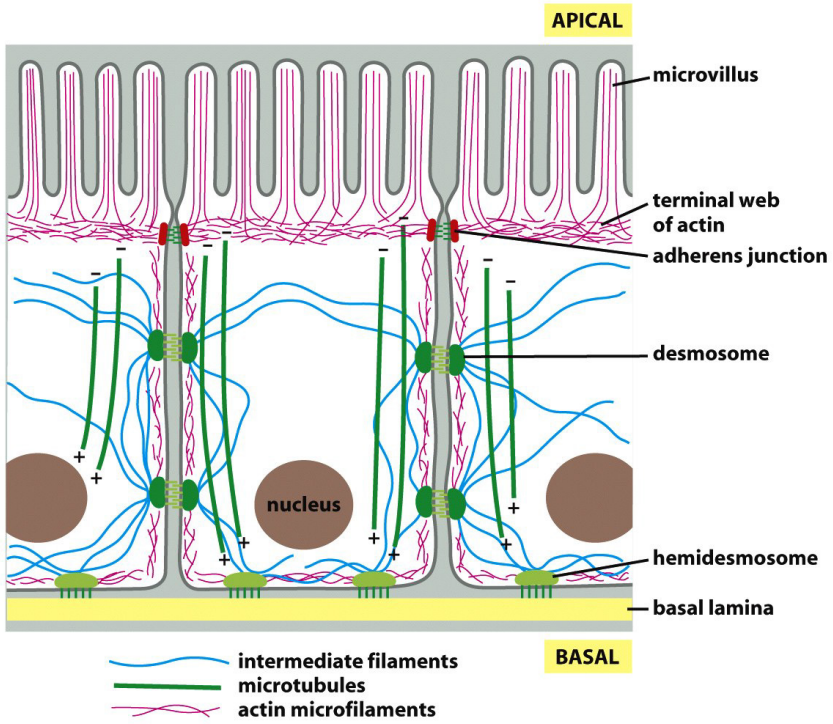

Figure 2.2: **In polarized epithelia adhesion structures connect the cytoskeleton to the basal lamina and surrounding cells.**
Figure adapted from [81] figure 16-5.

and desmocollin, which form homophilic contacts with the same proteins from the neighboring cell[84]. On the intracellular site thy cytosolic domains of desmoglein and desmocollin are connected to intermediate filaments *via* proteins like plakoglobin, plakophilin, desmoplakin and other anchoring and regulating proteins[85, 86]. Hemidesmosomes connect intermediate filaments to the basal lamina, a specialized extracellular structure composed of matrix proteins, that present adhesion points for integrins. Integrins are the dimeric transmembrane components of cell-matrix adhesion complexes that consist of various combinations of α- β-monomers dependent on the cell type and matrix composition. In the case of hemidesmosomes, integrin $\alpha_6\beta_4$ is linked to the intermediate filaments predominantly *via* plectrin and dystonin[84].

2.2.1 *Adherens junctions are mechanoresponsive structures*

An actin meshwork is outlining the cell cortex loosely associated with the plasma membrane, while adherens junctions (AJs) are the anchor points of contractile actomyosin network. In epithelial cells E-cadherin is the prime transmembrane protein that contributes on the extracellular side to the formation of AJs *via* homophilic *trans* dimerisation with E-cadherins from opposing cells and lateral clustering

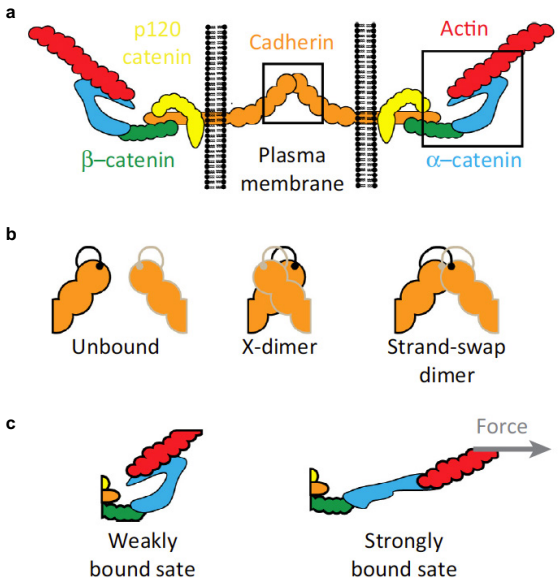

Figure 2.3: **E-cadherin mediated adherens junctions are the mechanoresponsive cell-cell contact anchor points for the actomyosin network in epithelial cells.**
The minimal AJ complex is built from E-cadherin, β-catenin and α-catenin that are linked to the actomyosin network. p120 catenin only indirectly involved via regulatory pathways. Mechanoresponses of the AJ complex are b) conformational changes from X- to strand-swapped dimer between extracellular E-cadherin domains of opposing cells and c) streatching of α-catenin increases binding to β-catenin and F-actin. Figure adapted from [94].

via transient *cis* interactions with E-cadherins within the same membrane[87–89]. The intracellular domain of E-cadherin offers binding sited for multiple adaptor proteins like β-catenin, which binds to α-catenin, which in turn can bind actin filaments[90–92] (figure 2.3). The connection of E-cadherin *via* β-catenin and α-catenin (also called CCC-complex) to the contractile actomyosin network, is the minimal structural unit of AJs that is sufficient to maintain actin associated cell-cell contacts. In addition, AJ can contain a large variety of regulatory signaling or actin binding proteins. For example p120-catenin is not physically linked to the actomyosin network, but can control mechanisms to stabilize AJs and increase actomyosin contractility.[93]

AJs are mechanoresponsive adhesion structures that react to mechanical cues with structural changes. The two terminal extracellular domains (EC12) of E-cadherin forms initial *trans* dimers with opposing E-cadherins in a so called X-dimer conformation (figure 2.3 b) that could be confirmed *via* crystal structure analysis [95]. These X-dimers are thought to be transient and under force change into a strand-swap dimer where the tryptophane residue at the second N-terminal position (W2) of one E-cadherin is flipping outwards into a binding pocket of the EC domain of the opposing E-cadherin[89,

90, 95]. This is the prevalent conformation in mature AJ complexes. On the intracellular site, α-catenin is binding very weakly to F-actin in the resting state, but strengthens its binding under tension. This catch bond behavior is facilitated by a tension induced conformational transition that exposes the tail domain which contains the actin binding domain (figure 2.3 c) [96–98]. Indeed the binding between the CCC complex and F-actin is so week without force that it is not possible to pull down actin *via* full length α-catenin in an *in vitro* cosedimentation assay[99], while the c-terminal tail domain does bind actin efficiently [96]. More recently, the force dependency could be confirmed *in vitro* *via* an optical trap based assay, that was used to slide an actin filament over an immobilized CCC complex [100].

2.2.2 *The E-cadherin is a key protein in adherens junction complexes*

E-cadherin consists of an extracellular part, that is structured into five homologous domains (EC1-5) (figure 2.4), which are connected *via* flexible hinge regions. Acidic amino acid residues in these hinge regions can form complexes with three Ca^{2+} per hinge[84]. This leads to a stiffening of the extracellular domains into a rod like shape. This stiffening is essential for the formation of *trans* dimers[101]. The extracellular domains also maintain the subtype specific binding between cadherins. While the epithelial E-cadherin binds to E-cadherin, N-cadherin, which is found in neurons and mesenchymal cells (e.g. fibroblasts), binds to N-cadherin. This homophilic binding behavior leads to a clustering of cells that express the same set of cadherins and is essential for the separation of different tissues[102]. Experiments with chimeric proteins that contained different numbers of the extracellular domain of E-cadherin fused with the rest of N-cadherin showed that the EC12 domain is sufficient to facilitate binding to full length E-cadherin.

Furthermore, the switch between E-cadherin and N-cadherin is a hallmark of the epithelial to mesenchymal transition (EMT). During EMT epithelial cells loose their stable cell-cell connections and turn into a more motile mesenchymal state. The reverse process called mesenchymal to epithelial transition (MET) as well as intermediated transition states also occurs and both are dynamically regulated in physiological processes during embryonal development and wound healing, but can also lead to fibrosis or cancer metastasis[76, 103].

Since E-cadherin is a transmembrane protein, it is expressed as a precursor protein and needs to undergo a maturation process to become fully functional (figure 2.4). The N-terminus of the precursor E-cadherin, the so called pro-domain, contains a signaling peptide that ensures correct localization of the future extracellular domain into the lumen of the ER and integration into its membrane during protein biosynthesis. The precursor E-cadherin is then transported

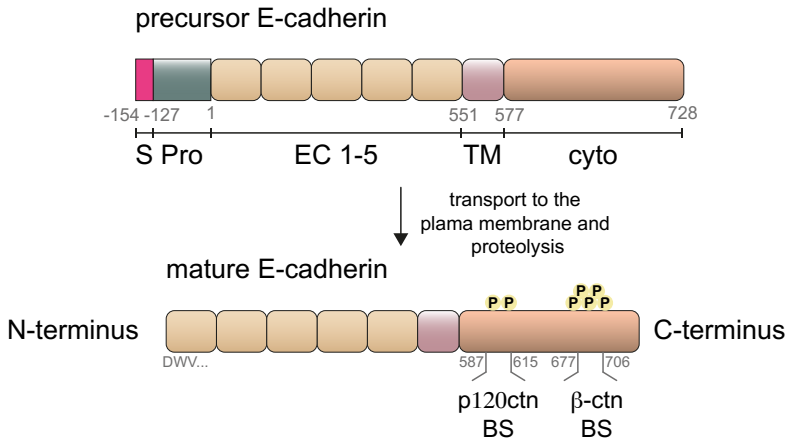

Figure 2.4: **E-cadherin domains form extracellular and intracellular connections.**
E-cadherin is expressed as a precursor protein and undergoes a maturation process before being presented aa a transmembrane protein in the plasma membrane. Figure adapted from [89].

in membrane vesicles *via* the Golgi apparatus to the plasma membrane. During this transport process, the pro-domain is cleaved off *via* furin protease [89] leaving the endogenous N-terminus DWV of mature E-cadherin. *In vitro* experiments with recombinantly expressed, unprocessed EC12 domains did show that even a single additional N-terminal methionin residue (MDWV) dramatically impaired the formation of EC12 dimers[95].

The C-terminal cytosolic domain of E-cadherin contains distinct binding sites for p120-catenin and β-catenin. While the p120-catenin is located close to the transmembrane domain, β-catenin binds close to the C-terminus. Multiple residues in the β-catenin binding region can be phosphorylated, which increases the binding affinity of β-catenin.

2.2.3 *The actomyosin network is anchored at the ECM via focal adhesions*

Like intermediated filaments, the actomyosin network is not only linked at cell-cell contacts *via* adherens junctions, but also *via* integrin mediated cell-matrix adhesion complexes called focal adhesions (FAs)[80, 84, 104] (figure 2.5). The initial connection between integrin dimers and F-actin is mediated by talin, a rod shaped protein with multiple actin binding sites and a globular head domain[105]. The head domain binds and activates the β-subunit of integrin dimers, while the rod domains of two talin proteins can dimerize with each other, thereby leading to an initial clustering of integrins[106]. Strain excepted *via* actomyosin contractility stretches the talin rod domain[107], which leads to exposure of cryptic actin and vinculin binding sites[108, 109]. The mechanoresponsive protein vinculin itself enables binding

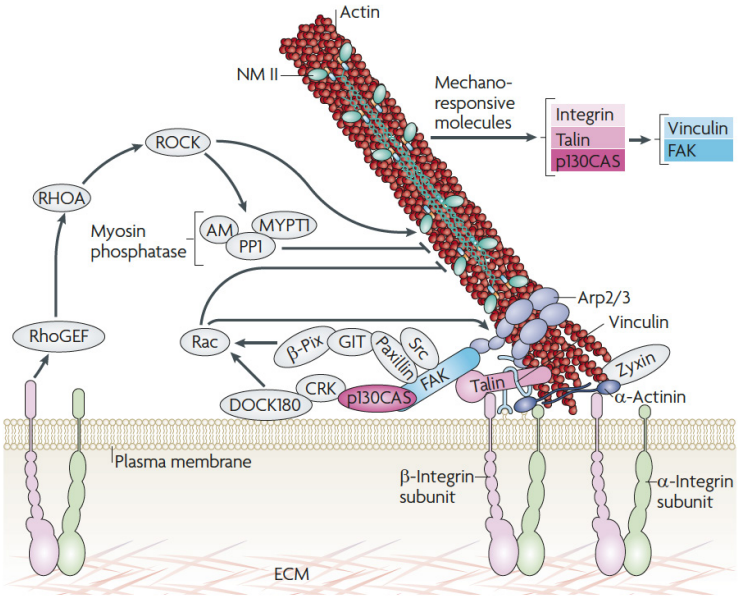

Figure 2.5: **Focal adhesions are multiprotein complexes that anchor actomyosin bundles to the ECM.**
Proteins recruited to FAs can bind directly to actin or activate regularory pathways for actin polymerization or myosin contraction. Figure adapted from [82].

to multiple actin filaments *via* stress induced unfolding of its tail domain[110]. The attachment of multiple actin filaments leads to binding of F-actin crosslinking proteins like α-actinin and Arp2/3[82], which drives the formation of interconnected bundles of F-actin and myosin II filaments called stress fibers thereby increasing the efficiency of actomyosin contractility. Another protein that can bind β-integrin and connect it indirectly to F-actin *via* recruitment of vinculin is paxillin. Like talin, paxillin contains binding sites for kinases like Src and focal adhesion kinase (FAK)[111] that can activate further regulatory signaling pathways. Many of these pathways include GTPases of the Rho protein family, e.g. RhoA and Rac. While Rac induces the inhibition of myosin phosphorylation which decreases actomyosin contractility, RhoA activates the Rho-associated protein kinase ROCK), which phosphorylates myosin and thus increases actomyosin contractility[81, 82].

2.3 HOW CELLS CAN MOVE - THE INTERPLAY OF ADHESION AND CONTRACTION

Single cells or cells at the edge of an epithelial cluster tend to form flat membrane protrusions called lamellipodia. The formation of lamellipodia derives from the constant pushing force of polymerizing actin filaments, that are cross-linked into a 2-dimensional branching network by the protein complex Arp2/3[81] and anchored to the under-

lying substrate *via* nascent adhesions (figure 2.6 a). The progression of lamellipodia is slower then the extension of F-actin, because the actin network is constantly dragged backwards creating a retrograde flow. Interactions of the back-flowing actin network with adhesion proteins induces shear stresses that activate a maturation into larger adhesion clusters and bundled attachments of actin filaments. In a distance of ca. 2-4 µm from the tip of a lamellipodium the architecture of the actin network changes into aligned actomyosin fibers that are connected to maturing FAs[82, 112], that can resist the increasing force load excepted by myosin contractions. In this region called lamellum, the retrograde flow of actin is reduced, which leads to a stabilization of the actomyosin network. The resulting stress fibers are firmly attached to the ECM *via* large elongated FAs and sustain constant pulling forces. The manifestation of FAs allowed further extension of the lamellipodia (figure 2.6b). Stress fibers can stretch several micrometers across the whole cell to a second FA structure. This double sided anchoring allows them to built up strong traction forces, that are transmitted *via* integrins to the ECM[80, 113] (figure 2.7a) The interconnected structure of the actomyosin network moves the cell body into the direction of lamellipodia formation and together with an orchestrated detachment of the adhesion structures at the trailing edge of the cell, this leads to migration of the cell.

In epithelial cells the tensile forces that are built up at the leading edge can be transmitted not only to FAs on the trailling edge, but also to AJs. As described in section 2.2.1 are mechanoresponsive load bearing structures like FAs, which leads to a 'tug of war' between these two actomyosin anchoring structures. Forces from the leading edge stimulate cells to move away from each other, while the force exerted on AJs increase cell-cell adhesion. Forces that are transmitted from the migrating cells at the edge to their neighboring cell can be propagated further over lengths of several cell diameters. These intercellular force transmission leads to stress at the cell-cell interfaces and induces tension within the tightly coupled epithelial layer that increase with distance from the leading edge [114]. Consequently, the mechanical coupling of epithelial cells also influences their migration. At AJs cells can experience shear stress (oriented along the cell-cell interface) or normal stress (oriented perpendicular to the cell-cell interface). It had been shown that cells tend to migrate collectively in directions correlated with high normal stress, which means the reduction of shear stress and thus, less neighbor exchange [115]. Therefore, on a short timescale an epithelial cell cluster acts as a solid elastic layer in which the relative position of the cells towards each other stays mostly constant. On longer timescales however cellular reorganizations and turbulences induced e.g. by cell death or cell division take over and the monolayer behavior can be regarded as liquid. [102] AJs are essential for this coordinated viscoelastic behavior as their dis-

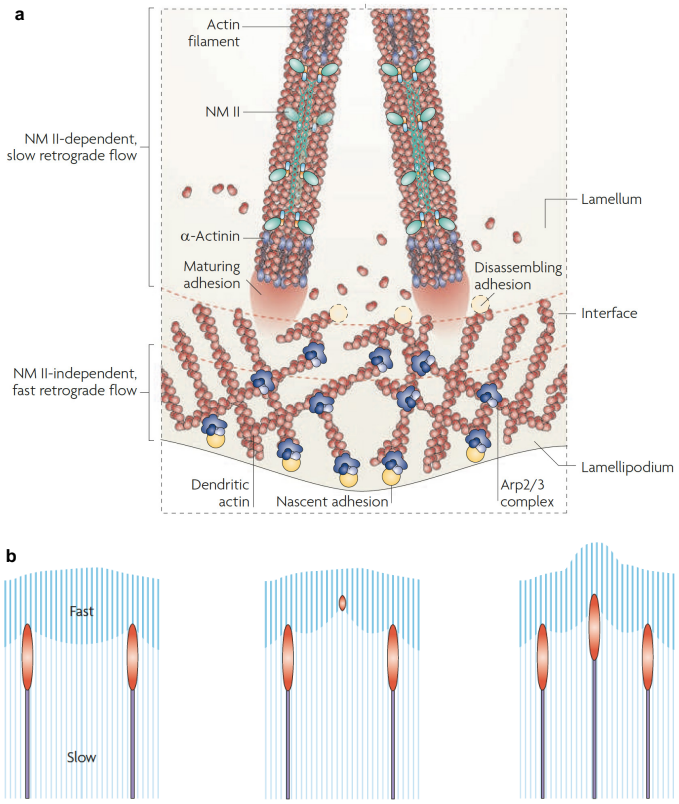

Figure 2.6: **Actin polymerization, cell-matrix adhesionand actomyosin contractility lead to migration.**
a) In lamellipodia polymerisation of the actin meshwork pushes the plasma membrane forward. FAs form at the interface to the lamellum initiate the formation of stress fibers. b) FAs built anchoring points that allow the cell to extend the lamellum and lamellipodia. Figure adapted from a) [82] and b) [112].

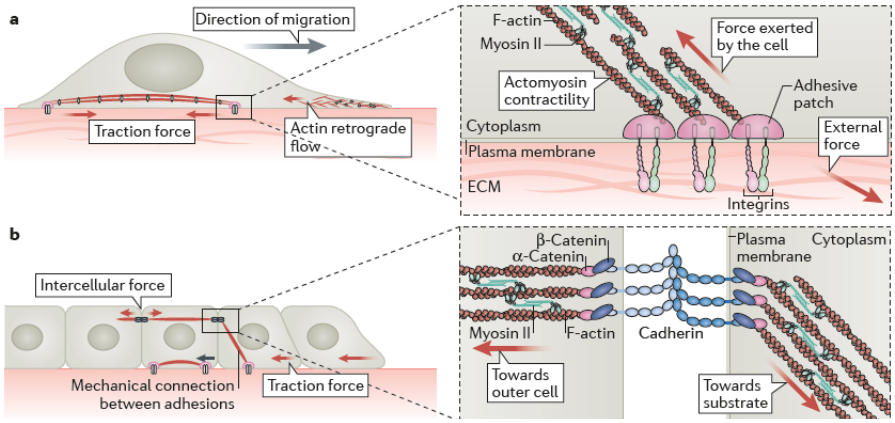

Figure 2.7: **Contractility and migration in single cells and epithelial monolayers.**
a) In single cells traction forces can be transmited across the cell via stress fibres that are anchored to the ECM via FAs. b) In epithelial cells forces excerted by caells at the migration edge can be transmitted into the cell layer via AJ.
Figure adapted from [113].

ruption leads to uncoordinated migration comparable to single cells, which also results in a reduced velocity of the layer[113].

3 MOTIVATION

3.1 A NEED FOR PRECISE CONTROL OF ADHESION COMPLEXES

As described in section 2.2 cell-cell and cell-matrix adhesions need to be co-regulated and outbalanced to maintain the integrity of epithelial cells[116]. On the other hand under certain circumstances e.g. wounding of the epithelial layer, the cell need to be able to downregulate cell-cell adhesions and become more motile to close the wound. These events are accompanied by multiple changes in the gene expression profile and dynamic regulation of biochemical signaling pathways. These complex processes are summarized under the term EMT[76]. The mechanisms of EMT can also lead to metastasis during cancer progression. Regarding the clonal origin of most tumors [117], the adhesive downregulation occurs in a single mutated cell or a small group of cells within the adhesive tissue. How the mechanical aspects of dynamically regulated cell adhesion contribute to EMT is poorly understood, mainly because methods to control cell adhesion with sufficient spatiotemporal precision but without systemic side effects are missing.

A general biological approach to study the function of a protein within a cell is to deplete it and study the occurring effects. This can be done either by a permanent, genetic knock out or a transient knock down on the translational level. Although being a very powerfull tool, this method is very limited to study dynamically regulated processes. Especially, in the context of cell adhesion complexes it is known that the downregulation of one protein can be compensated to a certain extend by another similar protein or activation of regulatory pathways. For example in epithelial cells the downregulation of E-cadherin can be compensated by P-cadherin (e.g. in A431 cells) or cadherin-6 (e.g. in MDCK cells)[118]. To investigate immediate mechanical effect of depletion of a target protein or structural complex, methods with higher spatiotemporal precision are necessary.

Laser ablation can be used to cut stress fibers within a cell [119] or selectively kill a cell within an epithelial monolayer [120] with very high spatiotemporal resolution, but this method is highly invasive and thus can cause dramatic unspecific side effects. Unwanted side effects are also an issue for the disruption of cadherin mediated cell-cell contacts *via* Ca^{2+} depletion (ref), since Ca^{2+} is a second messenger molecule that is involved in various processes inside a cell. Actomyosin contractility can be inhibited or stimulated with blebbistatin, but like Ca^{2+} depletion they act systemically on all cells within the

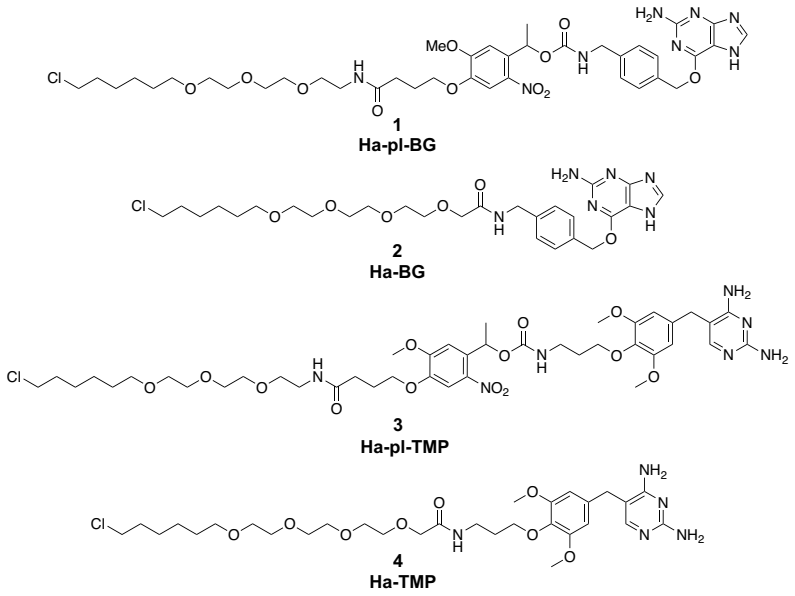

Figure 3.1: **Photocleavable and non-cleavable dimerizer for self-labelling protein tags taht will be applied in this study.**

culture dish and additionally blebbistatin is highly fluorescent and strongly interferes with GFP imaging[4].

3.2 MISSION STATEMENT - WHAT THE READER CAN EXPECT

3.2.1 *Aim of the study*

The aim of this project was to develop a method to control cell adhesion with light. Light was chosen as the intended trigger for the reasons discussed in section 1.1 like bioorthogonality and high spatiotemporal precision, but also it should be compatible with established imaging based methods to study cell migration and contractility. In a previous project at the Wombacher Lab, I developed a set of photocleavable and non-cleavable dimerizers (figure 3.1), of which the dimerizers Ha-TMP and Ha-pl-TMP were proven to be capable of translocating cytosolic proteins to subcellular compartments (e.g. sequestration at an intracellular membrane) by inducing protein-protein interactions between the DHFR tagged target protein and a Halo tagged localization domain [121].

Please note, that the reports of photoreactive dimerizer based on self-labelling protein tags discussed in section 1.4.2 were all published during the course of this PhD thesis project. The presented studies highlighted the broad potential of this cutting edge technology and encouraged me to develop the application for optochemically controlled adhesion complex formation presented in this thesis.

In the course of this project I wanted to establish the intracellular dimerization with the covalent-covalent binding Ha-BG and Ha-

pl-BG molecules and apply this state-of-the-art optochemical tool to control the formation or strengthening of cell adhesion complexes. I focused on the actomyosin connected adhesion structures FAs and AJs, because they are relatively well studied and known to be actively mechanoresponsive. Furthermore, some proteins have been previously identified as key players for the formation and enforcement of the adhesion complexes, and were therefore chosen as targets for establishing the method. Finally, I wanted to prove the mechanical functionality of the light controlled adhesion structures in the context of epithelial cell migration. Therefore, I applied some state-of-the-art technologies, that will be briefly explained in the following section.

3.2.2 *Selected methods to study epithelial cell migration and contractility*

As discussed in section2.3 epithelial cell migration is initiated at the free edge of a cell cluster *via* formation of filopodia and subsequent attachment of stress fibers *via* FAs. The pulling forces of the leading edge are counteracted by intercellular forces transmitted *via* AJs, which leads to collective migration. Thus, coordinated motion and collective contraction are measures for functional cell-cell adhesion [113].

To reduce complexity of the system and improve reproducibility, a rupture free wound healing assay (figure 3.2 a) can be performed. Cells are physically confined with a adhesion inert barrier e.g. made out of polydimethylsiloxane (PDMS). When the barrier is removed, the cells experience a cell free area along straight edge and start to migrate. The cell free area can be regarded as a model wound.

The collective migration behavior can be analyzed *via* particle image velocimetry (PIV) (figure b) a method derived from fluid dynamics to analyze streaming behaviors in gases and fluids by tracing the displacement of particles within over time. Therefore, two subsequent image frames of a time lapse recording are subdivided into smaller units called interrogation windows, that contain a small fraction of particles. The displacement of particles are compared by shifting each interrogation window in the next frame around its original position to find the best match according to a mathematically defined score[122]. The shift at each position is then assigned in a displacement vector field, which can be translated into a velocity vector field concerning the known time difference between two frames. In the context of cell migration, PIV can help to analyze the displacements within a cellular subpopulation, without the need to trace every cell separately. Spatial correlations and the overall correlation length can be calculated from the velocity fields, which are a measure collectively coordinated migration [123, 124].

Traction forces microscopy (TFM) allows to measure the tensile forces that cells exert on the ECM [125]. In a classical TFM experi-

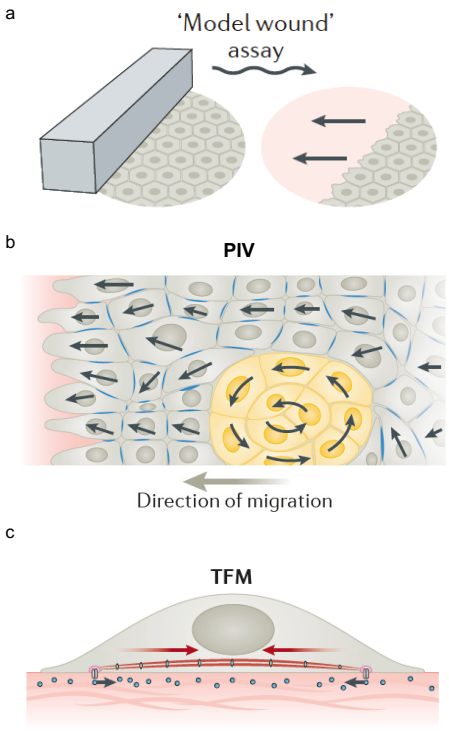

Figure 3.2: **Methods to study epithelial migration and contractility.** Sketches of a) a rupture free wound-healing assay, b) PIV analysis of cells in a monolayer and c) traction force microscopy (TFM). Figure adapted from [113]

ment, small fluorescent beads are incorporated in an elastic gel, which is functionalized with firmly coupled ECM molecules to allow cell attachment. When the cells adhere to the ECM molecules and start to exert traction forces, this leads to a deformation of the gel that can be traced *via* displacement of the beads directly underneath the gels surface. For a gel of known elastic modulus, the traction forces can be calculated by inverting the displacement field [114].

Part II

MATERIALS AND METHODS

4 MATERIALS

List of company abbreviations used

Company	**Abbreviation**
Acros Organics	Acros
Asta Tech Inc.	Asta
Bruker Daltronics	Bruker
Carl Roth	Roth
Eurisotop SAS	Eurisotop
GE Healthcare	GE
Gold Biotechnology	GB
KERN & SOHN	K&S
Macherey-Nagel GmbH & Co KG	Macherey
MCAT GmbH	MCAT
New England Biolabs GmbH	NEB
Novabiochem	Novab.
Scientific Industries	Sci. In.
Sigma-Aldrich	Sigma
Thermo Fisher Scientific	TF
Vacuubrand GmbH + Co KG	Vac.

4.1 CHEMICALS AND REAGENTS

Tween-20	Roth
Name	**Company**
1-Chloro-6-iodohexane	Sigma
20-Azido-3,6,9,12,15,18-hexaoxaicosan-1-ole	MCAT
4-[4-(1-Hydroxyethyl)-2-methoxy-5-nitrophenoxy]butyric acid	Sigma
4-Nitrophenyl chloroformiate	Sigma
6-((4-(Aminomethyl)benzyl)oxy)-9H-purin-2-amine	Asta
Acetic acid	Sigma
Acetonitril	Roth
Agar-Agar, Kobe I	Roth
Calcium chloride dihydrate	Merck
Celite® S filter aid, dried, untreated	Sigma

Tween-20	Roth
Chloroform-d	Eurisotop
Chloramphenicol	AppliChem
Coomassie Brilliant Blue R250	Sigma
D-(+)-Glucose	Sigma
Dichloromethane anhydrous, ≥99.8%, contains 40-150 ppm amylene as stabilizer	Sigma
N,N-Diisopropylethylamine 99.5%, biotech. grade	Sigma
N,N-Dimethylformamide puriss. p.a.	Sigma
Dimethyl sulfoxide (DMSO)	TF
DL-Dithiothreitol	Sigma
DNA Stain Clear G	SERVA
dNTP-Mix	TF
Ethylene glycol-bis(-aminoethyl ether) -N,N,N′,N′-tetraacetic acid (EGTA)	AppliChem
Ethylenediaminetetraacetic acid (EDTA, 0.5 M 100x)	TF
Ethyl acetate for HPLC, ≥99.7%	Sigma
Hydrogen	-
Methanol for HPLC, ≥99.9%	Sigma
Methanol-d_4	Eurisotop
Nickel(II) sulfate	Sigma
Palladium on activated charcoal (10 % Pd basis)	Sigma
Pyruvate	TF
Polygram Sil G/UV254 TLC plates	Macherey
PyBOP	Novab.
Potassium chloride (KCl)	Roth
Silica gel technical grade, pore size 60 Å, 230-400 mesh particle size, 40-63 µm particle size	Sigma
Sodium hydride 60 % dispersion in mineral oil	Sigma
Sodium Cloride (NaCl)	Merck
Sodium phosphate (Na_3PO_4)	Roth
Tetrahydrofuran, anhydrous	Sigma
Triethylamine puriss. p.a., ≥99.5% (GC)	Sigma
TRIS hydrochloride	Biomol

4.2 BIOCHEMICAL AND MICROBILOGICAL REAGENTS

Name	Cat. No	Company
Agarose	11404	Serva
Ampicillin	A0166	Sigma
Biotin	B4039	Sigma
Albumin fraction V (BSA)	8076	Roth
Fetal bovine serum (FBS)	-	Sigma
Geneticin	10131027	TF
Kanamycin	K-120-25	GB
Penicillin/Streptomycin (Pen/Strep)	15140122	TF
Trypsin	59427C	Sigma

4.3 ANTIBODIES

Abbreviations used:
Cat. No = catalog number, Comp. = Company, Appl. = application, Fin. conc. = final concentration, IF = immunofluorescence and WB = western blot
Conj. = Conjugation, A = Alexa Fluor, HRP = horseradish peroxidase, FITC = Fluorescein isothiocyanate, TRITC = Tetramethylrhodamine
DAPI = 4´,6-diamidino-2-phenylindole

4.3.1 *Primary antibodies*

Target protein	**Species**	**Cat. No**	**Comp.**	**Appl.**	**Fin. conc. [µg/ml]**
α-catenin (C-terminal)	Mouse	610193	BD	IF	1.06
				WB	0.11
α-catenin (N-terminal)	Rabbit	Ab51032	Abcam	IF	1.06
				WB	0.11
β-actin	Mouse	A1978	Sigma	WB	0.50
β-catenin	Mouse	610153	BD	IF	2.50
				WB	0.25
Desmo-plakin1	Guinea pig	DP-1	Progen	IF	1.00
E-cadherin (H-108)	Rabbit	Sc-7870	Sc	IF	2.00
				WB	0.20
E-cadherin	Mouse	Sc-8426	Sc	WB	0.20
GFP	Rabbit	A-11122	TF	WB	0.40
m-Cherry	Rat	M11217	TF	WB	0.40
N-cadherin	Mouse	610920	BD	WB	0.25

4.3.2 *Secondary antibodies*

Target species	Species	Conj.	Cat. No	Comp.	Appl.	Final conc. [µg/ml]
Mouse	Goat	A350	A-21049	TF	IF	10.0
Mouse	Goat	A405	A-31553	TF	IF	2.0
Mouse	Donkey	A647	A-31571	TF	IF	20.0
Rabbit	Goat	A350	A-21068	TF	IF	10.0
Rabbit	Goat	A647	A-21442	TF	IF	20.0
Guinea Pig	Goat	A647	A21450	TF	IF	2.0
Mouse	Goat	HRP	SC-2005	Sc	WB	0.4
Rabbit	Goat	HRP	SC-2004	Sc	WB	0.4
Rat	Goat	HRP	Ab97057	Abcam	WB	0.4

4.3.3 *Fluorescent Affinity Binders*

Name	Conj.	Cat. No	Comp.	Appl.	Final conc. [µg/ml]
DAPI	-	D9542	Sigma	IF	1.0
Phalloidin	A647	A22287	TF	IF	2.0
Phalloidin	FITC	P5282	Sigma	IF	2.0
Phalloidin	TRITC	P1951	Sigma	IF	2.0

4.4 DNA MODIFYING ENZYMES AND MASTER MIXES

All enzymes and master mixes were acquired from NEB.

Restriction enzymes		
AflII	BmtI-HF	NotI-HF
AgeI-HF	BsrGI-HF	PacI
AsiSI	DpnI	PmeI
BamHI-HF	FseI	SacII

Master mixes
Q5 High-Fidelity 2x Master Mix
Gibson Assembly 2x Master Mix

4.5 BUFFERS, SOLUTIONS AND MEDIA

4.5.1 *Buffer recepies*

FACS buffer	
FBS	10 %
EDTA	2 mM
in PBS	

TBST buffer (pH 7.5)	
TrisHCL	50 mM
NaCl	150 mM
Tween-20	0.1 %
in deionized H_2O	

TEV cut buffer (pH 8.0)	
Tris-HCl	50 mM
EDTA	0.5 mM
DTT	1 mM
in deionized H_2O	

Binding buffer/ buffer A (pH 7.4)	
Tris-HCl	50 mM
NaCl	0.3 M
Imidazol	30 mM
in deionized H_2O	

Eluition buffer/ buffer B (pH 7.4)

Tris-HCl	50 mM
NaCl	0.3 M
Imidazol	250 mM
in deionized H_2O	

10x TB buffer (pH 7.4)

Tris-HCl	0.5 M
NaCl	1 M
KCl	0.1 M
BSA	2% (w/v)
in deionized H_2O	

Strippin-Buffer (pH 7.4)

Na_3PO_4	20 mM
NaCl	0.5 M
EDTA	50 mM
in deionized H_2O	

Sodium chloride solution

NaCl	1.5 M
in deionized H_2O	

Nickel (II) sulfate solution

Nickel (II) sulfate	0.1 M
in deionized H_2O	

Comassie Staining solution

Comassie Brilliant Blue	0.05 % (w/v)
Isopropyl alcohol	25 % (v/v)
in deionized H_2O	

Comassie Destaining solution

Methanol	20 % (v/v)
Acetic acid	10 % (v/v)
in deionized H_2O	

Ponceau Red Solution	
Ponceau S	0.5 % (w/v)
Acetic acid	1 % (v/v)
in deionized H_2O	

4.5.2 *Cell culture media*

Name			**Cat. No**	**Company**
Dulbecco's modified Eagle's medium (DMEM)			41966-029	TF
+	Phenol Red			
incl.	Glucose	4.5 g/l		
incl.	Glutamax	4 mM		
incl.	Sodium Pyruvate	1 mM		
add	FBS	10 %		
opt.	Pen/Strep	1 %		
opt.	Geneticin	750 g/l		
Dulbecco's modified Eagle's medium (DMEM) no phenol red			31053-028	TF
-	Phenol Red			
incl.	Glucose	4.5 g/l		
incl.	Sodium Pyruvate	1 mM		
FluoroBrite			A1896701	TF
-	Phenol Red			
incl.	Glucose	4.5 g/l		
add	Glutamax	4 mM		
add	Sodium Pyruvate	1 mM		
add	FBS	10 %		
opt.	Pen/Strep	1 %		
opt.	Geneticin	750 g/l		
Opti-MEM			31985-062	TF

4.5.3 *Bacteria media*

Lysogeny broth (LB)-Medium	**LB Agar**
LB-Medium (Luria/Miller) 2.5 % (w/v) in sterile H_2O	Agar 2.0 % (w/v) in LB-Medium

4.5.4 *SDS page and western blot buffers*

Name	**Cat. No**	**Company**
RIPA lysis buffer	R0278	Sigma
Halt Protease and Phosphatase Inhibitor Single-Use Cocktail	78442	TF
NuPAGE LSD Sample Buffer	NP0007	TF
NuPAGE Sample Reducing Agent	NP0009	TF
Novex Sharp Pre-stained Protein Standard	LC5800	TF
MOPS SDS running Buffer (20x)	NP0001	TF
MES SDS running Buffer (20x)	NP0002	TF
Nitrocellulose membrane	88018	TF
NuPAGE Transfer Buffer	NP0006	TF
Ponceau Red	P3504	Sigma
BSA	8476	Roth
Amersham ECL Prime Western Blotting Detection Reagent	-	GE

4.6 KITS

Name	**Company**
Amaxa Cell Line Nucleofector Kit L	Lonza
Amaxa Cell Line Nucleofector Kit T	Lonza
ECL Primer Western Blotting Detecting Reagents	Amersham
QIAquick Gel Extraction Kit	Quiagen
QIAquick PCR Purification Kit	Quiagen
QIAprep Spin Miniprep Kit	Quiagen

4.7 DISPOSABLES

Name	Company
Cell culture flask 25 cm^2	Sarstedt
Cell culture flask 75 cm^2	Sarstedt
µ- Slides VI 0.4	Ibidi
12 Well Plate	TPP
6 Well Plate	TPP
Blotting Filter Paper 2.5 mm	TF
Nitro Cellulose Membrane 0.45 Micron	TF
4- 12 % Bis- Tris Gel 1.0 mm x10 wells	TF
4- 12 % Bis- Tris Gel 1.5 mm x15 wells	TF

4.8 CELL LINES AND BACTERIAL STRAINS

4.8.1 *Cell lines bought*

Name	Cat. No.	Company
A431	CRL-1555	ATCC
BT549	HTB-122	ATCC
MDA-MB-231	HTB-26	ATCC
MCF 7	HTB-22	ATCC
MDCK.2	00062107	Sigma

4.8.2 *Cell lines provided*

Name	Provider	Institute, Country
A431 α-catenin KO	Dr. T. Kato	Francis Crick Institute, UK
A431 D	Dr. R.M. Mège	Institut Jacques Monod, France
COS 7	Dr. U. Engel	Heidelberg University, Germany
MDCK.2 E-cadherin KO	Dr. R.M. Mège	Institut Jacques Monod, France
REF 52	Dr. B. Geiger	Weizmann Institute of Science, Israel

4.8.3 *Stable cell lines produced*

Original cell line	Plasmid used Code	Name
A431 D	pDO48	hE-cadherin GFP
	pDO52	EcGFP-α(280-906)
	pDO56	EcGFP-Halo_IRES_SNAP-mCherry-α(280-906)
A431 α-catenin KO	pDO23	mEmerald-α-catenin
	pDO52	EcGFP-α(280-906)
	pDO56	EcGFP-Halo_IRES_SNAP-mCherry-α(280-906)
MDCK II E-cadherin KO	pDO68	E-cadherin-Δ-cyto-Halo_ IRES_DHFR-EGFP-cytotail

4.8.4 *Bacterial strains*

Strain		Company
E. coli	DH5α	NEB
	KRX	Promega

4.9 MACHINES AND EQUIPPMENT

Name	Company
ABJ analytic scale	K&S
acuracy weighing machine AX 105 DeltaRange analytic scale	Mettler Toledo
Adventurer analytic scale	OHAUS
Agilent 1100 Series HPLC system equipped with diode array and fluorescence detector	Agilent
Amersham Imager 600	Amersham
Avanti J-26XP Ultracentrifuge with rotor JA-10 and JA-25.50	
ÄKTA pure 25 M, purifier system	GE
B28 plate incubator	Binder
Centrifuge 5417 R	Eppendorf
Centrifuge 5418	Eppendorf
DNAEngine, Thermocycler	Bio-Rad
EMB 1000-2 table scale	K&S
Excella E24R Incubator shaker	Eppendorf

Name	Company
FACS Melody	BD
Gene Pulser Xcell, electroporation system	Bio-Rad
Hei-VAP value G6 rotary evaporator	Heidolph
Heracell, carbon dioxide incubator	Hereaus
Heracell 240, carbon dioxide incubator	Hereaus
HisTrap HP 5 ml, IMAC column	GE
HisTrap HP 1 ml, IMAC column	GE
Lambda 25 UV/Vis spectrometer	PerkinElmer
Luna 3u C18(2) 100A, LC Column 100 x 0.3 mm, Ea	Phenomenex Ltd.
Megafuge 1.0 tabletop centrifuge	Hereaus
Microcentrifuge 5418 tabletop centrifuge	Eppendorf
micrOTOF-Q II high resolution mass spectrometer	Bruker
Mini-Sub Cell GT Systems agarose gel electrophorese chamber	Bio-Rad
Minitron Incubator AT73	INFORS
MinUVIS UV handlamp (30 W)	DESAGA
ND-1000 NanoDrop spectrometer	peqlab
Power Ease 90 W	TF
PowerPac Basic Power Supply	Bio-Rad
Prism Mini Centrifuge	Labnet
ROTINA 380 R tabletop centrifuge with rotor 1754	Hettich
SHAKER DRS-12 rocket shaker	neoLab
T100 Thermal Cycler, thermocycler	Bio-Rad
Thermomixer comfort	Eppendorf
UV-Transilluminator agarosegel documentation	peqlab
Vacuum pumping unit VP-2 autovac	Vac.
Varian Mercury Plus 300 MHz NMR spectrometer	Varian
Varian Mercury Plus 500 MHz NMR spectrometer	Varian
Vortex Genie II	Sci. In.
XCell SureLock SDS-electrophoresis system with power Ease 90W power supply	TF

Microscopes

Microscope	**Name**	**Stand**	**Company**	
	DMi8 inverted	DMi8	Leica	
	fluorescence wide-field			
Objective	Name	Company	NA	Imm.
	10 x HC PL FLUOTAR	Leica	0.32	dry
	63 x HC PL APO CS2	Leica	1.40	oil
Camera	Name	Company		
	sCMOS DFC9000GT	Leica		
Light source	Name	Power		
	X-Cite 200DC	200 W		
Filter sets	Filter	Excitation [nm]	Emission [nm]	
	DAPI	350/50	460/50	
	FITC	480/40	527/30	
	RHODAMINE	546/10	585/40	
	Y5	620/60	700/76	
	QSP-T	365/50; 488/20; 561/20; 638/20		
Laser scanner	Name	Excitation [nm]		
	Leica infinity scanner	405		

Microscope	**Name**	**Stand**	**Company**	
	Olympus IX inverted	DeltaVision	Olympus	
	fluorescence wide-field	Elite system		
Objective	Name	Company	NA, PH	Imm.
	10 x	Zeiss	0.30, PH1	dry
	20 x	Zeiss	0.50, PH1	dry
	60 x	Olympus	1.42	oil
Camera	Name	Company		
	CoolSNAP HQ ICX285	Photometrics		
Light source	Name	Power		
	SPECTRA X	220 W		
Filter sets	Filter	Excitation [nm]	Emission [nm]	
	GFP	475/28	525/48	
	mCherry	575/25	625/45	
	DAPI	390/18	435/48	
	Alexa 594	575/25	625/45	
	FITC	575/25	625/45	

Microscope	**Name**	**Stand**	**Company**	
	DM6000B microscope system		Leica	
Objective	Name	Company	NA	Imm.
	20 x	Leica	0.70	dry
	63 x	Leica	1.40	oil
Camera	Name	Company		
	DFC 365FX	Leica		
Light source	Name	Power		
	EL6000	120 W		
Filter sets	Filter	Excitation [nm]	Emission [nm]	
	DAPI	350/50	455/50	
	FITC	490/20	525/36	
	TRITC	555/26	605/52	
	Cy5	645/30	705/72	

5 CHEMICAL SYNTHESIS

5.1 GENERAL REMARKS

Chemicals were purchased from Sigma-Aldrich, MCAT GmbH, Asta Tech Inc., novabiochem, abcr GmbH & Co. KG, acros Organics and used as received. Solvents for nuclear magnet resonance (NMR) were purchased from euriso-top SAS. Thin layer chromatography (TLC) was performed with polygram Sil G/UV 254 plates. Spots on TLC plates were visualized with a UV hand lamp (λ=254 nm or 366 nm wavelength) or stained with ninhydrin, vanillin or potassium permanganate staining solution followed by heat treatment.

NMR spectra were measured on a Varian Mercury Plus 300 MHz spectrometer or a Varian 500 MHz NMR System. Chemical shifts were reported relative to solvent peaks according to Fulmer et al. [126] High resolution (HR) mass spectrometry (MS) was performed on a Bruker microTOF-QII mass spectrometer using electron spray ionization (ESI). Flash chromatography (FC) was done using silica gel with a pore size of 60 Å and a particle size range of 40-63 µm. All compounds were characterized by NMR (^{1}H, ^{13}C) and HR-MS/MS (ESI). Purity was further determined by RP-HPLC analysis *via* reinjection of the purified compound and integration of the UV absorbance signal at λ=280 nm. Analytical RP-HPLC was done on an Agilent 1100 series HPLC system using Phenomenex Luna 3µ C18 reversed-phase columns with a solvent gradient of 10 - 60 % solvent B over 60 min (Solvent A: H2O containing 0.1% trifluoroacetic acid (TFA); Solvent B: MeCN containing 0.1% TFA).

5.2 SYNTHESIS OF COMPOUND 5 HA-PEG(7)-N_3

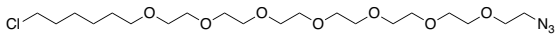

5

20-Azido-3,6,9,12,15,18-hexaoxaicosan-1-ole (411.53 mg, 1.17 mmol, 1.0 eq.) was dissolved in dry THF:DMF 7:1 (10 ml:1.5 ml, 0.1 M) at RT under Ar. The solution was cooled to 0° C in an ice water bath with constant stirring. NaH (93.6 mg, 2.34 mmol, 2.0 eq.) was added in small portions under constant Ar flow and stirring. Stirring continued at 0° C for 30 min before 1-chloro-6-iodohexane (266.6 µl, 1.76 mmol, 1.5 eq.) was added dropwise. The ice water bath was removed and the stirring was continued over night under Ar slowly warming to RT.

The NaH was quenched with ammonium chloride and the mixture was poured into water (40 ml). Sodium thiosulfate was added to reduce iodine and the mixture was extracted with EtOAc (3x 10 ml). The combined organic fractions were dried over magnesium sulfate and all volatile components were removed under reduced pressure. The crude product was purified *via* FC on silica gel (EtOAc) to yield 190.5 mg (35 %) of compound 5 as a yellow liquide.

^{1}H NMR (300 MHz, $CDCl_3$) δ 3.69 – 3.58 (m, 23H), 3.58 – 3.52 (m, 2H), 3.49 (t, J = 6.7 Hz, 2H), 3.42 (t, J = 6.6 Hz, 2H), 3.35 (t, J = 5.6, 4.6 Hz, 2H), 1.82 – 1.68 (m, 2H), 1.62 – 1.49 (m, 2H), 1.47 – 1.29 (m, 4H).

^{13}C NMR (75 MHz, $CDCl_3$) δ 71.18, 70.66, 70.63, 70.60, 70.57, 70.55, 70.54, 70.06, 69.99, 50.65, 45.00, 32.51, 29.42, 26.66, 25.38.

HR MS (ESI pso.) *m/z*: calculated for $C_{20}H_{40}ClN_3NaO_7^+$ $[M+Na]^+$: 492.2447, measured 492.2449.

5.3 SYNTHESIS OF COMPOUND 6 HA-PEG(7)-NH_2

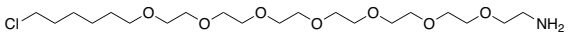

6

Compound 5 (190.5 mg, 405 µmol, 1.0 eq.) was dissolved in MeOH:EtOAc 5:1 (5 ml:1 ml, 0.07 M) at RT under Ar and stirring. A catalytic amount of Pd/C (42.9 mg, 40.5 µmol, 0.1 eq.) was added under constant Ar flow. H_2 was passed through the miture under constant stirring for 4 h at RT. The mixture was filtered through celite and volatile components were removed under reduced pressure. Compound 6 was obtained as a gray oil in a yield of 228.01 mg (>100 %, probably still containing solvent or Pd/C). Analytics were done from a previous batch.

^{1}H NMR (300 MHz, $CDCl_3$) δ 3.76 – 3.57 (m, 23H), 3.57 – 3.53 (m, 2H), 3.50 (t, J = 6.7 Hz, 2H), 3.42 (t, J = 6.6 Hz, 2H), 2.93 (t, J = 5.1 Hz, 1H), 1.82 – 1.67 (m, 2H), 1.64 – 1.50 (m, 2H), 1.49 – 1.27 (m, 4H).

^{13}C NMR (75 MHz, $CDCl_3$) δ 71.33, 71.17, 70.56, 70.54, 70.51, 70.50, 70.47, 70.39, 70.37, 70.36, 70.32, 70.25, 70.13, 70.07, 70.03, 45.01, 41.35, 32.51, 29.41, 26.66, 25.39.

MS (ESI pos.) *m/z*: calculated for $C_{20}H_{43}ClNO_7^+$ $[M+H]^+$: 444.2723, measured 444.3.

5.4 SYNTHESIS OF COMPOUND 7 HA-PEG(7)-PL-OH

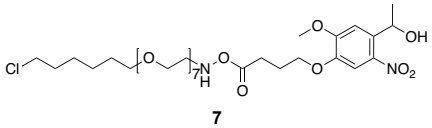

7

4-[4-(1-Hydroxyethyl)-2-methoxy-5- nitrophenoxy]butyric acid (80.9 mg, 270 µmol, 1.2 eq.) and PyBOP (140.5 mg, 270 µmol, 1.2 eq.) were

dissolved in dry DMF (2 ml, 0.14 M) under Ar in the dark and stirred for 2 h. Compound 6 (100 mg, 225 µmol, 1.0 eq.) was dissolved in dry DMF (2 ml, 0.11 M), supplemented with DIPEA (47 µl, 270 µmol, 1.2 eq.) and added dropwise to the mixture. Stirring continued over night at RT under Ar in the dark. The reaction mixture was poured into water (50 ml) and brine was added for better phase separation. Compound 7 was extracted with EtOAc (4x 20 ml). The cpmbined organic fractions were washed with brine supplemented water (30 ml) and dried over magnesium sulfate. All volatile components were removed under reduced pressure and a bronish yellow oil remained. Purification *via* FC on silica gel (DCM:MeOH 30:1 *v/v*) resulted in 130.2 mg (yield: 80 %) of a yellow oily residue.

^{1}H NMR (300 MHz, CD_3OD) δ 7.56 (s, 1H), 7.39 (s, 1H), 5.44 (q, J = 6.2 Hz, 1H), 4.07 (t, J = 6.2 Hz, 2H), 3.79 – 3.67 (m, 1H), 3.67 – 3.50 (m, 21H), 3.46 (t, J = 6.5 Hz, 2H), 3.41 – 3.32 (m, 7H), 3.22 (q, J = 7.3 Hz, 1H), 2.42 (t, J = 7.4 Hz, 2H), 2.16 – 2.06 (m, 2H), 1.79 – 1.70 (m, 2H), 1.62 – 1.52 (m, 2H), 1.46 (d, J = 6.3 Hz, 3H), 1.42 – 1.33 (m, 7H).

^{13}C NMR (75 MHz, CD_3OD) δ 173.77, 153.85, 146.64, 139.08, 137.43, 108.51, 108.41, 70.50, 69.83, 69.60, 69.48, 69.01, 68.10, 64.56, 54.20, 45.77, 45.71, 44.18, 42.17, 38.89, 38.77, 32.13, 31.83, 28.93, 26.12, 25.79, 25.68, 24.87, 24.84, 23.70, 17.11, 15.68, 11.56.

HR MS (ESI pos.) *m/z*: calculated for $C_{33}H_{57}ClN_2NaO13^+$ $[M+Na]^+$: 747.3441, measured 747.3435.

5.5 SYNTHESIS OF COMPOUND 8 HA-PEG(7)-PL-ACTIVATED

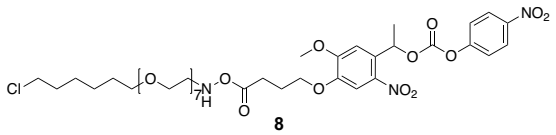

8

Compound 7 (130.2 mg, 179 µmol, 1.0 eq.) was dissolved in dry DCM (2 ml, 0.08 M). A solution of pyridine (36,2 µl, 447.5 µmol, 2.5 eq.) and 4-nitrophenyl chloroformiate (36.2 mg, 179 µmol, 1.0 eq.) in dry DCM (2 ml, 0.08 M) was added dropwise under constant stirring and Ar flow in the dark at RT. Stirring continued for 4 h before all volatile components were removed under reduced pressure. The crude product was purified *via* FC on silica gel (DCM, then DCM:MeOH 100:1, then 50:1, then 30:1 *v/v*) and yielded 94.58 mg (59 %) of a bright yellow oil.

^{1}H NMR (300 MHz, CD_3OD) δ = 8.28 – 8.20 (m, 2H), 7.58 (s, 1H), 7.44 – 7.37 (m, 2H), 7.19 (s, 1H), 6.39 (q, J=6.4, 1H), 4.09 (t, J=6.2, 2H), 3.97 (s, 3H), 3.61 – 3.57 (m, J=5.6, 22H), 3.56 – 3.50 (m, 6H), 3.44 (t, J=6.5, 2H), 3.36 (d, J=5.5, 2H), 2.40 (t, J=7.4, 2H), 2.15 – 2.05 (m, 2H), 1.78 – 1.68 (m, J=6.3, 5H), 1.60 – 1.50 (m, 2H), 1.49 – 1.35 (m, 4H).

^{13}C NMR (75 MHz, CD_3OD) δ = 173.73, 155.25, 154.00, 151.44, 147.59, 145.22, 139.80, 130.70, 124.67, 121.65, 108.41, 107.88, 73.17,

70.49, 69.81, 69.75, 69.70, 69.55, 69.42, 69.02, 68.09, 55.46, 44.15, 38.87, 32.09, 31.78, 31.73, 28.88, 26.09, 24.83, 24.73, 20.34.

HR MS (ESI pos.) *m/z*: calculated for $C_{40}H_{60}ClN_2NaO_{17}^+$ [M+Na]$^+$: 912..3503, measured 912.3469.

5.6 SYNTHESIS OF COMPOUND 9 HA-PEG(7)-PL-BG

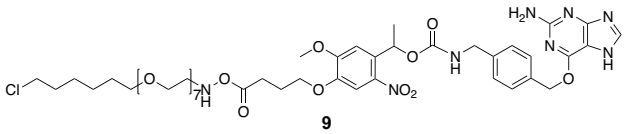

9
Ha-peg(7)-pl-BG

Compound 8 (94.58 mg, 106.2 µmol, 1.0 eq.) was dissolved in dry DMF (2 ml, 0.05 M) under Ar at RT. 6-((4-(Aminomethyl)benzyl)oxy)-9H-purin-2-amine (31.68 mg, 116.8 µmol, 1.1 eq.) and triethylamine (29,6 µl, 212.4 µmol, 2 eq.) were mixed in dry DMF (1.5 ml, 0.06 M) and the homogenous suspension was added dropwise to the solution of compound 8 and stirring continued over night at RT under Ar in the dark. All volatile components were removed under reduced pressure and the crude product was purified *via* FC on silica gel (DCM:MeOH 50:1 *v/v*). 35.93 mg (33 %) of a yellow oil were obtained from the pooled pure fractions (checked by TLC). Analytic RP-HPLC revealed 91 % purity (retention time = 25.43 min). The extinction coefficient at λ=280 nm of Ha-peg(7)-pl-BG (9) was assumed to be the same as for Ha-pl-BG (1) due to the same functional moieties: Ha-peg(7)-pl-BG$_{\varepsilon 280}$= 11.3 mM^{-1}cm^{-1}. Ha-peg(7)-pl-BG was dissolved in dry DMSO. A serial dilution was used to determine the concentration of this stock solution by measuring the absorption at λ=280 nm.

^{1}H NMR (500 MHz, CD_3OD) δ 7.85 (s, 1H), 7.61 (s, 1H), 7.44 (d, J = 8.1 Hz, 2H), 7.26 – 7.20 (m, 2H), 7.15 (s, 1H), 6.28 (q, J = 6.4 Hz, 1H), 5.57 – 5.46 (m, 2H), 4.32 – 4.15 (m, 2H), 4.08 (t, J = 6.2 Hz, 2H), 3.85 (s, 3H), 3.62 – 3.59 (m, 18H), 3.59 – 3.54 (m, 6H), 3.54 – 3.51 (m, 4H), 3.45 (t, J = 6.6 Hz, 2H), 3.37 (d, J = 5.4 Hz, 1H), 2.42 (t, J = 7.4 Hz, 2H), 2.11 (p, J = 6.7 Hz, 2H), 1.77 – 1.70 (m, 2H), 1.60 – 1.53 (m, 5H), 1.46 – 1.40 (m, 2H), 1.39 – 1.33 (m, 2H).

^{13}C NMR (126 MHz, CD_3OD) δ = 173.98, 160.24, 156.53, 154.23, 147.24, 139.59, 139.18, 135.52, 133.99, 128.22, 126.97, 108.82, 107.95, 70.73, 70.10, 70.09, 70.07, 70.04, 69.83, 69.72, 69.17, 68.60, 68.33, 67.22, 55.46, 44.33, 43.71, 39.03, 32.33, 32.06, 29.13, 26.32, 25.08, 25.04, 21.00.

HR MS (ESI pos.) *m/z*: calculated for $C_{47}H_{69}ClN_8NaO_{15}^+$ [M+Na]$^+$: 1043.4463, measured 1043.4434.

6 MOLECULAR CLONING

6.1 GENERAL REMARKS

Bacteria were cultured in selective LB medium for plasmid amplification and protein expression (see section 7.2). Antibiotics were dissolved in water (Ampicillin 100 mg/ml, Kanamycin 50 mg/ml) and stock solutions were stored at -20 °C. LB medium was freshly supplemented with antibiotics (final concentration Ampicillin 100 µg/ml, Kanamycin 50 µg/ml (30 µg/ml for low copy number plasmids). Plasmids were purchased from Addgene as agar stabs of transformed bacteria or provided by colleagues and collaboration partners as purified plasmids in water. pFC20A HaloTag T7 SP6 FlexiVector was purchased as lyophilized powder from Promega (Promega GmbH, Mannheim). Single stranded oligonucleotides (primer, see Appendix XY: Cloning Primer List) were purchased from IDT (Integrated DNA Technologies, BVBA, Leuven) with standard desalting purification. DNA modifying enzymes, buffer and master mixes were purchased from NEB (New England Biolabs GmbH, Frankfurt am Main). Linear DNA fragments were evaluated *via* agarose gel electrophoresis using SERVA DNA Stain Clear G (SERVA Electrophoresis GmbH, Heidelberg) supplemented agarose gels and visualization on a UV-Transilluminator (peqlab GmbH, Erlangen). DNA purification was done with kits purchased from Qiagen (QIAGEN GmbH, Hilden). Concentration and purity (A260/280) of eluated DNA was measured with a NanoDrop ND-1000 photo-spectrometer (peqlab). All generated plasmids were sent to Seqlab (Microsynth Seqlab, Göttingen) to check correct assembly of all ligation sites via Sanger sequencing using sequencing primers (see Appendix B.1.2) or standard sequencing primers provided by Seqlab.

6.2 PLASMID PREPARATION AND RESTRICTION DIGEST

Purified plasmids were transformed into chemocompetent *E. coli DH5α* *via* heat-shock transformation. 49 µl bacteria suspension were mixed with 1 µl plasmid solution (10-100 ng/µl in water) and incubated for 5 min on ice. Then the mixture was heated to 42 °C for 45 seconds in a waterbath and directly put back on ice for another 2 min. 1 ml prewarmed (ca. 37 °C) LB medium was added and the bacteria were incubated at 37 °C with 300 rpm shaking for 1 h. The bacteria were plated on selective LB-agar and incubated overnight at 37 °C. A single colony was picked and used to inoculate 10 ml selective LB medium

and grown over night at 37 °C, 150 rpm shaking. The overnight culture was used for preparation of glycerol stocks and plasmid purification using the QIAprep Spin Miniprep Kit. Glycerol stocks were made by mixing 500 µl of the bacteria suspension with 500 µl 80 % glycerol and kept at -80 °C for long term storage. Overnight cultures for plasmid purification were innoculated directly from the glycerol stocks if available.

Enzymes and buffers for restriction digests were used according to the manufacturers instruction. In case the small fragment was $\leq$ 50 bp, the linearized plasmid was prurified using the QIAquick PCR Purification Kit. Otherwise the large fragment was purified *via* gelextraction using the QIAquick Gel Extraction Kit.

6.3 POLYMERASE CHAIN REACTION

PCRs were set up using Q-5 High Fidelity 2X Master Mix following the manufacturers instructions. Annealing temperatures were calculated using the online tool NEB Tm Calculator (v1.9.13). Elongation times were adjusted according to the expected fragment length and the polymerase fidelity. If the recommended annealing temperature was 72 °C, the PCR protocol was set up as a 2-step protocol combining annealing and elongation as one step with a reaction time of the calculated elongation time plus 10 seconds. After PCR the reaction mix was supplemented with DpnI and incubated overnight to degrade template plasmids. PCR fragments were purified using the QIAquick PCR Purification Kit or *via* gelextraction using the QIAquick Gel Extraction Kit in case of side product formation.

6.4 GIBSON ASSEMBLY, TRANSFORMATION AND PLASMID PURIFICATION

All plasmids were produced *via* restriction site independent cloning according to Gibson et al. [127](so called Gibson Assembly) using the Gibson Assembly 2X Master Mix following the manufacturers protocol. 1 µl of the assembly mix was added to 49 µl suspension of electrocompetent *E. coli DH5α* on ice. The mixture was transferred into a prechilled 1 mm electroporation cuvette and shocked with 200 Ω, 25 µFd and a pulse of 1.8 kV/cm using a Gene Pulser Xcell electroporator (BioRad). The cells were immediately provided with 1 ml prewarmed LB medium and incubated for 1 h before they were plated on selective LB agar plates and incubated overnight at 37 °C. The next day, single colonies were picked for amplification in selective LB medium and plasmid purification as described in 4.2. Plasmids verified for the correct sequence were re-transformed into chemocompetent *E. coli DH5α* for plasmid preparation using the HiSpeed Plasmid Kit following the manufacturers instructions.

7 PROTEIN EXPRESSION AND PROCESSING

7.1 GENERAL REMARKS

EC12 proteins were expressed with an N-terminal 6xHis tag followed by a modified TEV-cleavage site for affinity based purification and subsequent proteolytic processing to obtain the correct N-terminus. Protein concentrations were measured with a NanoDrop ND-1000 photo-spectrometer (peqlab). Purification and processing were evaluated via SDS-PAGE and Western blot analysis (detailed protocol see section 8.1 and 8.2). The Äkta HPLC system and IMAC columns were washed and kept under 20 % ethanol after purifications.

7.2 PROTEIN EXPRESSION

Plasmids pNB01 and pNB02 were transformed into *E. coli KRX* (Promega, Mannheim) via the heat-shock protocol described in section 6.2. 10 ml selective LB medium was inoculated as starter culture with a single colony picked from a selective LB agar plate or directly from a glycerol stock and incubated overnight at 37 °C with rigorous shaking. The starter culture was used to inoculate a 1 l expression culture of selective LB medium. The expression culture was incubated at 37 °C with rigorous shaking until it reached an OD_{600} of 0.8-1 and then supplemented with 0.1 % w/v rhamnose to induce protein expression in KRX cells. The bacteria suspension was cultivated for additional 4 h under the before mentioned conditions. The expression culture was cooled to 0-4 °C on ice and pelleted by centrifugation with 6400 rcf for 10 min at 4 °C. The supernatant was discarded and the pellet was stored at -80 °C or kept on ice to proceed directly with protein purification.

7.3 PROTEIN PURIFICATION

The pellet from the protein expression culture was resuspended in 20 ml pre-chilled lysis buffer (Buffer A supplemented with 0.1 M PMSF protease inhibitor). The bacteria were ruptured with ultrasound using an Omni Ruptor 400 sonicator with 40 % power and pulser of 50 for 10 min on ice. The lysate was centrifuged with 174200 rcf for 30 min at 4 °C. The supernatant was carefully decanted and filtered through a 0.45 µm cellulose filter.

The cleared supernatant was loaded onto a 5 ml IMAC column (HisTrap, GE Healthcare) using the fully automated Äkta HPLC sys-

tem (Äkta pure 25 M) equipped with a 50 ml superloop, UV-Vis detector and fraction collector, operated with UNICORN Control Software v.6.3 (GE Healthcare). The purification was performed at a constant flow rate of 3 ml/min with buffer A (loading buffer) and buffer B (elution buffer) as mobile phase in different mix ratios. Before loading, the column was equilibrated with 4 column volumes (CV) buffer A. After loading the cleared supernatant, impurities were washed out with 5 CV buffer A. The liquid phase was changed to 20 % v/v buffer B in buffer A for 8 CV to wash out unspecifically bound proteins before running a gradient from 50 % to 100 % v/v buffer B in buffer A over 5 CV to elute the His tag bound protein. During the elution step, automated peak fractioning according to the slope change of the absorption value at λ=280 nm was activated. The column was washed with 6 CV buffer B and equilibrated with 6 CV buffer A for the next run.

The collected fractions were pooled and the buffer was exchanged to TEV buffer using Amicon Ultra-15 Centrifugal Filter tubes with a molecular cut off of 10 kDa (Merck Milipore). Therefore, the protein solution was reduced to ca. 200 µl and washed with 10 ml TEV buffer for three times. Finally, the protein was concentrated to 120 µM in TEV buffer.

7.4 TEV PROTEASE PROCESSING AND RE-PURIFICATION

To achieve the correct N-terminus of EC12 proteins the His tag was removed proteolytic treatment with TEV protease according to a protocol adapted from Ritterson et al.[128]. 1 µg of the purified EC12-GFP-Halo protein was diluted in 150 µl TEV buffer and 50 µl TEV protease (10 U/µl, invitrogen) was added. The reaction mixture was split in two fractions and incubated for 72 h at 4 °C (fraction 1) or RT (fraction 2). To remove the processed His tag and the protease (also carrying a His Tag) samples were purified using the Äkta HPLC system equipped with a 500 ml sample loop and a 1 ml IMAC column (both GE Healthcare) operated with a constant flow rate of 1 ml/min. The column was equilibrated with 5 CV buffer A to obtain a stable baseline signal for the absorption at λ=280 nm. When the sample was loaded onto the column, the flow through was collected manually until the absorption at λ=280 nm reached the baseline intensity again. The column was washed with additional 5 CV buffer A before running a gradient from 50 % to 100 % v/v buffer B in buffer A over 5 CV to elute the processed His tag and the protease. The eluate was collected manually. The column was washed with additional 5 CV buffer B and equilibrated with buffer A. The collected flow through was concentrated with Amicon 0.5 Centrifugal Filter tubes (Merck-Millipore) with a molecular cut off of 10 kDa and the

eluate was concentrated with the Amicon Ultra-15 Centrifugal Filter tubes.

In a second approach 200 µg purified EC12-GFP-Halo protein was incubated with 10 µl TEV protease at RT (sample 1) or 16 °C (sample 2) in a total volume of 40 µl. Additionally two samples were prepared according to the manufacturers protocol with 200 µg protein and 10 µl TEV protease in 1.5 ml TEV buffer (prepared from 20x TEV buffer (invitrogen) supplemented with 1 mM DTT) and also incubated at RT (sample 3) or on ice (sample 4). All samples were incubated for 72 h.

Ni-NTA-His-Bind Resin (Novagen) was used to remove the protease, cleaved His-tag and undigested protein from the samples. 100 µl resin was added to the digestion mix and incubated at 4 °C with constant agitation for 30 min. The resin was spun down for 30 seconds with 15 000 g and the supernatant containing the processed protein was removed carefully. The resin was washed 3x with 200 µl TEV buffer and then incubated with elution buffer B for 5 min at RT. The supernatant was removed carefully after pelleting the resin via centrifugation at 15 000 g for 30 seconds.

7.5 DIMERIZER TREATMENT OF EC12 PROTEINS

The processed and re-purified EC12 proteins were pre-incubated with an excess of Ha-BG or Ha-peg(7)-pl-BG and washed afterwards to achieve optimal dimerizer binding efficiency. The amount and volumes were adjusted to the yield of the respective processed protein batch. In detail, 1.4 nmol EC12-GFP-Halo (45 µl, 2.67 µg/µl) were incubated with 2.5 nmol Ha-BG (0.5 µl, 5 mM) for 15 min at RT. The proteins were washed 3x with 200 µl PBS using Amicon 0.5, 10 kDa tubes and finally concentrated to a 50 µM stock solution in 25 µl PBS. For Ha-peg(7)-pl-BG decorated EC12-GFP-Halo 0.6 nmol processed protein (60 µl, 9.5 µM) was mixed with 1 nmol of the dimerizer, incubated and washed as described above and finally concentrated to a 10 µM stock solution in 50 µl PBS.

The dimerizer decorated EC12 proteins were kept at 4 °C for maximum 24 h before using them in live cell experiments.

8 BIOCHEMICAL ANALYSIS

8.1 SDS-PAGE

Cells grown to 80-90 % confluence were washed twice with PBS, put on ice, submerged with prechilled RIPA lysis buffer supplemented with 0.5 mM EDTA and 1 % (v/v) Halt Protease and Phosphatase Inhibitor cocktail (all ThermoFisherScientific) and kept overnight at -80 °C. The lysate was defrosted on ice and collected with a cell scraper. Cell debris was pelleted via centrifugation at 4 °C with 14 000 rpm for 30 min, the supernatant was removed carefully and stored at -20 °C or used directly for SDS-PAGE analysis.

For qualitative analysis of purified proteins from bacterial expression or processing steps, samples were concentrated using Amicon 0.5 Centrifugal Filter tubes or diluted in their respective buffer to achieve comparable amounts of protein per samples (maximum 4 µg/sample).

Samples were mixed with self made SDS sample buffer (5:1 v/v) or 4x NuPAGE LDS Sample Buffer and 10x Sample Reducing Agent (13:5:2 v/v, ThermoFisherScientific) and denatured for 10 min at 95 °C. The samples and Novex Sharp Pre-stained Protein Standard (ThermoFisherScientific) were loaded onto a Novex 4-12 % Bis-Tris PAGE gel (ThermoFisherScientific) mounted in the XCell SureLock Mini-Cell SDS-Electrophorese system equipped with a PowerEase 90 W power supply and filled with MOPS SDS Running buffer (ThermoFisherScientific). Electrophoresis was done with constant voltage (200 V const., max. 120 mA) for 40-90 min according to the molecular weight of the target protein.

After electrophoresis PAGE gels were used for Western blot (see section 8.2) or stained with coomassie blue. The later was done by briefly boiling the gel in comassie blue solution, rinsing 2x with water and shaking the gel in comassie destaining solution over night. Images of Comassie stained gels were taken using a Amersham Imager 600RGB (GE Healthcare) with with white light epi illimination.

8.2 WESTERN BLOT AND IMMUNOCHEMILUMINESCENCE DETECTION

Following SDS-PAGE proteins were transferred from the gel onto a methanol activated nitrocellulose membrane (ThermoFisherScientific) using the XCell SureLock Mini-Cell equipped with a XCell Blot Module mounted according to the manufacturers recommendations. Blot-

ting was performed as wet blot in NuPAGE Transfer Buffer supplemented with 10 % (v/v) methanol with constant voltage (30 V const., maximum 220 mA) for 1 h. Successful transfer was validated via transiently staining the membrane with Ponceau Red solution.

To avoid unspecific antibody binding, the membrane was blocked with 3 % BSA in TBS-T (w/v) for minimum 1 h at RT. Primary antibodies (see table 4.3.1) were diluted 1:1000 - 1:5000 (v/v) according to the manufacturers recommendations in TBS-T with 1 % BSA (w/v) and incubated on the membrane overnight at 4 °C. The antibody solution was recovered and kept at -20 °C for later reuse and the membrane was washed 3x for 10 min with TBS-T at RT. HRP-coupled secondary antibodies were diluted 1:5000 (v/v) in TBS-T with 1 % BSA (w/v) and incubated on the membrane for 1 h at RT. Excess secondary antibodies were removed via 3x washing for 10 min with TBS-T at RT before incubating the membrane with ECL solution (GE Healthcare). The chemiluminescent signal was recorded using an Amersham Imager 600RGB in chemiluminescence mode with semiautomated exposure time.

8.3 IMMUNOFLUORESCENCE STAINING

Cells cultivated on round glass cover slips (∅ 12 mm, #1, Menzel) were washed twice with phenol red-free DMEM without supplements and fixed by perfusion with 4 % paraformaldehyde (PFA) and incubation for 20 min at RT. Fixed cells were washed twice with PBS and kept in PBS supplemented with 1 % PenStrep at 4 °C protected from light or used directly for indirect immunofluorescence staining. Therefore, fixed cells were permeabilized by incubation with 0.1 % Triton X-100 in PBS for 5 min at RT, blocked with 1 % BSA in PBS for 1 h and incubated with the primary antibody in 1 % BSA in PBS overnight at 4 °C. The next day, cells were washed three times for 10 min with 1 % BSA in PBS before adding the secondary antibody and optional with a fluorophore coupled phalloidin. After washing three times for 10 min, samples were mounted in Mowiol. If no Alexa 350 or Alexa 405 conjugated antibody was used, 1 % DAPI was added to the Mowiol before mounting the cells.

Images were taken with a Leica DM6000B upright fluorescent microscope equipped with a CCD camera (Leica DFC365 FX) and a 63x oil objective (HC PL APO, NA 1.4).

8.4 BEAD AGGREGATION ASSAY

To confirm functionality of recombinant expressed EC12-GFP-Halo the protein was immobilized on magnetic beads do perform a bead aggregation assay. 150 µl suspension of Halo ligand functionalized beads (Magne HaloTag Beads, Promega) were washed twice with 200

µl PBS and then incubated with 100 µl processed EC12-GFP-Halo (final concentration 0.46 µg/µl) for 1 h at RT with 800 rpm shaking. Fractions of the protein solution were taken before and after incubation with the beads and analyzed via SDS-PAGE.

The EC12-GFP-Halo loaded beads were diluted in 1000 µl TB buffer and split in two fraction. One sample was supplemented with 2 mM Ca^{2+} by adding 1 µl $CaCl_2$ stock solution (1 M), the other served as Ca^{2+} free control. Both samples we incubated for 1 h at RT with 800 rpm shaking then carefully transferred in a chambered coverslip (Nunc, ThermoFisher Scientific) and analyzed microscopically.

9 LIVE CELL IMAGING

9.1 CELL LINES AND CULTURE CONDITIONS

A431, BT549, MDA-MB 231, MCF-7 and MDCK.2 cells were purchased from atcc. A431 α-catenin KO cells were a kind gift from Takuya Kato (Francis Crick Institute, London). A431D and MDCK E-cadherin KO cells were provided from René-Marc Mège (Université Paris Diderot & CNRS, Paris). COS7 cells were a courtesy from Ulrike Engel (University of Heidelberg, Heidelberg)

All cells were maintained in growth medium consisting of Dulbecco's modified Eagle's medium (DMEM), high glucose supplemented with GlutaMAX, sodium pyruvate, 10 % fetal bovine serum (FBS) and 1 % penicillin–streptomycin, at 37 °C with humidified 5 % CO_2 atmosphere. Stable transfected cells were maintained in selection medium (DMEM, high glucose supplemented with GlutaMAX, sodium pyruvate, 10 % FBS and 750 µg/ml active Geneticin). Medium was exchanged every two to three days.

Cells were passaged by washing twice with PBS (Ca^{2+} and Mg^{2+} free), incubated for 5-10 min with 0.25 % trypsin-EDTA (ThemoFisherScientific) and resuspended in full medium in the desired density in a new flask. For experiments cells were counted with a Neubauer Haematometer or a Countess II FL Automated Cell Counter (ThemoFisherScientific) according to the manufacturers instructions. The cells were pelleted, resuspended in an appropriate volume of growth medium and seeded in the desired vessel. For Western blot analysis cells were seeded in 6 well plates ($2*10^5$ -10^6 cells per well according to the cell type). For indirect immunofluorescence staining cells were seeded on glass cover slips (∅ 12 mm, #1, Menzel) in a 6 well plate (4-5 cover slips per well, cell density as for western blot). For live cell experiments, cells were seeded on glass bottom petri dishes ((#1.5 cover slip, ibid, Martinsried), 8 well chambered cover glass (nunc Lab-Tek, ThermoFisherScientific) or in µ-channel slides (µ-Slide VI $^{0.4}$, ibidi) and incubated over night under standard conditions before performing the actual experimental procedure.

9.2 TRANSFECTION METHODS

9.2.1 *Non-liposomal transfection reagent*

Cells were seeded in 8 well chambered cover slips ($5*10^4$ cells per well) or µ-channel slides ($3*10^4$ cells per channel) and incubated over

night to reach 60-70 % confluency. The transfection mixture was prepared according to the manufacturers protocol by diluting a total amount of 200 ng plasmid DNA in 10 µl Opti-MEM (ThermoFisher-Scientific), adding another 10 µl Opti-MEM supplemented with 0.8 µl PromoFectin transfection reagent (PromoCell, Heidelberg) and gentle flipping. The mixture was added drop wise to a well or injected into a µ-channel. Cells were incubated over night under standard conditions.

9.2.2 *Electroporation*

Electroporation was performed using the Amaxa Nucleofector I Device (Lonza, Cologne). A431 α-catenin KO and A431D cells were transfected with Amaxa Cell line Nucleofector Kit T (program X-01; Lonza), MDCK.2 and MDCK E-Cadherin KO cells were transfected with Amaxa Cell line Nucleofector Kit L (program A-24; Lonza) following the manufacturers protocol. In brief, 10^6 cells were resuspended in 100 µl nucleofection solution with supplement, 2 µg plasmid DNA was added and the mixture was transferred into an electroporation cuvette (4 mm slit, provided in the kit). After the pulse, 500 µl prewarmed growth medium was added and the cells were injected directly into a µ-channel or transferred into a well of a 6 well plate containing 1 ml growth medium for antibiotic selection.

9.3 GENERATION OF STABLE CELL LINES

Cells transfected with plasmids carrying a neomycin selection marker ($neoR^+$) for expression in mammalian cells, were incubated in selection medium containing geneticin from one day after transfection. Antibiotic selection was done until all cells of a geneticin sensitive control sample died (usually 10-14 days). In case of morphological changes (e.g. less diffraction in phase contrast mode due to increased cell-cell adhesion) selected cell colonies were carefully detached with accutase (ThermoFisherScientific) picked with a micropipette, resuspended in growth medium and transferred into separated wells of a 12 well plate. The cells were incubated under standard conditions to form new colonies and the procedure was repeated 3-4 times until all colonies showed the desired phenotype.

9.4 FLUORESCENCE ACTIVATED CELL SORTING

In case transfected cells did not change their morphology or high expression levels were intended, antibiotic selected cells were sorted via fluorescence activated cell sorting (FACS) using a BD FACSAria III with 4 lasers (407/488/561/633), 11 colors (3-2-4-2) configuration (BD Biosciences, Heidelberg; performed in the ZMBH Flow Cytometry &

FACS Core Facility) or a BD FACS Melody with 3 laser (488/561/640), 8 colors (2-2-4) configuration.

After trypsinization, cells were resuspended in FACS buffer to a maximum number of $3*10^6$ and sorted into a 6 well plate containing 2 ml growth medium per well or into FCAS tubes containing 1 ml growth medium. Sorting was performed in purity mode selecting for high expression of the respective fluorescent marker protein. Cells sorted into plates were allowed to settle down for 2-3 h before exchanging the medium. Cells sorted into FACS tubes were washed with growth medium and seeded directly for live cell experiments or transferred into a cell culture flask.

9.5 LIVE CELL LABELING AND IMAGING

Transiently transfected or stable cells seeded for live cell imaging experiments were kept in imaging medium (FluoroBrite DMEM, high glucose supplemented with GlutaMAX, sodium pyruvate, 10 % FBS and 1 % penicillin–streptomycin or 750 µg/ml active geneticin) at 37 °C with humidified 5 % CO2 atmosphere during all live cell imaging experiments.

Cells were imaged with a Leica DMi8 inverted fluorescent wide-field microscope equipped with a X-Cite 200DC light source (200 W), a sCMOS camera (Leica DFC9000GT) using either 10x objective (HC PL FLUOTAR, NA 0.32, PH1) or 63x objective (HC PL APO CS2, NA 1.40 OIL UV) or a DeltaVision Elite system installed on an Olympus IX inverted fluorescence wide-field microscope equipped with a SPECTRA X light engine, a cooled CCD camera (CoolSNAP HQ/ICX285) and a custom built CO_2 and temperature controlled incubator using either a 10x objective (Zeiss 10X/0.30), a 20x objective (Zeiss 20 X/0.50) or a 60x objective (Olympus 60X/1.40).

For live cell labelling of self-labelling tags the cells were incubated for 30-60 min with the respective ligand coupled fluorophore (see table 9.1) diluted 1:1000 from the respective DMSO stock, washed three times with growth medium, incubated for 30 min and washed three times with imaging medium. Actin staining in living cells was done via incubation with 1 mM SiR-actin (SpiroChrom, Stein am Rhein) for minimum 1 h. The cells were washed with imaging medium directly before transferring them to the microscope.

Table 9.1: ligand coupled fluorophores. Self made * = provided by Wombacher's Lab

Name	Binding tag	Fluorophore	Cat. No	Company
SNAP-Oregon-Green	SNAP	Oregon-Green	S9104S	NEB
SNAP-Surface 488	SNAP	Atto 488	S9124S	NEB
Ha-diAcFl	Halo	Fluorescein	self made *	
Ha-TMR	Halo	Tetramethyl-rodhamine	self made *	

9.6 EXTRACELLULAR E-CADHERIN COMPLEMENTATION

In a µ-channel slide A431D cells stably expressing SNAP-E-cadherin345-mCherry were incubated with Ha-peg(7)-pl-BG bound EC12-EGFP-Halo protein (also see chapter 7) diluted in imaging medium in concentrations of 1 µM, 500 nM, 50 nM and 5 nM and non-transfected A431D cells were incubated with 1 µM Ha-peg(7)-pl-BG bound EC12 protein. After 2 h the protein solution was removed and the cells were washed with imaging medium. After re-administration of the protein solutions, cells were incubated over night. The next day, the cells were imaged 1 h after washing with imaging medium.

9.7 CHARACTERIZATION OF INTRACELLULAR DIMERIZATION AND PHOTOCLEAVAGE

9.7.1 *Dimerization conditions*

Dimerizers were diluted in imaging at least 1:1000 from the respective DMSO stock. Cells were washed with imaging medium before adding the dimerizer solution. To test the optimal conditions for intracellular chemically induced dimerization, A431D cells transiently transfected with Halo-GFP-Mito+ mCherry-SNAPf or Halo-GFP-Mito+mCherry-DHFR via electroporation (see section 9.2.2) were incubated with the respective dimerizer in different concentrations with and without washing in a µ-channel slide. For details about concentrations and incubation times of the various dimerizers please refer to tables listed in section 10.3.2. Dimerization efficiency was evaluated according to the sequestration of mCherry protein on the mitochondria via fluorescence live cell microscopy using the DeltaVision microscope system.

For reconstitution of AJs in cells stably expressing Ec-GFP-Halo and SNAP-mCherry-α(280-906) 200 nM Ha-pl-BG or 40 nM for Ha-BG were used, respectively.

9.7.2 *Photocleavage in the whole field of view*

To define minimal light intensities for efficient cleavage of the dimerizer, cells A431D cells transiently transfected with Halo-GFP-Mito+ mCherry-SNAPf were incubated with 200 nM Ha-pl-BG for 6 h in a µ-channel slide. Using the DMi8 microscope system with the 63x objective, cells that showed efficient sequestration of mCherry protein at the mitochondria were exposed to repetitive 20 ms pulses of near UV light (DAPI filter λ=350/50, 100 % intensity). Images were taken between each pulse in green and red fluorescence channel to follow the signal distribution of the GFP and mCherry proteins. Exposure conditions that lead to an efficient release of mCherry protein from the mitochondria were tested on cells treated with 40 nM Ha-BG to validate stability of the protein complexes induced with the non-cleavable dimerizer and general photo-toxic effects under these conditions.

Cells stably expressing Ec-GFP-Halo and SNAP-mCherry-α(280-906) treated with Ha-pl-BG were exposed to 4x20 ms near UV light with the before mentioned parameters to dissolve AJs.

9.7.3 *Photocleavage in defined pattern*

Cleaving dimerizer in defined pattern was done using the DMi8 microscope system equipped with a 405 nm laser (40 mW) in a Leica Infinity Scanner FS and QSP-T filter cube.

For cleaving with subcellular precision, the 63x objective and ND 100 % was used. Intensities were tested as desired above for photocleavage in the whole field of view by stepwise decreasing the spot size or increasing laser power, scan speed and the number of iterations. Dissociation of AJs in defined subcellular regions in A431 α-catenin KO cells stably expressing Ec-GFP-Halo and SNAP-mCherry-α(280-906) treated with Ha-pl-BG was performed with 10 % laser power, scan speed 10, spot size 0.68 µm and 20 iterations.

The 10x objective and ND 100 % was used to cleave the dimerizer in defined subregions of a cellular monolayer. A431 α-catenin KO cells with Ha-pl-BG reconstituted AJs were scanned with increasing laser power, scan speed and the number of iterations or decreasing spot size. Efficient cleavage of the dimerizer was determined indirectly via morphological changes of the targeted cell, which is increased diffraction in Phase contrast mode due to dissociation of the AJs. A431 α-catenin KO cells with Ha-BG reconstituted AJs were used to confirm

that the morphological changes were not induced by phototoxic or unspecific cellular stress reactions.

In collective migration and traction force microscopy experiments 50 % laser power, scan speed 10, spot size 1.54 µm and 20 iterations were used. The parameters were validated for each experimental setup with changes in the optical path (e.g. cells in glass coverslip or on hydrogels).

9.8 COLLECTIVE MIGRATION ANALYSIS

9.8.1 *Experimental procedure*

One well silicone culture-inserts (ibidi, cut 2 well inlet, growth area 0.22 cm^2) were placed in a glass bottom culture dish (#1.5 coverslip, ibidi). 4 x 10^4 cells were seeded in 80 µl growth medium and incubated overnight in standard culture conditions. The growth medium in the inlet was replaced with growth medium containing the dimerizer and incubated for 4 - 6 h. The inlet was removed and cells were carefully washed with phenol red-free DMEM and the dish was finally filled with imaging medium with or without the dimerizer. Phase contrast images were taken with the Leica DMi8 microscope using the 10x objective 2x2 binning in 5 min intervals starting 1 h after removing the inlet.

9.8.2 *Data analysis*

Displacement vectors of moving cells between two consecutive phase contrast images were calculate using a custom-made PIV algorithm.[129–131] In brief, the images were drift corrected using cell free areas as reference for image alignment. The signal-to-noise ratio set to 1.3 and threshold for normalized mean to 2.0. If necessary the two values were adjusted according to the image quality. An absolute displacement cut off was set that was four times higher as the extrapolated mean displacement to reduce high noise peaks. The image pairs were subdivided into 32x32 pixel interrogation windows with 50 % overlap for displacement comparison. Displacement vectors were calculated for the whole field with a nodal distance of 16 pixel (equals 20.7 µm grid space) using cubic splines based interpolation. Displacement vector fields were displayed in pixel values (setting microns per pixel value to 1.0).

The correlation length of the lateral velocity displacement vectors were then calculated using a custom-made MatLab script as described by Das et al.[123] with modifications for analysis of continuous time lapse recordings. Displacement vectors were divided by the time difference between two successive frames to convert them into velocity vectors. Velocity vectors r_{ij} were allocated to the central coordinates

Table 9.2: Gel mixtures for TFM measurements [µl]

Young´s Modulus [kPa]	0.2	6
PBS	450.25	386.53
Acrylamide 40%	37.5	93.72
Bis-acrylamide 2%	7.5	15
Beads	2	2
APS 10%	2.5	2.5
TEMED	0.25	0.25

(i, j) of each 16x16 pixel window. Each vector consist of a lateral component (U_{ij}, along the migration front e.g. perpendicular to the dominant direction of cell migration) and an axial component (V_{ij}, perpendicular to the migration front). The fluctuations along and perpendicular to the migration front (u_{ij}, v_{ij}) were calculated as:

$$u_{ij} = U_{ij} - \sum_{i=1,m} \sum_{j=1,n} U_{ij}/(m \times n) = U_{ij} - U_{mean} \tag{9.1}$$

$$v_{ij} = V_{ij} - \sum_{i=1,m} \sum_{j=1,n} V_{ij}/(m \times n) = V_{ij} - V_{mean} \tag{9.2}$$

With U_{mean} and V_{mean} being the mean velocities along and perpendicular to the migration front. Since axial migration perpendicular to the migration front is intrinsically highly correlated in the chosen experimental setup, only the lateral velocity correlation function was calculated as:

$$C_r = \frac{\langle u(r´) \times u(r´ + r) \rangle_{r´}}{\sqrt{\langle u(r´)^2 \rangle \times \langle u(r´ + r)^2 \rangle}} \tag{9.3}$$

with $\langle \ldots \rangle$ being the average and r being the norm of r_{ij}, which is $r = \| r_{ij} \|$. The lateral correlation diameter was defined as the point where the lateral correlation function (3) reaches the lower threshold of 0.01.

9.9 TRACTION FORCE MICROSCOPY

9.9.1 *Preparation of gels*

Preparation of gels for traction force microscopy (TFM) was done as described previously [132, 133]. In brief, glass bottom dishes (#0 coverslips, Cellvis) were incubated for 15 min with 7.14 % 3-(trimethoxysilyl)propyl methacrylate (Sigma) and 7.14% acetic acid diluted in ethanol (v/v/v). The surfaces were washed twice with ethanol and dried carefully.

Polyacrylamide (PAA) gels containing dark red fluorescent carboxylated polystyrene beads were casted on methacrylate activated surfaces. For imaging of cell monolayer migration 0.5 µm beads (Fluoresbrite 641, Polysciences) were used, whereas TFM experiments of small cell clusters were performed on gels containing 0.2 µm beads (FluoSpheres (660/680), ThermoFisherScientific). In order to achieve different stiffnesses of the gel mixtures were prepared as shown in table 9.2 resulting in 3% acrylamide with 0.03% bis-acrylamide in PBS for 0.2 kPa gels and 7.5% acrylamide with 0.06% bis-acrylamide in PBS for 6 kPa gels with 0.05% ammonium persulfate (APS) as radical starter and a catalytic amount of N,N,N´,N´-tetramethylethylenediamine (TEMED). 22 µl of the mixture were placed on an activated surface and covered with an 18 mm round coverslip to generate a flat surface. The gel was polymerized for 1 h at RT and then submerged with PBS for 30 min before lifting the coverslip with a scalpel.

The gel surfaces were coated with collagen type I (from rat tail, Millipore) to facilitate cell adhesion. 75 µl of a 2 µg/µl solution of the photoreactive cross-linker sulphosuccinimidyl-6-(4´-azido-2´-nitrophenylamino) hexanoate (Sulfo-SANPAH, ThermoFisherScientific) in water was added onto the gel and activated by exposure to UV light (λ= 365 nm, 15 W, 3 cm distance). The gel was washed twice with 10 mM HEPES buffer for 3 min on the orbital shaker, covered with 500 µl of a collagen type I solution (100 µg/ml in PBS) and incubated over night at 4 °C.

9.9.2 *Experimantal procedure*

The collagen coated gels were washed vigorously with PBS. One well silicone culture-inserts that had been submerged with 1 % (w/v) BSA in PBS for 30 min were placed carefully in the center of a gel. As described for collective migration analysis, 4 x 10^4 cells were seeded in 80 µl growth medium and incubated in standard culture conditions until cells attached to the surface. The dimerizers were added and incubated for 6-8 h or overnight to allow the cells to form an intact monolayer. 1 h prior to imaging, the inlet was removed and the cells were washed with phenol red free medium before adding the respective dimerizer dissolved in imaging medium.

The migrating cellular monolayer was imaged in phase contrast mode and the position of the beads underneath the surface of the gel was recorded in fluorescent mode using the relative focus control of the DMi8 microscope equipped with the 10x objective and the 405 nm laser. Images were taken with 2x2 binning in 5 min intervals for 2-4 h before cleaving the dimerizer in defined regions of the monolayer as described in section 9.7.3. Image recording continued for another 2-4 h before trypsinizing the cells and taking reference images of the position of the beads in the relaxed gel.

9.9.3 *Data analysis*

Displacement of the beads was calculated using the custom-made PIV algorithm already presented for collective cell migration analysis (section 9.8.2), but comparing each image of the time lapse series with the reference image. Additionaly to the parameters described in section 9.8.2 the Young´s modulus of the respective gel was entered and the Poisson´s ratio was set to 0.5. For TFM analysis the actual pixel size of 1.295 µm per pixel was used to calculate displacement vectors in a grid space of 20.7 µm. Traction forces were reconstructed from these vectors via regularized Fourier Transform Traction Cytometry[134] with a regularization parameter chosen by Generalized Cross Validation [135] that was kept constant for all frames of one time lapse recording. For TFM analysis of migrating monolayers padding was set to 1.0 to circumvent edge problems (i.e. the recorded field of view was mirrored in all directions along the edge of the image). In case of small cell clusters a Tukey $\alpha$was used instead and adjusted to reduce the influence of cell free areas whithout effecting areas where the gel was deformed by the cells.

Part III

RESULTS AND DISCUSSION

10 TOOL DEVELOPMENT

10.1 HALO AND SNAP TAGGED TARGET PROTEINS CAN BE DIMERIZED INSIDE LIVING CELLS

Since the goal was the reconstitution of mechanotransductive protein complexes, the first aim was to achieve mechanically stable protein-protein interaction that are interlinked in a covalent-covalent manner. Motivated by the previous results using Halo and DHFR tagged proteins and data presented by the Wymann lab[55, 56] the first attempt was to increase the length of the peg linker between the chlorhexane and benzylguanin moieties. Erhardt *et al.* could double the dimerization rate of intracellular SNAP and Halo tagged proteins *via* extending the linker by one ethylene glycol (EG) and one CH_2-CH_2 bond[55]. The photocleavable dimerizer presented by Zimmermann *et al.* is highly similar to Ha-pl-BG, but has a linker that is three ethylene glycol units longer[56]. Therefore, the photocleavable dimerizer Ha-peg(7)-pl-BG was synthesized in a 5 step reaction as described in figure10.1. 20-Azido-3,6,9,12,15,18-hexaoxaicosan-1-ole was coupled to 6-chloro-1-iodohexane to form compound 5 and the azide group was hydrolyzed to obtain compound 6. The terminal amino group of compound 6 was then connected to the terminal carboxyl group of the O-nitrobenzyl linker in a standard peptide coupling reaction to yield compound 7. The amino-methyl functionalized benzylguanine was then coupled under basic conditions to the hydroxy group of compound 7 *via* the carbamate activated carboxylic acid ester intermediate 8. Analysis *via* HR-MS, NMR and RP-HPLC confirmed the composition und purity of compound 9 (Ha-peg(7)-pl-BG).

Sequencing revealed that the previously used human O^6-alkylguanine-DNA alkyltransferase (hAGT) (previously sold by Covalys as SNAP tag) carried mutations for improved substrate binding compared to endogenous hAGT, but was missing mutations for decreased affinity towards DNA and improved protein stability after substrate binding [136, 137]. Thus, in a second attempt the hAGT sequence in the hAGT-mCherry plasmid was replaced with an improved SNAP tag sequence. The new generated SNAP-mCherry plasmid was cotransfected with a plasmid coding for TOMM20-Halo in COS7 and REF52 cells. The Halo tagged TOMM20 localizes at the outer mitochondrial membrane whereas the SNAP tagged mCherry is expressed cytosolically. As shown in figure 10.2 a), after addition of 10 µM Ha-peg(7)-pl-BG the SNAP-mCherry protein is sequestered at the mitochondria indicated by significantly increased fluorescent intensity compared

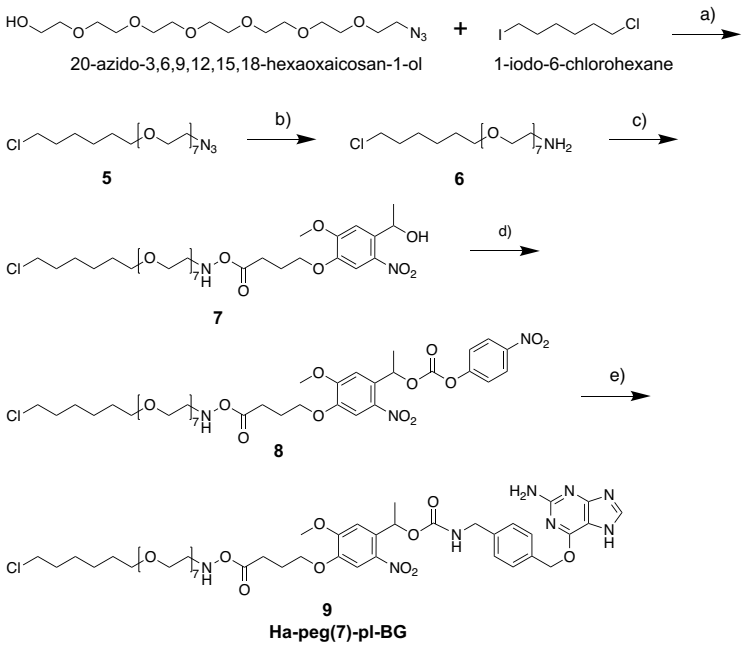

Figure 10.1: **Synthesis of Ha-peg(7)-pl-BG.**
The photocleavable dimerizer Ha-peg(7)-pl-BG was assembled in a five step reaction. Reagents and conditions: a) THF:DMF 7:1, NaH, 0 °C-RT, overnight. b) MeOH:EtOAc 5:1, Pd/C, H_2, RT, 4 h. c) 1. DMF, 4-[4-(1-Hydroxyethyl)-2-methoxy-5- nitrophenoxy]butyric acid, PyBOP, RT, 2 h; 2. 6, DIPEA, RT, overnight. d) DCM, 4-nitrophenyl chloroformiate, pyridine, RT, 4 h. e) DMF, 6-((4-(Aminomethyl)benzyl)oxy)-9H-purin-2-amine, triethylamine, RT, overnight.

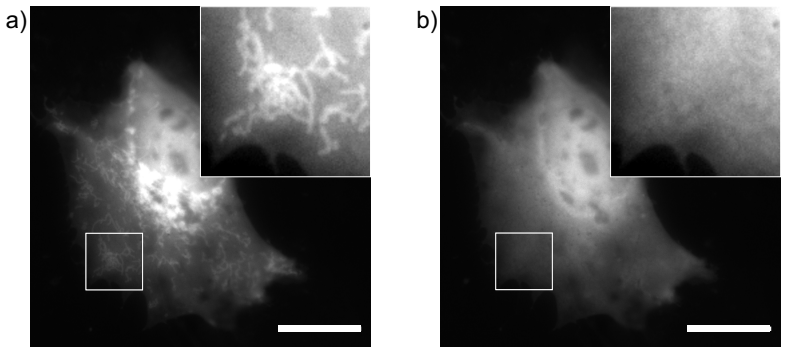

Figure 10.2: **Ha-peg(7)-pl-BG induces the sequestration of SNAP-mCherry *via* dimerization with TOMM20-Halo that is reversed upon exposure to UV light.**
a) In COS7 cells transiently expressing the cytosolic target protein SNAP-mCherry and the mitochondrial localization doamin TOMM20-Halo addition of the photocleavable dimerizer Ha-peg(7)-pl-BG induces sequestration of SNAP-mCherry at the mitochondria. b) Exposure to UV light (1 s, λ=390/18 nm) cleaves the dimerizer and releases sequestered SNAP-mCherry into the cytosol. Inserts are contrast adjusted 3x zoom of the white outlined area in the main image. Scale bar: 20 µm.

to the cytosolic background. Reversibility of the sequestration was demonstrated by exposure to UV light figure 10.2 b). Comparisons of Ha-peg(7)-pl-BG and the shorter Ha-pl-BG in their ability to induce binding of SNAP-mCherry to TOMM20-Halo in cotransfected cells revealed that the sequestration activity of the shorter dimerizer was slightly faster and reached similar levels in efficiency. Furthermore, efficient sequestration could be found also for reduced dimerizer concentrations of 1 µM for both dimerizer. A quantitative analysis was not applicable because the sequestration rate varied dramatically from cell to cell because of different ratios of expression levels of SNAP-mCherry and TOMM20-Halo proteins. This was most likely due to a high variation in the uptake of the two cotransfected plasmids.

10.2 THE COMBINATION OF HALO, SNAP AND DHFR TAGGED PROTEINS ALLOWS MULTIPLEXED DIMERIZATION

The next aim was to test the possibility for multiplex sequestration of target proteins through combination of the SNAP/Halo setup with the previously established DHFR/Halo setup. Three plasmids coding for TOMM20-Halo, SNAP-mCherry and EGFP-DHFR, respectively, were introduced into COS7 and REF52 cells *via* transient transfection. Sequentially, addition of 1 µM Ha-peg(7)-pl-BG induced the sequestration first of SNAP-mCherry at the mitochondria while EGFP-DHFR remained cytosolic (see figure 10.3 a) and subsequent addition of 1 µM Ha-pl-TMP also recruited EGFP-DHFR to the mitochondria

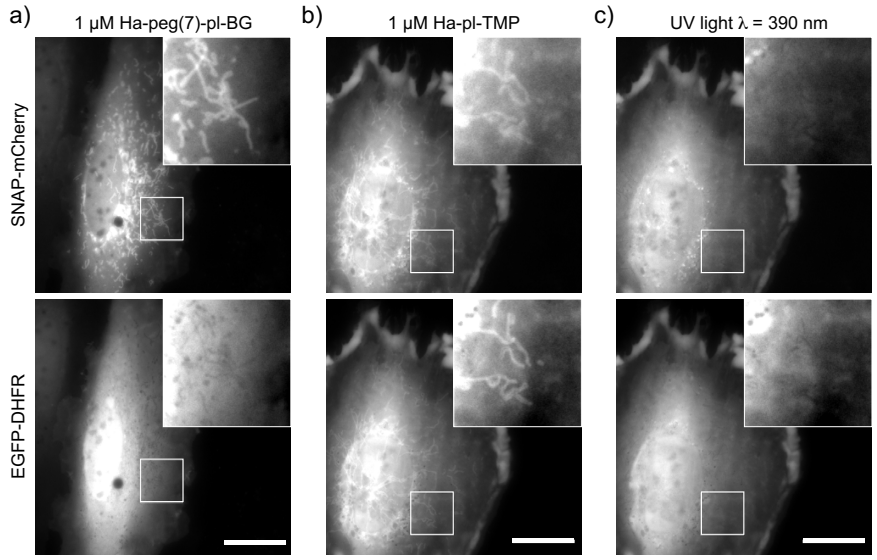

Figure 10.3: **SNAP and DHFR tagged proteins are sequestered subsequently *via* dimerization with a Halo tagged localization domain and released simultaneously by UV light.**
REF52 cells transiently expressing SNAP-mCherry, EGFP-DHFR and TOMM20-Halo show a) mitochondrial sequestration of SNAP-mCherry, but not EGFP-DHFR after addition of Ha-peg(7)-pl-BG. b) Only after addition of Ha-pl-TMP, EGFP-DHFR dimerizes with TOMM20-Halo and is cosequestered at the mitochondria with SNAP-mCherry. c) Irreadiation with UV light (1 s, λ=390/18 nm) cleaves the dimerizers and simultaniously releases both proteins. Inserts are contrast adjusted 3x zoom of the white outlined area in the main images. Scale bars: 20 µm.

as shown in figure 10.3 b). Exposure to UV light released both target proteins coinstantaneously by cleaving the photo linker of Ha-peg(7)-pl-BG and Ha-pl-TMP. Similar results could also be obtained using Ha-pl-BG in combination with Ha-pl-TMP. Note that combinations of the photocleavable dimerizers used in these experiments with the photostable dimerizers Ha-BG or Ha-TMP in principle would also allow to release only one of the target proteins after the sequential recruitment to a Halo tagged interaction partner. Therefore, multiplex dimerization offers a variety of combinatorial possibilities and has a great potential in studying the effects of protein-protein interactions or for applications in synthetic biology[51].

10.3 DIMERIZATION WITH BIFUNCTIONAL SMALL MOLECULES DEMANDS FOR STOICHIOMETRIC OPTIMIZATION

To reach maximum efficiency for chemically induced dimerization each target protein would need to bind one dimerizer and one localization domain. Despite the fact that cotransfection of monocistronic plasmids offers high flexibility in testing different combinations target proteins as presented in chapter 11, it leads to the problem of stoichio-

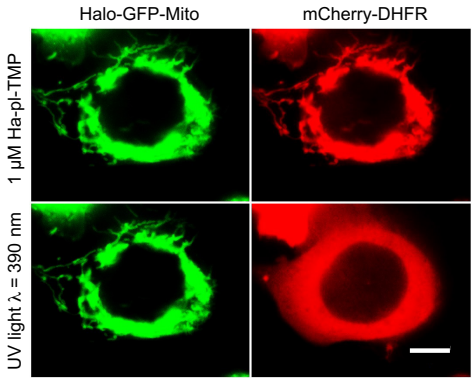

Figure 10.4: **Expression from bicistronic vectors enables highly efficient sequestration of cytosolic target proteins.**
DLD1 R2/7 cells expressing Halo-GFP-Mito and mCherry-DHFR after transient transfection with the bicistronic plasmid Dual ctrl1 show virtually complete sequestration of mCherry-DHFR after administration of Ha-pl-TMP. The cytossolic localization of mCherry-DHFR after irreadiation with UV light (1 s, λ=390/18 nm) proves that the mitochondrial sequestration was specifically induced by Ha-pl-TMP treatment. Scale bar: 20 µm.

metric mismatch of dimerization proteins expressed in the cell. If the cytosolic target protein is expressed in high excess compared to the localization domain, the amount of sequestered protein might not be detectable in the high cytosolic background even if 100 % of the localization domains bind a target protein. Apart from that, the number of dimerizers needs to be carefully adjusted as well. Self-evidently, the tagged proteins cannot form hetero-dimers if no or too little dimerizer is present. But on the other hand, an excess of dimerizer leads to an increased number of monomeric reacted SNAP and Halo tagged species, because if both proteins bind one dimerizer each, they cannot for a hetero-dimer either.

10.3.1 *Use of bicistronic vectors optimize expression level ratios*

To make sure each of the target proteins is expressed in every transfected cell, ideally the sequences coding for both proteins is introduced *via* one bicistronic vector. For example, the protein coding regions can be connected *via* a viral Internal Ribosome Entry Site (IRES). Depending on the expressing cell type this leads to a 1:1 expression or an excess of the upstream construct. Ballister *et al.* [57] presented a construct were the Halo and GFP tagged localization domain (Halo-GFP-Mito) is cloned upstream and the DHFR tagged mCherry target protein (mCherry-DHFR) downstream of the IRES in one plasmid. DLD1 R2/7 cells were transiently transfected with this plasmid and incubated with 1 µM Ha-pl-BG. As shown in figure 10.4virtually complete sequestration of DHFR tagged mCherry was achieved.

10.3.2 *High dimerizer doses impair protein complex formation*

The bicistronic Halo-GFP-Mito and mCherry-DHFR coding plasmid (in the following called Dual ctrl1) was used to test optimal concentrations and incubation times for the dimerizers Ha-TMP and Ha-pl-TMP. The molecules were administered to the transiently transfected A431D cells and the samples were checked after 1 h and after 3 h. Then the dimerizer were washed out and the samples were checked after 1 h, after 2 h and after 16 h. Sequestration efficiencies were rated qualitatively on a scale form "+" (barely detectable) to "+++++" (virtually complete). The results are presented in table 10.1 and 10.2. Interestingly the larger molecule Ha-pl-TMP had a much better sequestration efficiency compared to the photostable Ha-TMP in the tested concentrations. Ha-pl-TMP shows excellent sequestration efficiency for all tested concentrations. The slight decrease after 3 h compared to 1 h for high concentrations indicates an oversaturation of dimerizer i.e. formation of monomeric reacted Halo and DHFR tagged species. This interpretation is further supported by the fact the sequestration efficiency reached the maximum level again after washing out the excess dimerizer allowing new expressed proteins to bind the monoreacted species. For early timepoints Ha-TMP shows a much weaker and slower sequestration rate. This could be either to a lower cell permeability or an impaired binding of the two interaction partners. In case of low permeability, higher concentrations should lead to better results, but for the highest concentration tested here (20 µM Ha-TMP) no sequestration could be detected before removing excess dimerizer. Instead, the sequestration rate increased moderate with longer incubation, but continued rising even after the dimerizer was washed out reaching maximal level for 0.2 µM concentration. For 20 µM Ha-TMP a good sequestration rate was found only 16 h after washing. Therefore, it was concluded that Ha-TMP has a good cell permeability and that high concentrations led to a complete oversaturation. The slow turn on could be explained with an impaired binding of two proteins, which might be because of sterical hindrance due to the short linker between the Halo ligand and the TMP moiety. To test also the optimal incubation conditions for Ha-BG and Ha-pl-BG the DHFR tag in Dual ctrl1 was replaced with a SNAP tag. According to the procedure desired for Dual ctrl1 the resulting plasmid Dual ctrl2 was introduced into A431D cells and incubated with Ha-pl-BG and checked after 1 h and 3 h. After washing the samples were checked after 2 h and 16 h. The results are shown in table 10.3. Optimal sequestration was found with 1 µM Ha-pl-BG after 3 h incubation and 2 h after washing. Similar to Ha-pl-TMP high concentrations led to lower efficiency after 3 h compared to 1 h incubation but slowly recovered after washing. Low concentrations gave good results after longer incubation and after washing. Therefore, it

Table 10.1: **Testing optimal concentration and incubation time for Ha-pl-TMP.**

Time point		Ha-pl-TMP concentration					
		0 nM	8 nM	40 nM	0.2 µM	1 µM	5 µM
After addition	1 h	-	+++++	+++++	+++++	+++++	+++++
	3 h	-	+++++	+++++	+++++	++++	+++
After washing	1 h	-	+++++	+++++	+++++	+++++	++++
	2h	-	+++++	+++++	+++++	+++++	+++++
	16 h	-	+++++	+++++	+++++	+++++	+++++

Table 10.2: **Testing optimal concentration and incubation time for Ha-TMP.**

Time point		Ha-TMP concentration					
		0 nM	40 nM	0.2 µM	1 µM	5 µM	20 µM
After addition	1 h	-	-	+	+	-	-
	3 h	-	+	+++	+++	++	-
After washing	1 h	-	+++	+++++	++++	++++	-
	2 h	-	++++	+++++	+++	+++	-
	16 h	-	++++	+++++	++++	++++	+++

was tested if lower concentrations could lead to efficient dimerization after longer incubations. Dual ctrl2 expressing cells were constantly incubated with Ha-pl-BG or Ha-BG and checked after 1 h, 3 h, 5 h and 8 h. To test how long the complexes are stable, the cells were washed after 24 h and checked again the next day. Results shown in tables10.4 and 10.5 confirm that even nanomolar concentrations of Ha-pl-BG and Ha-BG con induce efficient dimerization without saturation effects. Furthermore the formed complexes are stable for at least 24 h after removing the dimerizer solution. Ha-peg(7)-pl-BG was not considered for detailed testings of incubation conditions, because Ha-pl-BG showed sufficient dimerization efficiency.

In summery, the combination of expression from bicistronic vectors and longer incubation with nanomolar dimerizer concentrations led to reproducible formation of protein complexes that are stable for up to 48 h.The covalent-non-covalent binding dimerizers Ha-pl-TMP and Ha-TMP led to faster and more efficient dimerization over a broad range of concentrations, whereby Ha-TMP might work efficiently even in lower doses then the ones tested. But also the covalent-covalent binding Ha-pl-BG and Ha-BG showed significant formation protein hetero-dimers that should be stable stable even under high tensile forces. In respect of the planned experiments, this gives flexibility to study the processes of cell adhesion and migration even in long time lapse experiments.

Table 10.3: **Testing optimal concentration and incubation time for Ha-pl-BG.**

Time point		Ha-pl-BG concentration					
		0 nM	40 nM	0.2 µM	1 µM	5 µM	20 µM
After addition	1 h	-	-	+	++++	+++	++
	3 h	-	+	+++	+++++	++++	+
After washing	2 h	-	+++	++++	+++++	++++	+
	16 h	-	+++	+++	++++	++++	++

Table 10.4: **Testing long term incubation and Ha-pl-BG induced complex stability.**

Time point		Ha-pl-BG concentration					
		0 nM	1.6 nM	8 nM	40 nM	200 nM	1 µM
After addition	1 h	-	-	-	+	+	++
	3 h	-	-	-	+	+++	+++
	5 h	-	-	+	++	+++	+++
	8 h	-	-	+	++	+++	+++
	24 h	-	-	+	++	+++	++++
	48 h	-	-	+	++	++++	+++++

Table 10.5: **Testing long term incubation and Ha-BG induced complex stability.**

Time point		Ha-BG concentration					
		onM	0.32 nM	1.6 nM	8 nM	40 nM	200 nM
After addition	1 h	-	-	-	-	-	+
	3 h	-	-	+	++	+++	+++
	5 h	-	-	+	++	++++	++++
	8 h	-	-	++	+++	++++	++++
	24 h	-	-	++	++++	+++++	+++++
	32 h	-	-	++	++++	++++	++++

11

DEFINITION AND EVALUATION OF TARGET PROTEINS

Having established the method of protein sequestration *via* photocleavable dimerizers, the next aim was to test potential target proteins. Therefore, three different concepts of how to apply the dimerizer tool were investigated. The first concept was based on retention of target proteins. The was idea to prevent proteins from reaching their place of activity by trapping them in a cellular compartment where they have no function. A big advantage of this concept is, that the proteins only need to be fused with self-labelling tag and are fully functional. This conforms to a functional knock down without perturbations of the expression levels or protein structure. Thus, it is applicable for a broad range of target proteins even without detailed knowledge about the structure of their binding sites for interacting proteins. Furthermore, when proteins that are active e.g. at the plasma membrane, are sequestered at the outer mitochondrial membrane, their turn on after release would be limited only by diffusion through the cytosol. This should allow to study even processes with super high turn on kinetics.

In contrast, the second concept was built on recruitment of target proteins. Known binding sites of interacting proteins could be replaced with the self labelling tags. This would put the protein-protein interaction under control of the presence of a dimerizer. Advantageous of this approach would be a very low background activity, since the proteins should not be able to interact without dimerizer. Additionally, protein complexes induced by the photocleavable dimerizer could be dissolved with ultra high spatiotemporal resolution, therefore giving the possibility to study fast turn off effects.

The third concept was the dimerizer induced complementation of split proteins. Proteins that are interlinking other proteins in a multi-protein complex *via* different domains that are structurally independent from each other (i.e. domain A is folding correctly without domain B and vice versa), could be expressed as two separate constructs. If each is carrying a self labelling tag at the position of the missing domain, dimerization of the two domains should also reconstitute the interlinking function of the protein. The advantage compared to the second concept would be that only one protein needs to be genetically modified to control the formation of the targeted multi-protein complex.

Different target proteins were tested for their potential as a switch for cell adhesion following the three concepts “retention”, “recruitment” and “complementation”. Each target protein was fused with a

self-labelling tag and a fluorescent protein to to follow its cellular localization and translocation in live cell experiments. Although it had been shown that bicistronic vectors can improve the expression ratios of two dimerizer targeted proteins, cotransfection of monocistronic vectors was the method of choice, because it offers a higher flexibility to test various combinations of potential target proteins. The most promising combinations were then to be cloned into a bicistronic vector for further experiments.

11.1 RETENTION OF FOCAL ADHESION PROTEINS

The FA complex proteins vinculin and paxillin were chosen as targets for the retention approach. Terminal fluorescent fusion proteins are well established and do not effect their functionality [111, 112, 138, 139]. Since proteins are constantly exchanged with a cytosolic pool even in mature FAs[106, 138, 140], it should be possible to sequester the full amount of expressed protein over time. The final goal was to retain vinculin and paxillin within the same cell and release them separately or together as a stimulus to increase cell-matrix adhesion. Therefore, vinculin was fused N-terminally with DHFR tag while paxillin was equipped with N-terminal SNAP tag. To follow the sequestration and reintegration into FAs after release EGFP and mCherry were inserted with the tag, respectively. In a first step, each protein was transiently expressed together with a Halo tagged TOMM20 in COS7 and REF52 cells. The mitochondria in COS7 cells are particularly large, which is favorable for sequestration. REF52 cells however form large and well defined FA structures, which should be easier to detect after releasing the proteins. Using the fluorescently labeled TOMM20-mCherry-Halo was very helpful for evaluating if the vinculin accumulations found after dimerizer treatment were still in FA structures or sequestered on the mitochondria by overlaying the two fluorescence signals (see figure 11.1 a). The mCherry in TOMM20-mCherry-Halo was exchanged with EGFP to achieve an easier discrimination for paxillin localization as well (figure 11.1 b).

Both target proteins could successfully be sequestered at the mitochondria after addition of the respective dimerizer. But from the overlay it was also visible that a significant amount remained in the cytosol, of which some fraction did integrate in FA structures as indicated by the clusters that do not overlap with the mitochondrial signal.

An attempt to improve sequestration efficiency was to replace the DHFR tag with a modified mutant that is destabilizing the protein it is fused with when it is not bound to TMP[141]. The aim of this DD tag was to have the level of vinculin low before the dimerizer is added and stabilize only those proteins that are bound to a dimerizer. When releasing the sequestered DD tagged vinculin by cleaving

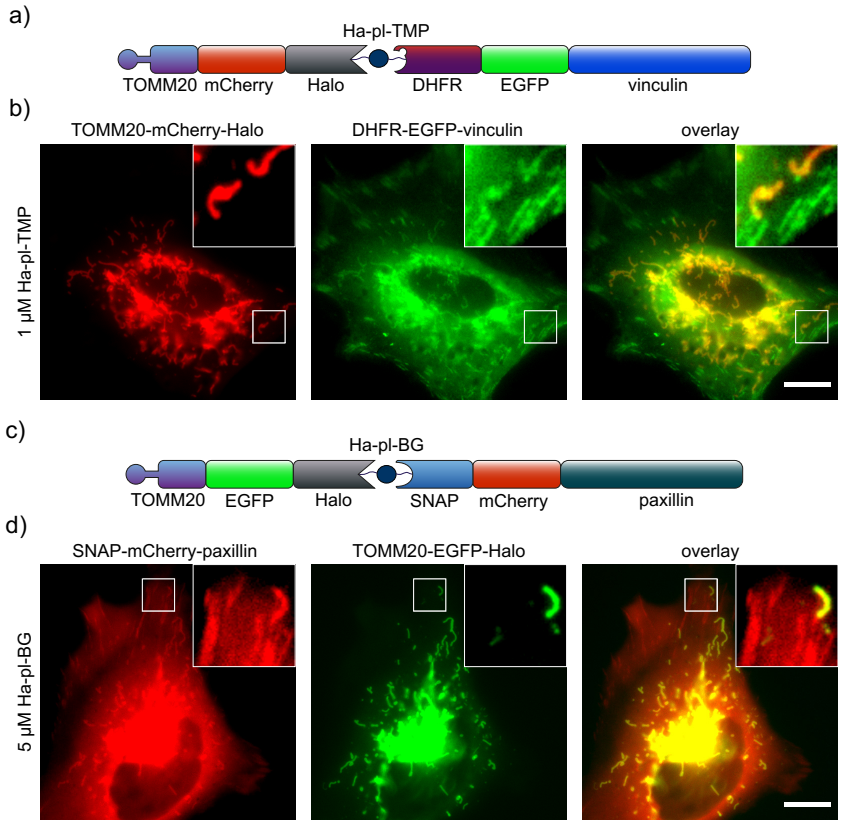

Figure 11.1: **Efficiency of vinculin and paxillin retention *via* sequestration at the mitochondria is not high enough to prevent incorporation in FAs.**

a) Sketch of the Ha-pl-TMP induced protein dimer of TOMM20-mCherry-Halo and DHFR-EGFP-vinculin. b) REF52 cells transiently expressing DHFR-EGFP-vinculin and TOMM20-mCherry-Halo show vinculin accumulation at the mitochondria and in FAs after incubation with Ha-pl-TMP. Vinculin sequestered at the mitochondria appears in yellow in the overlay of mCherry (mitochondria) and the GFP (vinculin) signal, while clusters in FAs appear in green. c) Sketch of the Ha-pl-BG mediated dimer of TOMM20-EGFP-Halo and SNAP-mCherry-paxillin fusion proteins. d) REF52 cells transiently expressing SNAP-mCherry-paxillin and TOMM20-EGFP-Halo show accumulations of paxillin at the mitochondria and in FAs after incubation with Ha-pl-BG. Mitochondrial located paxillin appears in yellow in the overlay of mCherry (paxillin) and the GFP (mitochondria) signal, while clusters in FAs appear in red. Inserts are contrast adjusted 3x zoom of the white outlined area in the main images. Scale bars: 10 µm. Sketches not to scale.

the dimerizer the TMP moiety should stay bound to the DD tag and the released proteins should stay stabilized. As shown in supplementary figure A.1, the DD tag is binding Ha-pl-TMP and can be translocated to the mitochondria, but apparently the destabilizing effect is not strong enough to reduce the level of tagged vinculin to the desired level.

Furthermore it was tried to remove the fraction of tagged proteins integrated in FAs. Cells coexpressing DHFR-EGFP-vinculin and TOMM20-mCherry-Halo were treated with accutase. This enzyme mix is detaching cells by digesting matrix proteins like collagen, but preserves most of the proteins on the cell surface, allowing a fast reattachment of the cells as soon it is removed. By detaching the cell from the surface, FAs should be dissolved and all vinculin should be cytosolic. In presence of the dimerizer the cytosolic pool should be sequestered before they can reintegrate in FAs. When seeding cells detached with accutase in presence of Ha-pl-TMP, no DHFR-EGFP-vinculin was found at the mitochondria, but integrated in FAs.

At this stage of the project it was shown that functional vinculin and paxillin can be sequestered at the mitochondria in living cells. However, to achieve a functional knock down a very high efficiency in sequestration would be necessary, which could not be achieved under the tested parameters. As discussed before, the expression ratio of target to localization domain is a critical parameter for an efficient sequestration. Although the two plasmids were cotransfected in ratios 1:2 (target:TOMM20) the amount of target protein appeared to be always much higher then what could be sequestered on the mitochondria. Expressing target and localization domain from a bicistronic vector could help to overcome this problem. But to achieve a functional change in cell-matrix adhesion this system should be applied in cells that do not express an endogenous pool of the respective target protein (KO cells). Such cells were currently not at hand.

11.2 RECRUITMENT OF ADHERENS JUNCTION PROTEINS

For the recruitment concept adherens junctions were chosen as target structures. The linear connection between E-cadherin and F-actin *via* the CCC complex offers good potential and multiple variabilities in replacing protein-protein binding domains. Since the final goal was to control cell-cell adhesion *via* dimerizer induced formation of AJs, a cell line had to be chosen, that is deficient of AJs but can form stable cell-cell contacts if the missing components are introduced. Therefore, the expression levels of AJ components were analyzed for a variety of cell lines (see Figure 11.2). REF52 cells are rat fibroblasts and express only very low levels of all tested adhesion components. They served as models for mesenchymal cells that show no features of an epithelial phenotype. BT549, MDA-MB 231 and MCF-7 cells are epithelial

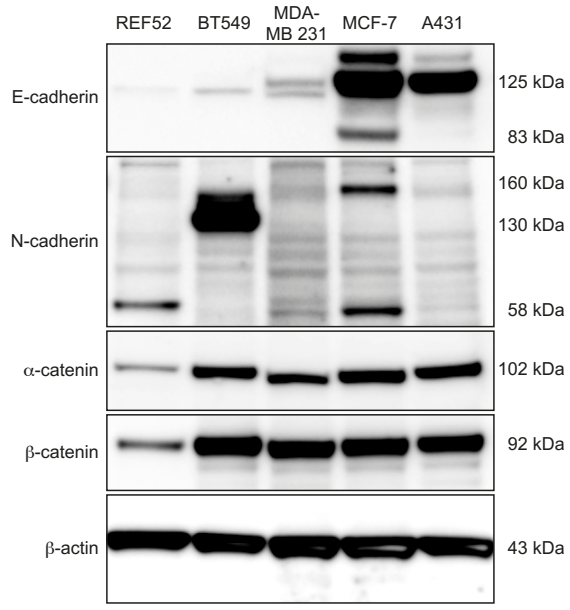

Figure 11.2: **Expression levels of adherens junctions components are dependent on the cell type.**
The expression levels of all AJ components are reduced in REF52 fibroblasts. Expression patterns of E-cadherin and N-cadherin are varying between the epithelial cell lines BT549, MDA-MB 231, MCF-7 and A431 wild type cells (A431) depending on their respective degree of cancer progression, while α- and β-catenin levels are not effected. β-actin serves as loading control.

breast cancer cells that are widely used as models for different stages of EMT. While MCF-7 cells do express high levels of E-cadherin and show an epithelial like phenotype, BT549 cells switched completely to N-cadherin expression and are phenotypically mesenchymal as they grow as single cells (see supplementary figureA.2). MDA-MB 231 cells reflect an intermediate stage of EMT, since they do not express E-cadherin nor N-cadherin and show a mesenchymal phenotype without strong cell-cell connections (also supplementary figure A.2). A431 cells are epidermoid carcinoma cells with a strong epithelial phenotype that is also reflected in high levels of E-cadherin and no N-cadherin expression. All four epithelial cells show similar expression rates of α- and β-catenin. Furthermore, E-Cadherin deficient mutants of A431 (A431D) and gene edited A431 α-catenin knock out cells were used to test the dimerizer induced recruitment of AJ proteins. For a detailed description of the A431 mutants, please refer to section 12.1. A431 wild type (WT) and knock out (KO) cells were difficult to transfect and thus cotransfection of two monocistronic vectors for testing target proteins was not possible. Therefore, the cloned fusion proteins were tested in REF52, MDA-MB 231 and MCF-7 cells for stability and functionality *via* expression after transient transfection and the most promising candidates will be tested in A431 KO cells for their ability to rescue the morphology of the wild type phenotype.

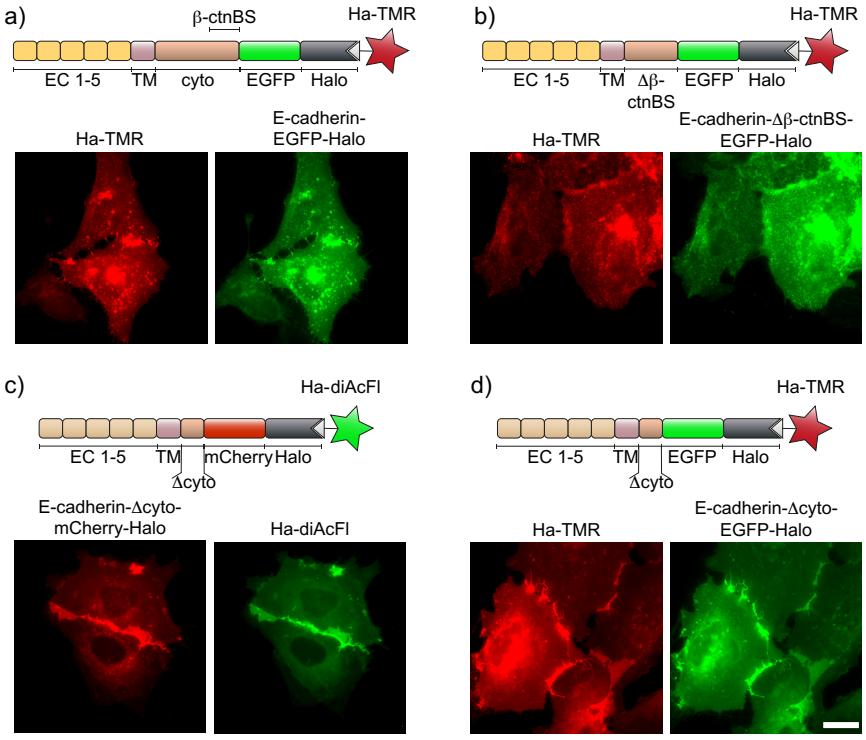

Figure 11.3: **E-cadherin-Halo mutants localize in the plasma membrane and can be stained with Halo ligand conjugated fluorophores.** a) Full length E-cadherin-EGFP-Halo, b) the β-catenin binding site ($\Delta\beta$-ctnBS) depleted mutant E-cadherin-$\Delta\beta$-ctnBS-EGFP-Halo and c)+d) mutants deficient of all protein binding site of the cytosolic domain E-cadherin-Δcyto-mCherry-Halo and E-cadherin-Δcyto-EGFP-Halo are found to localize in the plama membrane upon expression in MDA-MB 231 cells and can be fluorescently labelled at their Halo tag *via* treatment with a)+b)+d) 5 µM Halo-TMR or c) 1 µM Halo-Fl. Sketches above the fluorescence images illustrate the respective fusion protein constructs. Scale bar is 20 µm. Sketches not to scale.

The first step was to test if the c-terminal intracellular domain of E-cadherin (aa578-728), which includes the β-catenin binding site (aa677-706), can be replaced with a Halo tag. Two variants were tested, replacing only the β-catenin binding site ($\Delta\beta$-ctnBS, truncation at aa694-706) or the full cytosolic tail (truncation at aa583-706). For analysis in live cell fluorescence microscopy EGFP or mCherry were inserted with the Halo tag. A full length E-cadherin with N-terminal EGFP and Halo tag served as positive control. To confirm functionality of the Halo tag the cells were stained with the cell permeable fluorophores Halo-TMR or Halo-Fl. As shown in figure 11.3 all Halo tagged E-cadherin mutants could be expressed and stained successfully. They are predominantly located in the plasma membrane and vesicular clusters inside the cells as expected for transmembrane proteins. The signal is higher at cell-cell contact areas of two transfected cells due to an overlap of plasma membranes form both cells. In-

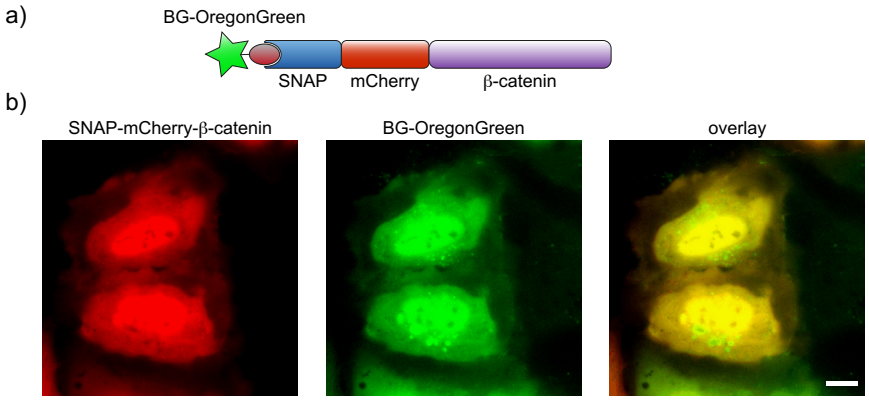

Figure 11.4: **SNAP-mCherry-β-catenin is found in the cytoplasma and nucleus and can be labeled with fluorophore coupled SNAP ligands.**
a) Illustration of the labeling of a SNAP-mCherry-β-catenin fusion protein with the fluorescent SNAP tag substrate BG-OregonGreen. b) SNAP-mCherry-β-catenin expressed in MDA-MB 231 shows high nuclear accumulation. Incubation with 5 µM BG-OregonGreen leads to efficient labeling of the SNAP tag and accumulation of the synthetic fluorophore, but not SNAP-mCherry-β-catenin in vesicular structures (green spots in the overlay). Scale bar 10 µm. Sketch not to scale.

terestingly, the E-cadherins without cytosolic domain (figure 11.3 c) and d)) seem to be more stable then the full length (figure 11.3 a)) or the $\Delta\beta$-ctnBS mutant (figure 11.3 b)). Nevertheless, if fluorescently tagged β-catenin was expressed together with full length E-cadherin-EGFP-Halo both proteins accumulated in cell-cell contact areas of co-transfected cells thereby indicating a functional interaction (see supplementary figure A.3 a)).

In a second step, the catenins were evaluated for their potential as target proteins. β-catenin was N-terminally fused with a SNAP and mCherry tag, expressed in MDA-MB 231 cells (figure 11.4) and MCF-7 cells (supplementary figure A.3) and stained with the SNAP ligand BG-OregonGreen. In MDA-MB 231 cells the protein was found in the cytosol and nucleus, whereas in MCF-7 cells it showed a strong association with the plasma membrane. This reflects the behavior of endogenous β-catenin in the absence or presence of functional AJs (see also figure 12.2). Coexpression with E-cadherin-EGFP as shown in supplementary figure A.3 resulted in co-accumulation of both proteins, proofing that tagging of both, E-cadherin and β-catenin does not interfere with their natural ability to bind to each other.

Remarkably, only low expression rates of the β-catenin construct could be achieved. Higher loads of plasmid and transfection agents led to increased cell death when transfecting the SNAP-mCherry-β-catenin plasmid, while control transfections with e.g. SNAP-mCherry showed high transfection rates. Thus, high expression of exogenous β-catenin seemed to be cytotoxic in these cells.

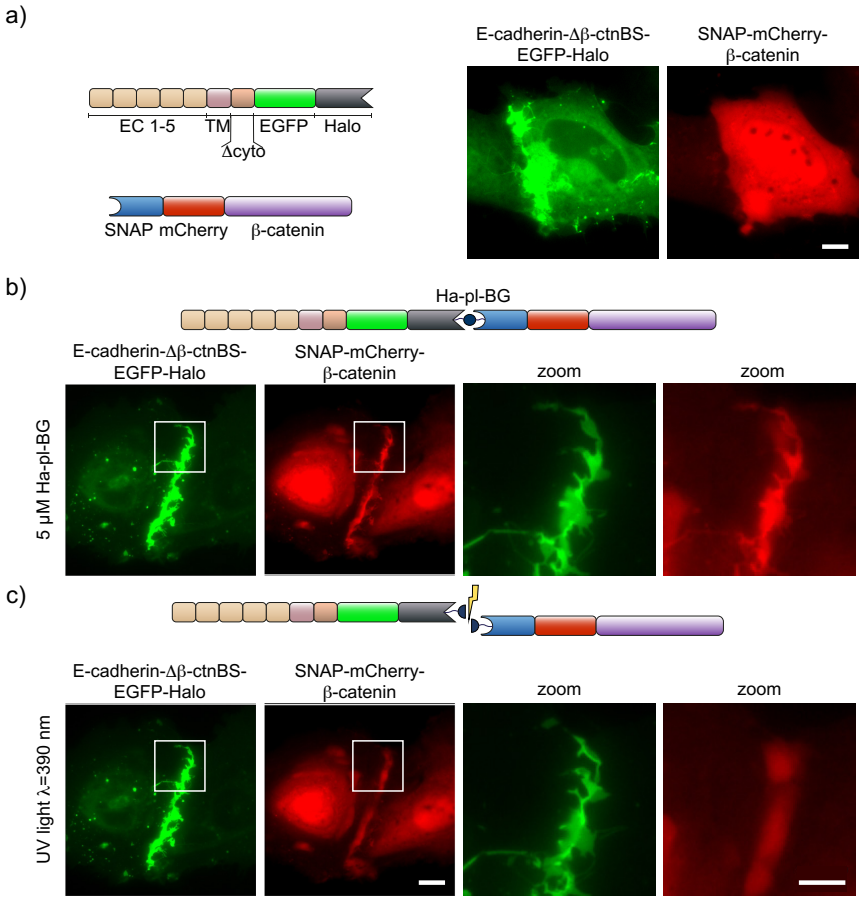

Figure 11.5: **SNAP-mCherry-β-catenin colocalizes with** E-cadherin-$\Delta\beta$-ctnBS-EGFP-Halo **only after incubation with Ha-pl-BG.**
a) Coexpressed in REF52 cells the membrane localized E-cadherin-$\Delta\beta$-ctnBS-EGFP-Halo and the cytosolic SNAP-mCherry-β-catenin show no colocalization. b) After addition of the Ha-pl-BG SNAP-mCherry-β-catenin is recruited to clusters of E-cadherin-$\Delta\beta$-ctnBS-EGFP-Halo. A Ha-pl-BG induced dimers is illustrated on top. c) Exposure to UV light cleaves the dimerizer and reverses colocalization of E-cadherin-$\Delta\beta$-ctnBS-EGFP-Halo and SNAP-mCherry-β-catenin.
The white frames indicate areas shown as zoom on the right next to the images. Scale bars: 10 µm; 5 µm for the zoomed images. Sketches not to scale.

Finally, E-cadherin-Δβ-ctnBS-EGFP-Halo and SNAP-mCherry-β-catenin were coexpressed in REF52 cells and treated with Ha-pl-BG dimerizer (figure 11.5). Without the dimerizer (figure 11.5 a)) the β-catenin binding deficient E-cadherin was membrane localized and showed increased signal in cell-cell contact areas due to overlapping plasma membrane structures, but could not form defined clusters. The β-catenin on the other side was found in high levels in the cytosol and nucleus, but not enriched at the plasma membrane. However, after incubation with 5 µM Ha-pl-BG (figure 11.5 b) β-catenin colocalized with E-cadherin rich structures at the interface of cotransfected cells. The well defined colocalization could be dissolved *via* UV light exposure (1 s, λ=390/18 nm), proofing that the recruitment of SNAP-mCherry-β-catenin to E-cadherin-Δβ-ctnBS-EGFP-Halo was specifically induced by the photocleavable dimerizer. Thus, the interaction of E-Cadherin and β-catenin was chemically reconstituted and could be abrogated with light.

Since REF52 cells do express only very low levels of α-catenin, functional AJ complexes could not form. The coexpression of E-cadherin-Δβ-ctnBS-EGFP-Halo and SNAP-mCherry-β-catenin in MDA-MB 231 cells was not possible, because of cytotoxicity as discussed earlier in this section. This could be explained with the relatively low level of endogenous β-catenin found REF52 in comparison to cells MDA-MB 231 cells. Therefore, the level of recombinant expressed β-catenin alone did not reach a critical level REF52 cells, while the combination of high endogenous expression combined with exogenous expression is killing MDA-MB 231 cells.

α-catenin, the third component of the minimal AJ complex was tested as a target for chemically induced protein complex formation. To overcome the problems of β-catenin overexpression encountered in the previous setup, the aim was to recruit α-catenin directly to E-cadherin. As discussed in section2.2.1, fusion proteins of E-cadherin and α-catenin had been shown to maintain the connection to the actomyosin network although they do not contain β-catenin binding sites.[96, 142] Such a chimeric construct could be obtained from the Troyanovsky lab. E-cadherin-Δcyto-GFP-α-catenin(280-906) (short EcGFP-α(280-906)) contained an E-cadherin that was truncated from aa596 and an α-catenin lacking the first 279 aa connected *via* GFP. That means the E-Cadherin is missing the cytosolic domain including the binding sites for β-catenin and p120-catenin and α-catenin is missing the N-terminal domain, that is responsible for binding to β-catenin and homodimerization. To put the formation of this E-cadherin-α-catenin complex under control of a dimerizer a Halo tag with a stop codon, an IRES sequence and a SNAP-mCherry tag were inserted between GFP and α-catenin. The resulting plasmid was a bicistronic vector for co-expression of Ec-GFP-Halo and SNAP-mCherry-α(280-906) that could be tested directly in A431 knock out cells. When A431D

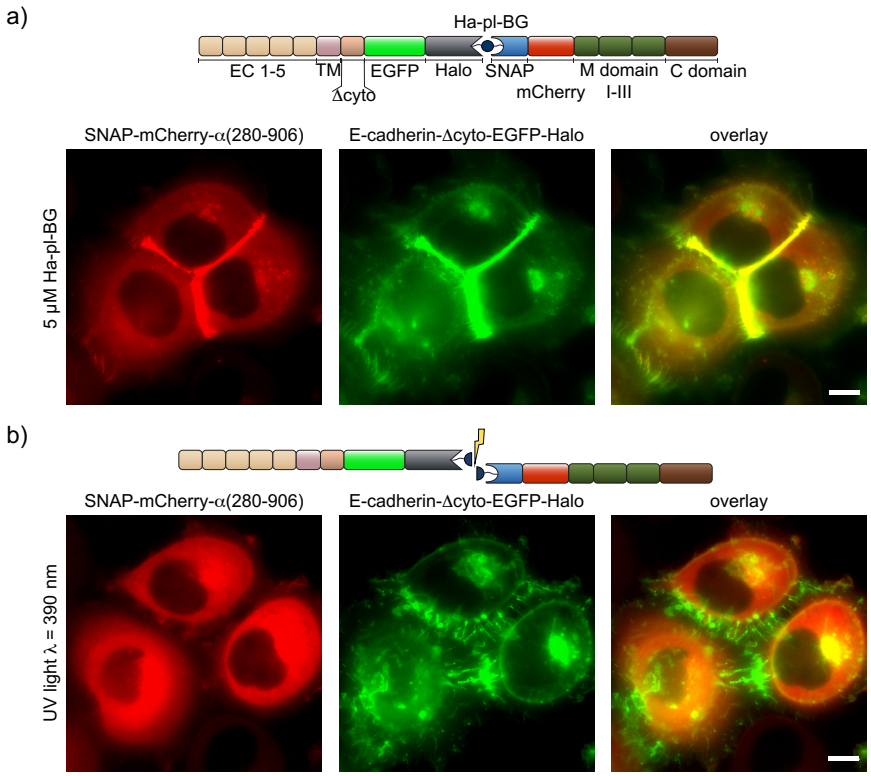

Figure 11.6: **Dimerizer induces the formation of E-cadherin-α-catenin complexes, that cluster along cell-cell contact areas and dissipate after illumination with UV light.**

a) The sketch shows the expected protein complex that forms via Ha-pl-BG mediated binding between E-cadherin-Δcyto-EGFP-Halo and SNAP-mCherry-α(280-906). Indeed, A431D cells expressing the tailless E-cadherin-Δcyto-EGFP-Halo and SNAP-mCherry-α(280-906) from a bicistronic vector show strong colocalization of the two fusion proteins at the cell-cell contact areas after incubation with Ha-pl-BG. b) The Ha-pl-BG mediated dimers are decomposed upon UV light illumination. SNAP-mCherry-α(280-906) is released into the cytosol and E-cadherin-Δcyto-EGFP-Halo forms transient irregular clusters while the cells are drifting apart from each other.
Scale bar 10 µm. Sketches not to scale.

cells transfected with this plasmid were incubated with Ha-pl-BG, not only colocalization of Ec-GFP-Halo and SNAP-mCherry-α(280-906) was induced , but the E-cadherin-α-catenin complex formed linear cluster along the cell-cell contact areas (figure 11.6 a). When cleaving the dimerizer with UV light (figure 11.6 b)), the α-catenin construct was immediately released form the linear clusters and the cells detached forming elongated tethers between them. These tethers were particularly visible because of the high content of the E-cadherin construct. Furthermore, the small cluster of cells seemed to fall apart according to the position of the nuclei, which is supporting the impression that the linear clusters were holding the cells together.

In summary, the recruitment of AJ proteins is a promising way to control cell-cell adhesion. To confirm that the dimerizer induced protein complexes do resemble functional adherens junctions further analysis had to be done (please refer to chapter 12), but at this stage, recruitment of α-catenin to tailless E-cadherin showed the best performance and was therefore the focus of further experiments. The recruitment of β-catenin was impaired by several problems. First of all, high expression of SNAP-mCherry-β-catenin was not possible in MDA-MB 231 cells presumably to cytotoxic effects. This could be avoided either by putting SNAP-mCherry-β-catenin expression under the control of a weaker or inducible promotor or making stable cell lines of cells selected for an tolerated expression level. Furthermore, the E-cadherin-$\Delta\beta$-ctnBS-EGFP-Halo fusion protein was less stable than the tailless E-cadherin constructs. This might be due to the fact that tailless E-cadherin is also missing structures that are targeted to induce internalization or degradation like two cut sites for proteases and the two phosphorylation sites in the p120-catenin binding site[89] (see section **??**). In principle, β-catenin recrution could be facilitated with tailless E-cadherin as well, which would also offer the possibility to induce a sequential recruitment of β-catenin and α-catenin by multiplexed dimerization as demonstrated in section 10.2.

A big advantage of the recruitment concept in comparison to the retention approach is that the complex formation efficiency does not have to be 100 %. A cytosolic pool of unbound target protein should be rater buffering high doses of dimerizer then having negative effects as long the amount of formed clusters is sufficient to induce a physiological effect.

11.3 COMPLEMENTATION OF SPLIT E-CADHERIN

Instead of recruiting binding partners to a protein that is deficient of the endogenous binding domain, it should also be possible to recruit the separately expressed binding domain and thereby reconstitute the full functionality of the protein. E-cadherin offers two interesting target sites for this complementation approach. On the one hand, the

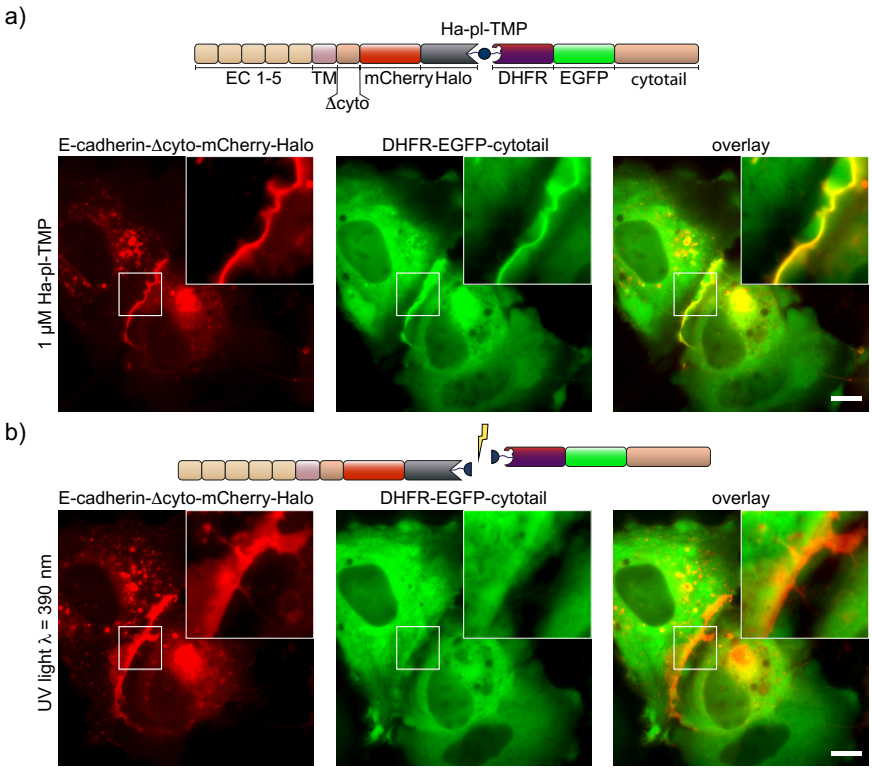

Figure 11.7: **Intracellular reconstitution of split E-cadherin *via* chemically induced dimerization leads to accumulation at cell-cell contact areas that can be dissolved *via* UV illumination.**
a) Tailless E-cadherin-Δcyto-mCherry-Halo and DHFR-EGFP-cytotail are connected via Ha-pl-TMP to form a protein dimer, that combines the extra- and intracellular binding sites of E-cadherin. In REF52 cells this leads to coaccumulation of the reconstituted E-cadherin at cell-cell contact areas indicated via colocalization (yellow in overlay) of the tailless E-cadherin (red) and the cytosolic domain (green). b) Exposure to UV light (λ= 390 nm) cleaves the dimerizer and releases the cytosolic domain from its membrane localization. Scale bars 10 µm. Sketches not to scale.

extracellular domains, that have been shown to be essential for epithelial adhesion (see section **??**) and can serve as adhesive ligands even as recombinantly expressed fragments immobilized on surfaces[143–145]. On the other hand, the intracellular cytosolic domain that mediates the connection to the acto-myosin network *via* catenins (see section 2.2.1) and can induce physiological changes if expressed separately in epithelial cells [146–148].

The intracellular reconstitution of split E-cadherin is technically similar to the recruitment of binding proteins as described in the previous section 11.2. The cytosolic domain of E-cadherin (aa578-728) was fused C-terminally to a DHFR-EGFP construct and expressed in REF52 cells together with E-cadherin-Δcyto-mCherry-Halo. Treated with Ha-pl-TMP the GFP tagged cytosolic domain was enriched at cell-cell interface colocalizing with the mCherry tagged tailless E-

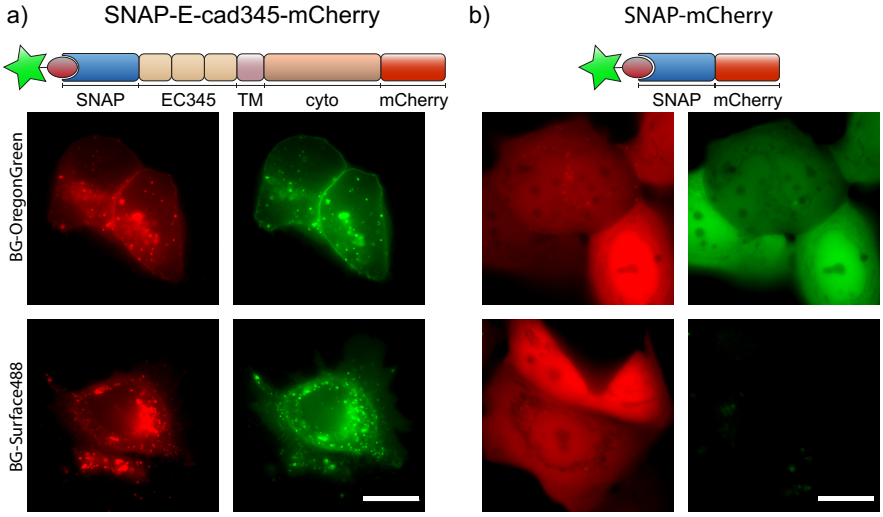

Figure 11.8: **SNAP-E-cadherin345-mCherry is located in the plasma membrane presenting the SNAP tag to the extracellular space.** MCF-7 cells expressing a) SNAP-E-cadherin345-mCherry or b) SNAP-mCherry were treated with either with BG-OregonGreen (upper row of fluorescent images) or BG-Surface488 (lower row) for fluorescent labeling (green) of the SNAP tag. While the cell permeable BG-OregonGreen labels both proteins, the non-permeable BG-Surface488 in bound only be extracellularely presented SNAP tag of the E-cadherin construct. Scale bars are 10 µm. Sketches not to scale.

cadherin (figure 11.7). Similar to the recruitment of α-catenin(280-906) to tailless E-cadherin (figure 11.6) the dimerizer induced complexes accumulated in linear structures along the contact area. After cleaving the dimerizer the cytosolic domain was released immediately and the accumulation of tailless E-cadherin became less defined, however no tethers did form nor did the cells change their position relative to each other. As discussed for the case of β-catenin recruitment, REF52 cells do express only very little amounts of β-catenin and α-catenin. Therefore, the reconstitution of split E-cadherin might have failed to induce the formation of AJs in these cells because it could not be connected to the actomyosin network.

For reconstitution of the extracellular domain the sub-domain 1 and 2 (EC12) were replaced by SNAP tag and expressed in mammalian cells, while an EC12-Halo fusion protein was recombinantly expressed in bacteria. For analysis in live cell experiments, the mammalian construct was fused with an intracellular mCherry tag (SNAP-E-cadherin345-mCherry). The SNAP tag was inserted in exchange of the EC12 domain (aa1-221) only, i.e. preserving the signal peptide for localization into the ER lumen and the pro-domain for proteolytic processing of the N-terminus to achieve extracellular presentation of SNAP-E-cadherin345-mCherry. Functionality and extracellular localization were tested by expressing SNAP-E-cadherin345-mCherry in MCF-7 cells and staining it with the cell permeable BG-OregonGreen

and the non-permeable BG-Surface488 dyes (figure 11.8). SNAP-mCherry expressing cells served as a control for the non-permeability of BG-Surface488. While SNAP-E-cadherin345-mCherry was stained with both dyes, the cytosolic SNAP-mCherry could be stained with BG-OregonGreen only. Thus, the SNAP tag of the cadherin construct must be presented on the extracellular side of the plasma membrane.

Note that the high amount of SNAP-E-cadherin345-mCherry in intracellular clusters could be explained with the inability to form extracellular *trans*-dimers that stabilize the membrane localization of E-cadherin. The construct is expected to be highly internalized as long it is deficient of the EC12 domain, but should stabilize as soon the extracellular domain is reconstituted.

The EC12 domain was fused C-terminally with a Halo tag (EC12-Halo) for expression in *E. coli*. In a second version an EGFP optimized for bacterial expression systems [149] was inserted between the EC12 and Halo domain (EC12-EGFP-Halo). While EC12-EGFP-Halo should serve as an easily detectable probe to establish the method, EC12-Halo was intended to be used in actual live cell experiments. The proteins carried an N-terminal His tag for purification from the bacterial expression culture *via* immobilized metal ion affinity chromatography (IMAC). Because the correct processing of the N-terminus is crucial for *trans*-dimer formation between extracellular domains of E-cadherin[95] the His tag was followed by a TEV protease recognition site (His_{TEV}, amino acid sequence ENLYFQ'X with ' being the actual cut site and X the P1' residue). According to Ritterson *et al.*[128] the P1' position was changed from serine (S) or glycine (G) in the original recognition site to aspartic acid (D) to obtain the right N-terminal sequence of EC12 after proteolytic processing (see figure 11.9a). Since the TEV protease used for this purpose also carried a His tag, the mixture could be easily purified *via* IMAC yielding only processed EC12 protein in the flow through. For the EC12-EGFP-Halo construct the processing quality was validated *via* Western blot analysis (figure 11.9 b). Fractions from the purified but unprocessed protein (1), from the proteolytic reaction (2), the re-purified, processed protein (3) and the immobilized fraction (4) were detected with an antibody against GFP (showing processed and unprocessed EC12-EGFP-Halo) and an antibody against the His tag (showing unprocessed protein and the TEV protease). Comparing lane 1 and 2 of the His tag stained membrane, it is obvious that His tag was efficiently removed from EC12 protein. The weak band in lane 3 on the His tag stained membrane was most likely due to unspecific binding of the anti-His tag antibody to the EC12 construct, because unprocessed protein was immobilized on the IMAC column in the re-purification. Indeed, lane 4 showed the pooled and concentrated eluate from the re-purification, which contains the TEV protease and unprocessed EC12 protein. Furthermore, direct comparison of lane 3 and 4 on the His tag stained membrane re-

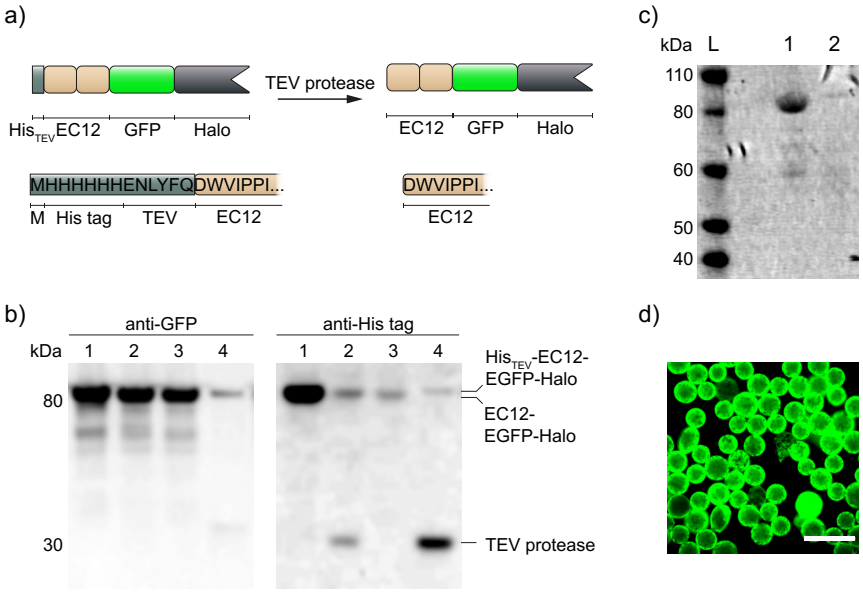

Figure 11.9: **Proteolytic processing of EC12 proteins from bacterial expression generates the endogenous N-terminal sequence.**
a) EC12-EGFP-Halo is expressed in bacterial cultures with a N-terminal His tag, that needs to be removed via proteolytic cleavage with TEV protease. b) Evaluation of N-terminal processing via immunochemical staining for GFP and His tag in Western blot analysis: purified His_{TEV}-EC12-EGFP-Halo (86.5 kDa, lane 1) is treated with a His tagged TEV protease (30 kDa) in a proteolysis reaction mix that remeoves the His tag (lane 2). When passed through an IMAC column only the processed EC12-EGFP-Halo (84.8 kDa) can be detected in the flow through (lane 3), while the TEV protease and unprocessed His_{TEV}-EC12-EGFP-Halo are retained at the column and can be eluted subsequently (lane 4). anti-GFP staining shows the amount of EC12 protein recoverd after each step, anti-His tag staining validates the presence of His tag in the respective bands. Please note, the anti-His tag antibody showes little cross-reactivity with processed EC12-EGFP-Halo. c) Coomassie stained SDS-PAGE gel showing the amount of EC12-EGFP-Halo before (lane 1) and after (lane 2) incubation with Halo tag binding magnetic beads. d) The EC12-EGFP-Halo binding to the beads can be visualized via fluorescence microscopy. M: N-terminal methionin resudue that results from an ATG start codon, His tag: poly-histidin tag for protein purification via IMAC, IMAC: immobilized metal ion affinity chromatography, TEV: recognition site for proteolytic cleavage with TEV protease, L: protein ladder. Scale bar 100 µm. Sketches not to scale.

vealed a small shift between the hight of the band further supporting the opinion that lane 3 contained only processed EC12-EGFP-Halo (84.8 kDa) whereas the heavier unprocessed protein (86.5 kDa) was found in lane 4. To conclude, EC12-EGFP-Halo was successfully processed and re-purified.

Next, the functionality of EC12-EGFP-Halo was tested in vitro. The processed protein was efficiently immobilized on Halo ligand coated magnetic beads (figure 11.9 c+d) thereby proofing the functionality of the Halo tag. A bead aggregation assay was performed with the EC12-EGFP-Halo decorated beads as described in Zhang *et al.* [150] to proof the formation of EC12 trans dimers under high calcium conditions, but no differences on bead aggregation could be detected with or without calcium. Most likely, the beads used in this assay were to heavy to be held together by EC12 fragments, because it had been shown previously, that at least EC1-3 are necessary to achieve a significant formation of aggregated beads, while only the full extracellular domain EC1-5 can fulfill the full adhesive potential [143].

Since in the presented setup, EC12 will be combined with EC345 on the cell surface *via* the dimerizer, it was assumed that the reconstituted extracellular domain should acquire a significant adhesive strength further supported *via* lateral clustering. Since the dimerizer did not need to be highly cell permeable, the larger Ha-peg(7)-pl-BG dimerizer was used in this case. Processed EC12 protein was coupled with Ha-peg(7)-pl-BG, washed to remove unbound dimerizer and administered to A431D cells stably expressing SNAP-E-cadherin345-mCherry (see figure 11.10) in different concentrations. After 2 h the cells incubated with 1 µM or 500 nM dimerizer coupled EC12 protein showed a significant accumulation of the EGFP labeled protein on the cell surface and in intracellular clusters strongly colocalizing with the mCherry signal from SNAP-E-cadherin345-mCherry. The specificity of dimerizer mediated binding between EC12-EGFP-Halo and SNAP-E-cadherin345-mCherry was further supported by the finding, that enrichment of EC12-EGFP-Halo did not happen on untransfected A431D cells. Although in the transfected cells the signals were higher at cell-cell contact areas due to the overlap of membranes, no specific clustering could be observed. To check if the expected E-cadherin clusters need longer time to form, incubation with dimerizer bound EC12 protein was continued over night. After 24 h, even the 50 nM protein solution lead to a significant staining of SNAP-E-cadherin345-mCherry expressing cells. However, no specific clustering of E-cadherin could be detected for the different samples. Instead, the mCherry positive intracellular aggregates did increase dramatically, indicating that no functional E-cadherin could be formed.

Despite the challenges encountered in the presented experiments, extracellular complementation of E-cadherin has some conceptional

advantages compared to the intracellular complementation approach. First of all, only one fusion protein has to be expressed in the cells, omitting the problem of coexpression in suitable ratios. Second, the purified extracellular domains can be preincubated with an excess of dimerizer to ensure high binding efficiencies. Unbound dimerizer can then be washed out to avoid single reacted protein species as discussed in section 10.3. Third, since the dimerization happens in the extracellular space, cell permeabilization is not a limiting step and the cells can be supplied with new protein repeatedly without the risk of oversaturation. Finally, additional modifications can be introduced easily in the EC12 fragment in biochemical in vitro reactions.

The encountered problems could be explained by various scenarios. On the one hand, the aggregation of SNAP-E-cadherin345-mCherry is much higher then observed in the cytosolically truncated E-cadherin mutants presented in section 11.2. The extracellular truncation may lead to increased endocytosis, because this E-cadherin version cannot be stabilized at the cell membrane *via trans*-interaction with E-cadherins from neighboring cells. This could be evaluated by measuring the diffusion rate within the membrane in comparison to a full length E-Cadherin in a FRAP experiment. An adaptation form classical FRAP measurements as demonstrated by Hong *et al.* [151], the internalization rate could be measured using a photoconvertable fluorescent protein like Dendra2. In case high internalization rates are an issue, stabilizing mutation could be introduced in the juxtamembrane region as was shown by Hong *et al.* for C-terminally truncated E-cadherins. Notably, the three point mutations K584R, L587V and L588A were included in the EcGFP-α(280-906) and thus also in the Ec-GFP-Halo construct derived from this plasmid. The E-cadherin-Δcyto-mCherry-Halo plasmid used for intracellular reconstitution of E-cadherin on the other hand was truncated before these critical residues at position V583.

Regarding the EC12 construct, mass spectrometry measurements could confirm the correct processing of the N-terminus and the efficiency of binding the Ha-peg(7)-pl-BG dimerizer in addition to the in vitro characterization performed here. Western blot analysis of cell lysate could be done to proof the binding efficiency of EC12-EGFP-Halo and SNAP-E-cadherin345-mCherry after the experiments presented in figure 11.10. Another critical point is the sterical confirmation of the reconstituted complex. Reconnection of EC12 and EC345 is maintained *via* EGFP-Halo and the SNAP tag domain, each of them being larger than a single EC domain. The large protein sequence inserted in the extracellular domain might interfere with lateral clustering and the ability to stiffen under high Ca^{2+} conditions, since the $Ca^{2+}$are complexed in the hinge region between the EC domains, which is disrupted between EC2 and 3 in the presented setup. In has been reported, that replacing e.g. the EC 3 and 4 domain with pro-

tein domains of similar size and shape leads to homophilic binding efficiencies as low as for EC12[143]. Therefore, the split for extracellular complementation of E-cadherin should be made in another position. Insertions of multiple protein domains has been reported to be possible e.g. between the EC5 and the transmembrane region of E-cadherin [152]. As discussed in section ?? the full extracellular domain EC1-5 recombinantly expressed by mammalian cells, is known to have strong adhesive potential. Although the yield from mammalian expression cultures is known to be much lower then from bacterial expression systems, a big advantage would be that mammalian cells do process the N-terminus of the protein endogenously making the proteolytic treatment presented for EC12 fragments obsolete. The EC1-5-SNAP proteins presented by Fichtner *et al.* [144] could be combined with an E-cadherin in which the full extracellular domain had been replaced by a Halo tag. Concerning that EC1-5 proteins are widely used for surface functionalizations to maintain cell adhesion *via* cadherins, this approach has good potential to reconstitute functional E-cadherins.

Nevertheless, regarding the good results achieved with the recruitment of catenins and the intracellular complementation of E-cadherin and for the temporal restrictions of this project, the extracellular complementation strategy was set on hold.

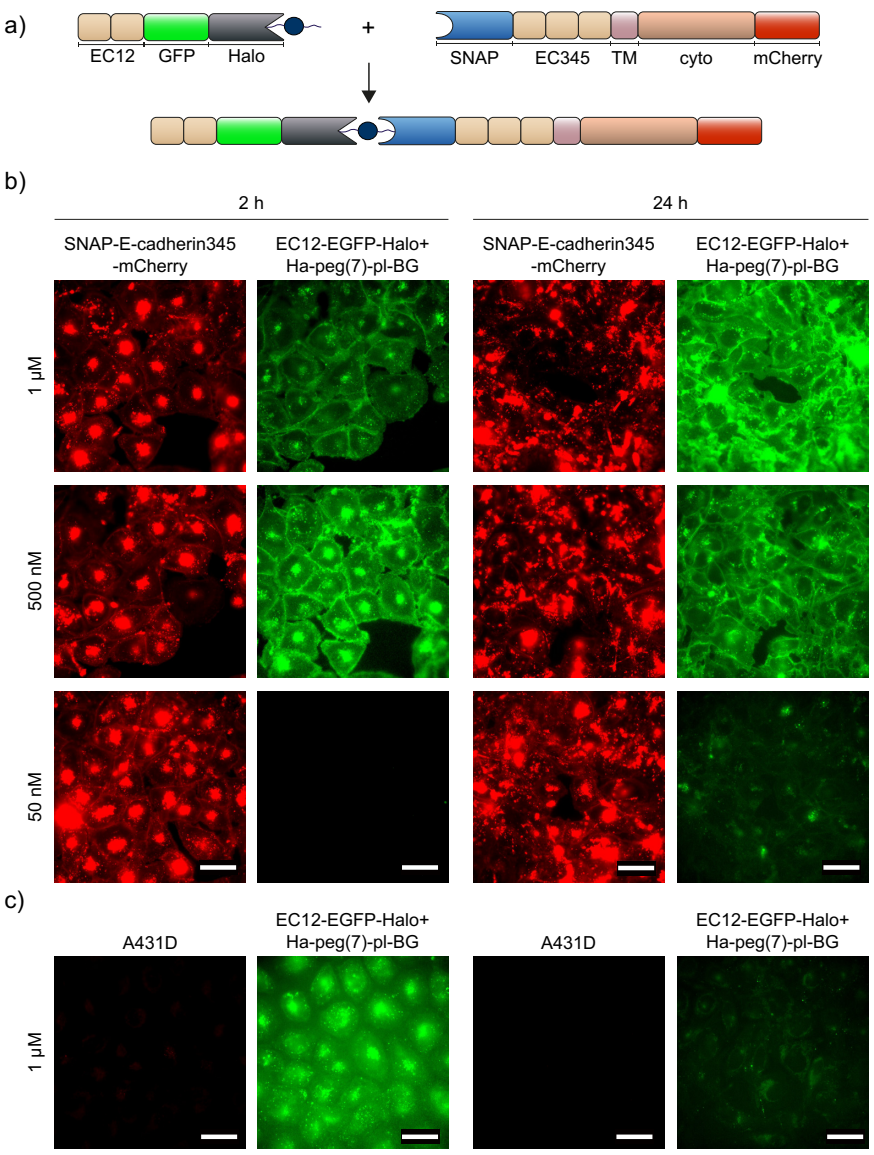

Figure 11.10: **Complementation of extracellular E-cadherin domains has no effect on E-cadherin accumulation at cell-cell interfaces.** a) EC12-EGFP-Halo can be dimerized via Ha-peg(7)-pl-BG with SNAP-E-cadherin345-mCherry to reconstitute the extracellular domain of E-cadherin. b) N-terminally processed and dimerizer conjugated EC12-EGFP-Halo is binding to SNAP-E-cadherin345-mCherry expressed on the surface of stable transfected A431D cells depending on the protein concentration. After 2 h and 24 h incubation the reconstituted E-cadherins do not cluster at cell-cell surfaces, but form aggregates within the cells. c) Untransfected A431D cells do not bind dimerizer conjugated EC12-EGFP-Halo on the cell surface, but also internalize the protein. Images are diplayed with higher contrast correction then in b) to visualize the intracellular aggregates, that occur to a much lower extend then in SNAP-E-cadherin345-mCherry expressing cells. Scale bars: 40 µm. Sketches not to scale.

12

CHARACTERIZATION AND EVALUATION OF DIMERIZER INDUCED CELL ADHESION

12.1 CHARACTERIZATION OF A431 MUTANT CELLS

Direct comparison of a knock out mutant with their respective wild type equivalent is a widely used approach to test the functionality of recombinantly expressed proteins. Ideally, the recombinant expression of a protein that was depleted in the cell should recover the wild type phenotype. This concept is known as rescue transfection. Regarding the promising results that were achieved via dimerization of Ec-GFP-Halo and SNAP-mCherry-α(280-906) expressed from a bicistronic vector (hereafter referred to as Dual1), the cells were characterized more detailed. The dimerizer induced complex resembles the chimeric fusion construct Ec-GFP-α(280-906), and should share functional features of both, E-cadherin and α-catenin. Therefore, an A431 α-catenin knock out cell line (A431 α-catenin KO cells) was included in these experiments in addition to the E-cadherin deficient A431D cells. Since it was planned to use the cells in collective migration experiments where a homogeneous expression level throughout the cell population would be favorable, all analysis were made from stable transfected cell lines. In addition to Dual1 transfected KO cells, cell lines transfected with the chimeric Ec-GFP-α(280-906) fusion protein or a fluorescently tagged full length version of the KO protein, that is E-cadherin-GFP in A431D and mEmerald-α-catenin in A431 α-catenin KO cells were used as controls for rescue of the wild type phenotype. Although the transfected plasmids carried a resistance marker for antibiotic selection, cells tended to reduce the expression levels of recombinant proteins. Therefore, the cells were freshly sorted for high expression levels before each collective migration experiment.

12.1.1 *Expression levels of adherens junction proteins in stable cell lines*

The expression levels of endogenous and recombinant E-cadherin and α-catenin was investigated via Western blot analysis. As shown in figure 12.1, A431D did not express E-cadherin whereas endogenous E-cadherin was found in wild type A431 cells (A431 WT) with a molecular weight of ca. 120 kDa according to the protein standard used in this experiment. The discrepancy to the value of 80 kDa calculated for the processed E-cadherin from the amino acid sequence is because the majority of cellular E-cadherin is unprocessed and carries the pro-domain resulting in 97 kDa molecular weight calculated

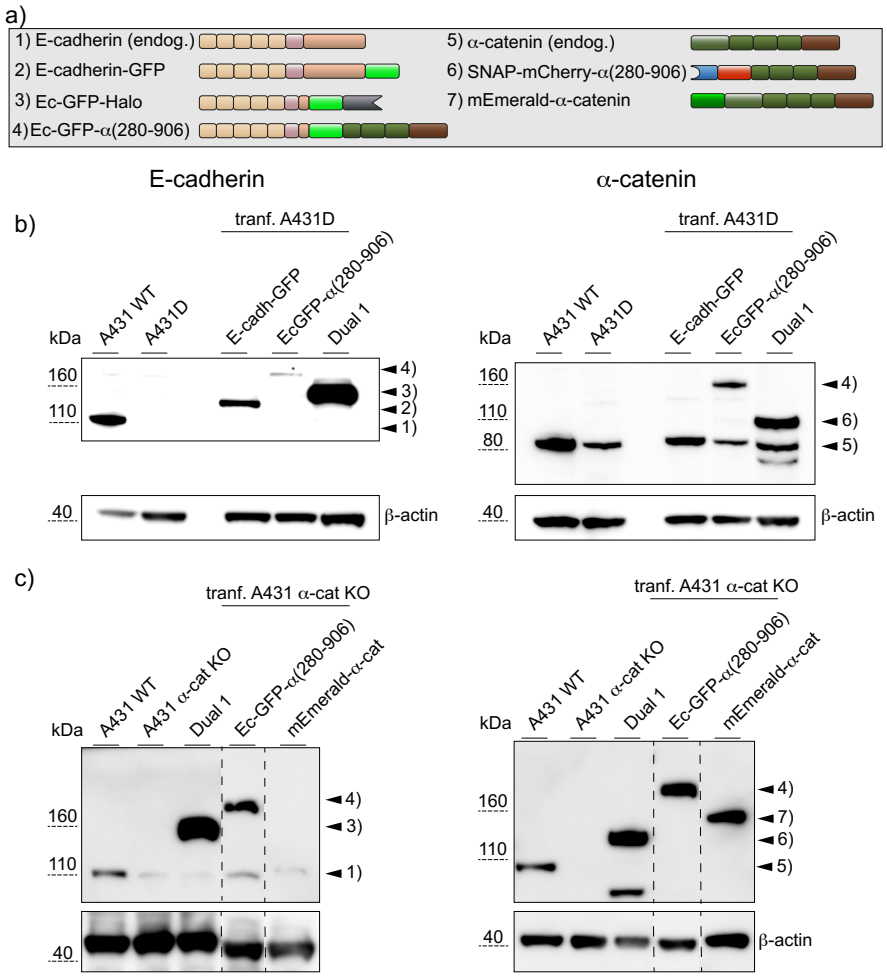

Figure 12.1: **Western blot analysis of A431 mutants for expression of E-cadherin and α-catenin constructs.**
a) Illustration of the different E-cadherin and α-catenin constructs expressed in A431 mutants in comparison to the endogenous proteins. Dual1 cells express Ec-GFP-Halo and SNAP-mCherry-α(280-906). b) Immunochemical detection of E-cadherin (left) and α-catenin constructs (right) expressed in stable transfected A431D cells in comparison to A431 WT ynd untransfected A431D cells. Numbers on the right site of the blot correspond to the constructs illustrated in a) and indicate the hight expected according to the molecular weigth. α-catenin constructs Ec-GFP-α(280-906) and SNAP-mCherry-α(280-906) (expressed by Dual1 cells) are expressed in addition to endogenous α-catenin. The extra band of low molecular weigt detected in α-catenin stainings of Dual1 cells could not be assigned. β-actin serves as loading control. Original images of the blots are presented in supplementary figure A.4 a). c) Stable transfected A431 α-catenin KO cells analyzed in the same setup as described in b). Endogenous E-cadherin is expressed in A431 α-catenin KO cells in very low amounts. Also for A431 α-catenin KO Dual1 cells an unassignable band was found in the α-catenin detection. Lanes in the images shown in c) were rearranged for better comparability with results from b). Cut sites are indicated in dashed lines. Original images of the blots are presented in supplementary figure A.5. endog.: endogenous, transf.: transfected. Sketches not to scale.

for the amino acid sequence. The additional difference arises from heavy glycolisation as reviewed in eg. van Roy et al.[89]. Small discrepancies also arise for the fusion constructs E-cadherin-GFP (124 kDa), Ec-GFP-α(280-906) (180 kDa) and Ec-GFP-Halo (145 kDa) indicating successful glycosilation (all molecular weights calculated from the amino acid sequence including the pro domain). Note, that the expression levels of the three recombinant E-cadherins differ significantly for A431D cell lines due to problems with stable expression levels. Endogenous α-catenin (102 kDa) was expressed in all A431D cell lines and A431 WT. The expression level in A431D cells was significantly lower than in A431 WT cells, but could be fully recovered in A431D cells expressing E-cdherin-GFP. Since the antibody used for α-catenin detection recognized the C-terminus of α-catenin, the 145 kDa band of Ec-GFP-α(280-906) is visible in addition to the endogenous α-catenin of Ec-GFP-α(280-906) transfected A431D cells. For A431D cells transfected with Dual1, additionally to the endogenous α-catenin and the recombinant SNAP-mCherry-α(280-906) (119 kDa) a third band of ca. 85 kDa was detected that could not be specified further. The level of endogenous α-catenin in A431D cells transfected with Ec-GFP-α(280-906) or Dual1 was comparable to A431D rather then A431 WT cells, indicating that endogenous α-catenin is not affected in these cells.

For A431 α-catenin KO cells the expression level of endogenous E-cadherin was highly reduced in comparison to A431 WT cells. While in Dual1 transfected cells the endogenous E-cadherin was barely detectable over the strong signal from recombinant Ec-GFP-Halo, cells expressing Ec-GFP-α(280-906) on the other hand showed levels comparable to A431 WT for endogenous E-cadherin in addition to the heavier chimeric fusion protein. This could be interpreted as a sign for a rescue in phenotype. For mEmerald-α-catenin transfected A431 α-catenin KO cells however, the detected amount of endogenous E-cadherin was much lower then for Ec-GFP-α(280-906) transfected cells. If this reflects the true expression level or is due to a technical problem in the revelation of the membrane would need to be evaluated in a repetition of this experiment.

The absence of endogenous α-catenin was confirmed for A431 α-catenin KO cells, whereas the recombinant mEmerald-α-catenin (128 kDa), Ec-GFP-α(280-906) and SNAP-mCherry-α(280-906) were expressed in high amounts compared to the level of endogenous α-catenin in A431 WT.

12.1.2 *Cellular localization of adherens junction proteins in rescue transfected cell lines*

The cellular localization of adherens junction proteins was analyzed via fluorescent immunohistochemical staining of paraformaldehyde

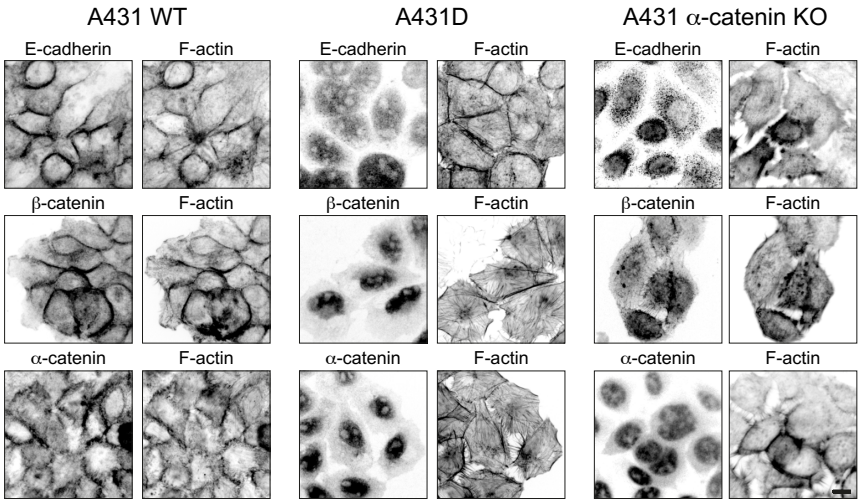

Figure 12.2: **Cellular localization of adherens junctions components in A431 wild type and knock out cells.**
Fluorescent immunohistochemical staining for E-cadherin, β-catenin or α-catenin, respectively and costaining for F-actin in A431 WT, A431D and A431 α-catenin KO cells illustrates the localization of the CCC complex components inside the cells. For more detailed desrciption please refer to the main text. Scale bar 10 µm. Sketches not to scale.

fixated cells. Fluorescently tagged recombinant proteins were detected by the fluorescent signal of their tag. E-cadherin fusion constructs were additionally detected with an anti-E-cadherin antibody to confirm the coherence between the GFP signal and E-cadherin detection and to potentially detect additional pools of endogenous E-cadherin that did not colocalize with the recombinant protein. In A431 WT cells E-cadherin, β-catenin and α-catenin accumulated at the plasma membrane at cell-cell interfaces forming functional AJs as indicated by the co-accumulation of F-actin. By contrast, in A431D cells β-catenin and α-catenin were found predominantly in the nucleus, while staining for E-cadherin resulted in a low undefined signal in the perinuclear region and actin was mainly organized in stress fibers stretching between focal adhesions. In A431 α-catenin KO cells E-cadherin was found to be accumulated in small vesicles in the perinuclear region. β-catenin showed an undefined localization varying from cell to cell with a slight tendency for the plasma membrane or the nucleus. Despite the absence of α-catenin confirmed via western blot analysis (see figure 12.1) immunofluorescence detection with the antibody against the N-terminus of α-catenin showed nuclear localization for A431 α-catenin KO cells. Since this was not the case for the transfected A431 α-catenin KO cells, this is considered to be an experimental artifact.

E-Cadherin-GFP expressed in A431D cells (figure 12.3 a) localized mainly in the plasma membrane and accumulated in cell-cell contacts together with β-catenin, α-catenin and F-actin in forming AJs. Expres-

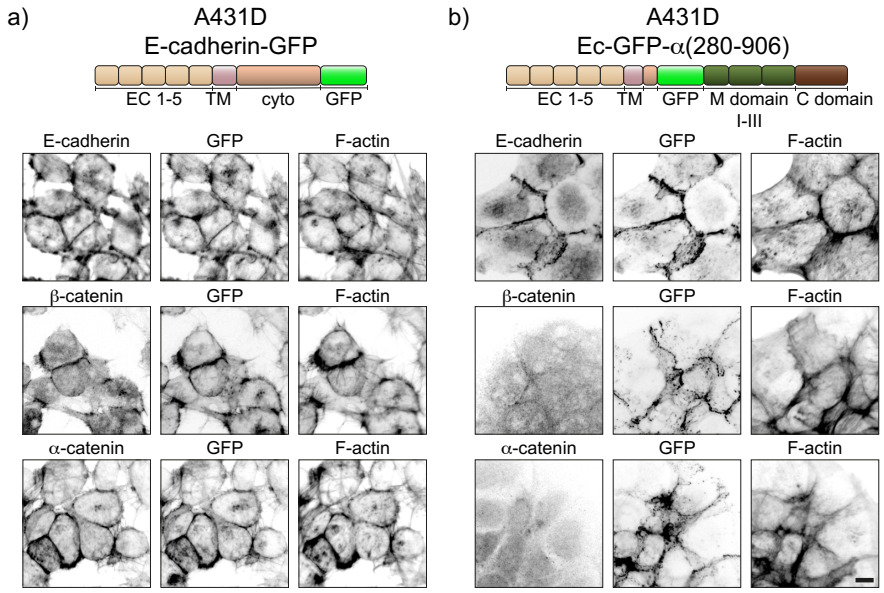

Figure 12.3: **Cellular localization of adherens junctions components in rescue transfected A431D cells.**
Fluorescent immunohistochemical staining for E-cadherin, β-catenin or α-catenin, respectively and costaining for F-actin together with fluorescent signal from the GFP tag illustrates the localization of the CCC complex components with a) E-cadherin-GFP and b) Ec-GFP-α(280-906) inside stable transfected A431D cells. For more details please refer to the main text. Scale bar 10 µm. Sketches not to scale.

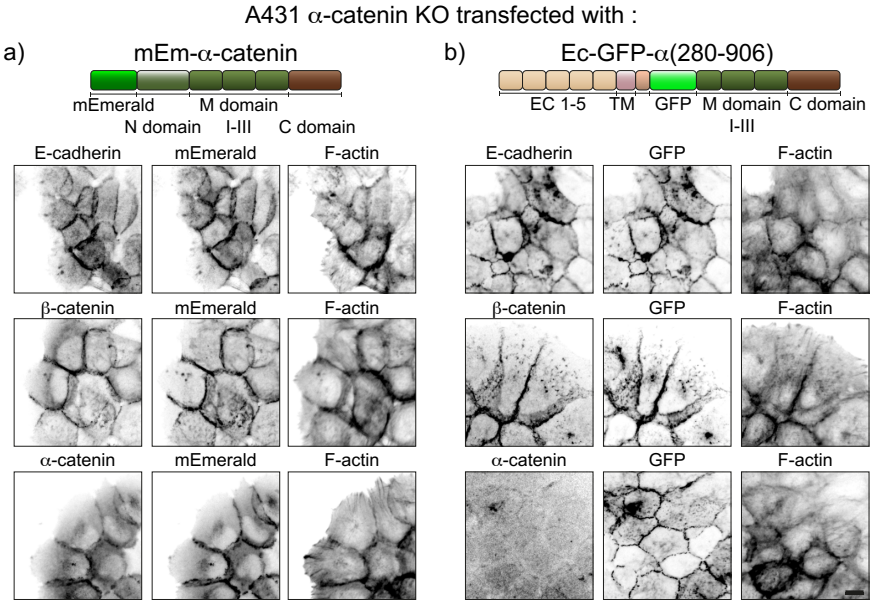

Figure 12.4: **Cellular localization of adherens junctions components in rescue transfected A431 α-catenin KO cells.**
Fluorescent immunohistochemical staining for E-cadherin, β-catenin or α-catenin, respectively and costaining for F-actin together with fluorescent signal from the GFP tag illustrates the localization of the AJ components with a) mEmerald-α-catenin and b) Ec-GFP-α(280-906) inside stable transfected A431 α-catenin KO cells. For more details please refer to the main text. Scale bar 10 µm. Sketches not to scale.

sion of Ec-GFP-α(280-906) (figure 12.3 b)also led to clusters of the E-cadherin fusion construct at cell-cell contacts and co-accumulation of F-actin, but β-catenin and α-catenin were not recruited to these clusters. Instead they showed an undefined localization with a tendency for nuclear localization.

Expression of mEmerald-α-catenin in A431 α-catenin KO cells (figure 12.4 a) rescued the colocalization of E-cadherin, β-catenin and α-catenin together with F-actin accumulation at cell-cell contact sites in AJ complexes. Interestingly, expression of Ec-GFP-α(280-906) (figure 12.4 a) did not only lead to clustering of the chimeric fusion construct and F-actin colocalization, but also induced β-catenin co-accumulation at cell-cell contacts.

In summary, the immunostainings confirmed the expected arrangement of E-cadherin, β-catenin, α-catenin and F-actin in functional AJs in A431D cells transfected with E-cadherin-GFP and A431 α-catenin KO cells transfected with mEmerald-α-catenin. Expression of Ec-GFP-α(280-906) induced cell-cell contact formation and F-actin reorganization, but was missing β-catenin recrution in A431D cells. Although Ec-GFP-α(280-906) did not contain a β-catenin binding site the colocalization of β-catenin in A431 α-catenin KO cells could be possibly explained by an indirect recruitment via lateral cadherin clustering. The

Ec-GFP-α(280-906) get stabilized at the plasma membrane via extracellular trans dimerization with E-cadherin from opposing cells and on the other hand via binding to the actomyosin network as shown by enrichment of F-actin at these clusters. Via lateral clustering the E-cadherin domain of Ec-GFP-α(280-906) can also recruit endogenous E-cadherin, which in turn binds β-catenin even without direct connection to the actomyosin network. Therefore, β-catenin recruitment is dependent on endogenous E-cadherin, which in turn explains why β-catenin is not affected in A431D cells.

12.1.3 *A431D and A431 α-catenin KO cells respond differently to dimerizer induced adherens junctions*

Ha-pl-BG and Ha-BG are covalently bound by Halo tag and SNAP tag. Therefore, the formation of the dimeric complex between Ec-GFP-Halo and SNAP-mCherry-α(280-906) (short: E-cadherin-α-catenin complex) could be analyzed via western blot of protein samples electrophoretically separated in a polyacrylamide gel under denaturing conditions. A431D cells expressing Dual 1 were incubated for 9 h with the photocleavable Ha-pl-BG dimerizer or the photostable Ha-BG dimerizer and lysed directly or after exposure to UV light (λ= 365 nm) from a table top UV lamp. E-cadherin and α-catenin were detected via immunoblotting using an antibody against the unmodified extracellular domain of E-cadherin and C-terminal domain of α-catenin. As shown in figure12.5 without the dimerizer SNAP-mCherry-α(280-906) was found in a single band with a molecular weight (MW) of 119 kDa. When incubated with either Ha-pl-BG or Ha-BG (both: MW ca. 1 kDa), an additional band was detected. The hight of the band fit to the expected MW of 265 kDa for the covalent-covalent dimerized Ec-GFP-Halo (MW 145 kDa) and SNAP-mCherry-α(280-906). This heavy band was not present when Ha-pl-BG cells had been exposed to UV light, but was found in similar intensity in lysate from cells treated with Ha-BG with or without UV exposure. The same pattern was also found when detecting E-cadherin on the membrane, but the relative amount of E-cadherin that contributed to the dimer was much lower than for α-catenin.

The data proofed, that the heavier band was indeed the E-cadherin-α-catenin complex and that this complex could be specifically disintegrated with UV light if Ha-pl-BG was used to induce dimerization. In the reported case, the dimerizer were applied in concentrations found to be optimal in the mitochondrial sequestration experiments presented in section10.3.2. Because Ec-GFP-Halo and SNAP-mCherry-α(280-906) are connected via an IRES sequence on the vector, the E-cadherin construct is tendentially expressed in a higher level than the α-catenin fusion protein. Since also less then 50 % of SNAP-mCherry-α(280-906) were bound in the complex, it should be possible to im-

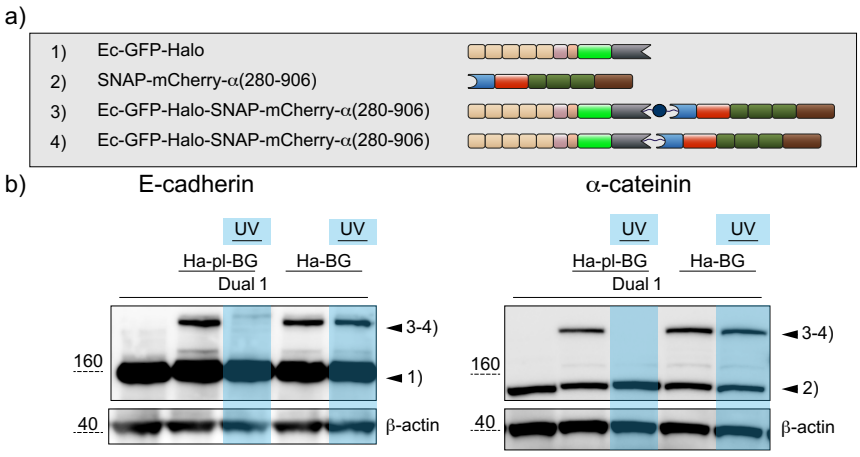

Figure 12.5: **Western blot analysis of dimerizer treated and UV exposed A431D Dual1 cells.**
a) Illustration of Ec-GFP-Halo and SNAP-mCherry-α(280-906) and the dimeric complexes that form in A431D Dual1 cells via treatment with photocleavable Ha-pl-BG (3) or non-cleavable Ha-BG (4). b) Immunochemical detection of E-cadherin (left) and α-catenin constructs (right) expressed in stable transfected A431D cells show additionally heavy bands for the dimeric Ec-GFP-Halo-SNAP-mCherry-α(280-906) complex. Dimers formed via Ha-pl-BG are dissociated upon UV light (λ=365 nm) exposure, while Ha-BG induced dimers stay intact. Sketches not to scale.

prove that ratio by longer incubation time or optimized dimerizer concentrations.

To check the effects on cellular localization of AJ components after E-cadherin-α-catenin dimer formation and light induced dissociation of the complex, cells were treated as described above but fixed with PFA and analyzed via immunohistochemical fluorescent staining (figure 12.6). Dual1 transfected A431D cells showed high amounts of recombinant E-cadherin in the plasma membrane, but did resemble the E-cadherin knock out phenotype considering nuclear localization of β-catenin and stress fibre organization of F-actin. Recombinant SNAP-mCherry-α(280-906) was mainly found in the perinuclear region as detected by mCherry fluorescence. After incubation with the photocleavable dimerizer Ha-pl-BG, SNAP-mCherry-α(280-906) was recruited to colocalize with Ec-GFP-Halo at the plasma membrane. Accumulation of dimerizer induced E-cadherin-α-catenin complexes at cell-cell contacts were associated with an enrichment of F-actin. Therefore, it can be assumed that the E-cadherin-α-catenin complexes are functionally connected to the actomyosin network. When Ha-pl-BG treated cells were exposed to UV light, they switched back to the knock out phenotype with perinuclear SNAP-mCherry-α(280-906) and Ec-GFP-Halo being found in the plasma membrane. Dual1 expressing A431D cells treated with the non-cleavable dimerizer Ha-BG instead did not react to the UV exposure, but kept the F-actin

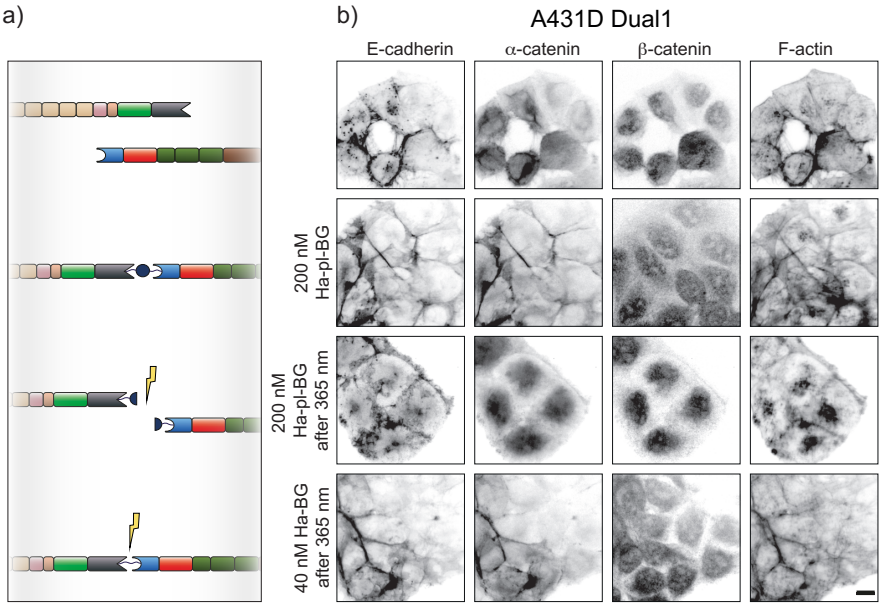

Figure 12.6: **Light controlled dissociation of dimerizer induced E-cadherin-α-catenin complexes in A431D cells do not affect β-catenin localization.**

a) Illustration of dimer formation and dissociation between Ec-GFP-Halo and SNAP-mCherry-α(280-906) in A431D Dual1 cells via treatment with photocleavable Ha-pl-BG or non-cleavable Ha-BG and UV light irradiation (indicated by the flash). b) Immunohistochemical stainings for β-catenin and F-actin recorded together with fluorescent signals from GFP (fused to E-cadherin) and mCherry (fused to α-catenin) show the rearrangement of AJ components within the cell before (first row), after incubation with Ha-pl-BG (second row) and after additional treatment with UV light (third row, λ=365 nm). The fourth row shows UV exposed cells that had been treated with Ha-BG. β-catenin localization is not effected by the formation or dissociation of E-cadherin-α-catenin complexes. Scale bar 10 µm. Sketches not to scale.

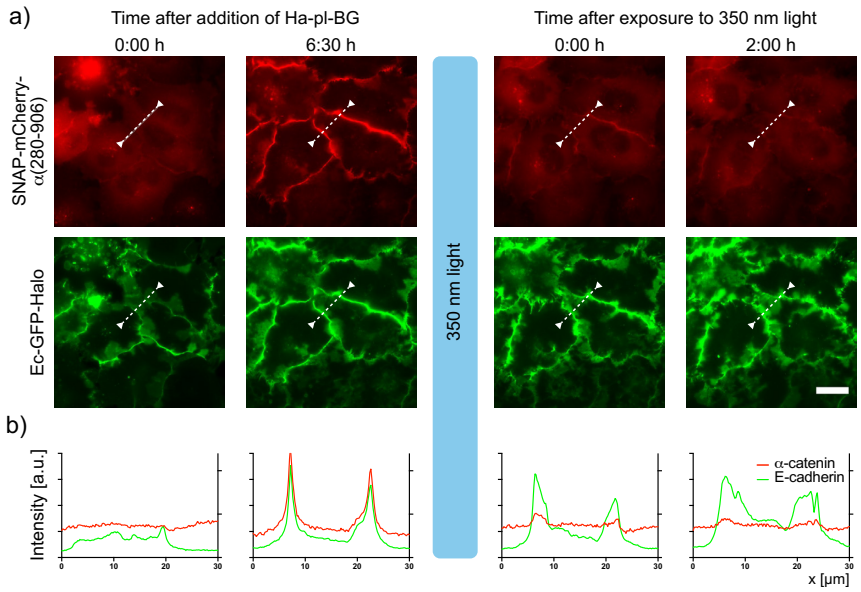

Figure 12.7: **Dynamic formation of dimerizer induced E-cadherin-α-catenin complexes in A431D Dual1 cells can be reversed by UV light.**

a) Fluorescent timelapse recordings of A431D Dual1 cells show the formation of E-cadherin-α-catenin complexes after addition of Ha-pl-BG via colocalization of Ec-GFP-Halo and SNAP-mCherry-α(280-906) that is efficiently reversed after exposure to UV light (λ=350/50 nm). b) A line plot of the fluorescence intensity values for E-cadherin (GFP) and α-catenin (mCherry) along the white dashed line between the arrow heads in the fluorescence images shown in a). Scale bar 20 µm.

linked E-cadherin-α-catenin complexes. β-catenin localization was not affected during the formation and dissociation of E-cadherin-α-catenin complexes in A431D cells. Using live cell fluorescence microscopy (figure 12.7) it was possible to follow the recruitment of SNAP-mCherry-α(280-906) to Ec-GFP-Halo over time. Note that the cells were forming extensive overlappings with each other that were visible due to the GFP labeled membranes. Addition of Ha-pl-BG induced a translocation of SNAP-mCherry-α(280-906) from the cytosol to the plasma membrane via dimerization with Ec-GFP-Halo. After ca. 4 h the colocalization reached its maximum and stayed stable for several hours. Despite forming structures with high density of the E-cadherin and α-catenin constructs, reflected by high intensities of GFP and mCherry fluorescence, respectively, the dimerized complex was also detected in the overlapping extrusions. UV light (λ=350 nm) did cleave the dimerizer and released SNAP-mCherry-α(280-906) from the plasma membrane back into the cytosol. The peaks of Ec-GFP-Halo localization became broader which indicated less rigid organization of the cell-cell contact area. Directly after the light pulse some fractions of the α-catenin construct remained at the regions with previously high concentration of the E-cadherin-α-catenin complexes.

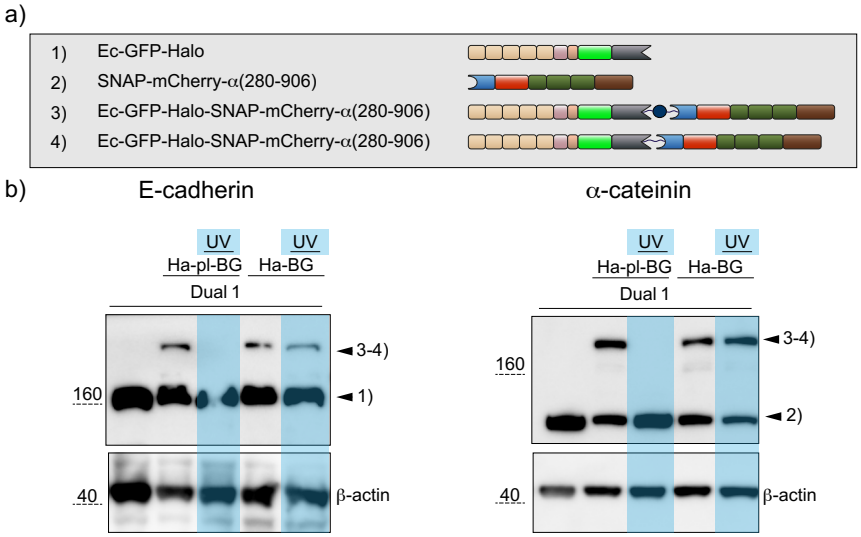

Figure 12.8: **Western blot analysis of dimerizer treated and UV exposed A431α-catenin KO Dual1 cells.**
a) Illustration of Ec-GFP-Halo and SNAP-mCherry-α(280-906) and the dimeric complexes that form in A431α-catenin KO Dual1 cells via treatment with photocleavable Ha-pl-BG (3) or non-cleavable Ha-BG (4). b) Immunochemical detection of E-cadherin (left) and α-catenin constructs (right) expressed in stable transfected A431D cells show additionally heavy bands for the dimeric Ec-GFP-Halo-SNAP-mCherry-α(280-906) complex. Dimers formed via Ha-pl-BG are dissociated upon UV light (λ=365 nm) exposure, while Ha-BG induced dimers stay intact. Sketches not to scale.

However, these remainings dissolved within 30 min and while also the Ec-GFP-Halo localization became more dispersed.

When testing the effects of dimerizer treatment and subsequent UV exposure in Dual1 expressing A431α-catenin KO cells, western blot analysis showed the same pattern of E-cadherin-α-catenin dimer formation that was reversible for Ha-pl-BG but not for Ha-BG treated cells (see figure12.8).

In immunostainings Dual1 transfected A431α-catenin KO cells looked similar to their A431D counterpart, regarding the localization of E-cadherin, SNAP-mCherry-α(280-906) and F-actin, but additionally to the nuclear localization β-catenin showed colocalization with clusters of the recombinant Ec-GFP-Halo at the plasma membrane (see figure 12.9). Although in close proximity to each other, cells were not connected to each other. Treatment with Ha-pl-BG led to the formation of E-cadherin-α-catenin dimers that colocalize with β-catenin. These complexes showed a strong accumulation in linear structures at cell-cell contact areas and association with F-actin forming closely connected cell clusters. Exposure to UV light induced decomposition of the tightly bound cell clusters leaving only tethered connections between retracted cells. This was clearly related to a disruption of the E-cadherin-α-catenin complexes as SNAP-mCherry-α(280-906)

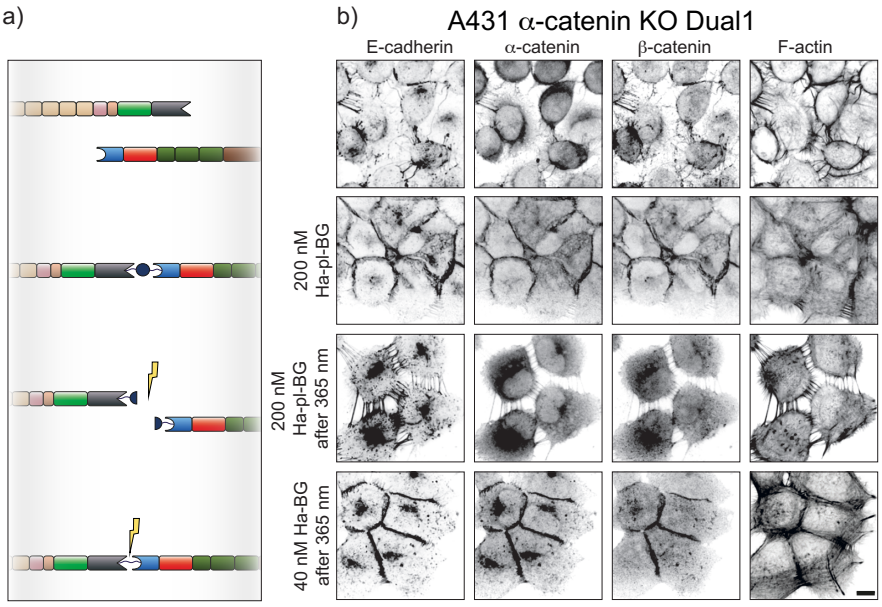

Figure 12.9: **Dimerizer treated A431 α-catenin KO Dual1 cells form straight cell-cell contacts containing β-catenin and disintegrate under formation of tether like structures after exposure to UV light.**

a) Illustration of dimer formation and dissociation between Ec-GFP-Halo and SNAP-mCherry-α(280-906) in A431 α-catenin KO Dual1 cells via treatment with photocleavable Ha-pl-BG or non-cleavable Ha-BG and UV light irradiation (indicated by the flash). b) Immunohistochemical stainings for β-catenin and F-actin recorded together with fluorescent signals from GFP (fused to E-cadherin) and mCherry (fused to α-catenin) show the rearrangement of AJ components within the cell before (first row), after incubation with Ha-pl-BG (second row) and after additional treatment with UV light (third row, λ=365 nm). The fourth row shows UV exposed cells that had been treated with Ha-BG as negative controls for dimerizer cleavage. β-catenin localization follows the formation and dissociation of E-cadherin-α-catenin complexes. Scale bar 10 µm. Sketches not to scale.

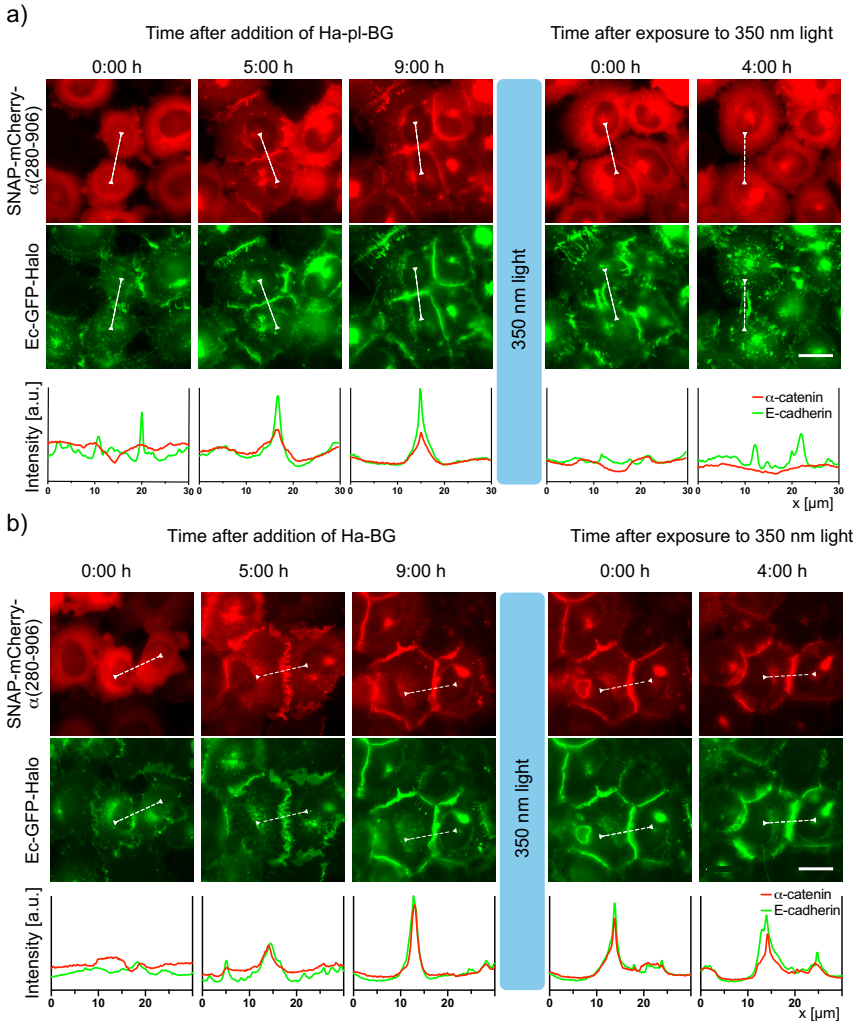

Figure 12.10: **Dimerizer induced E-cadherin-α-catenin complexes in A431 α-catenin KO Dual1 cells mature into defined linear complexes that are dissolved immediately after light induced dissociation.**

a) Fluorescent timelapse recordings of A431 α-catenin KO Dual1 cells after addition of Ha-pl-BG show the formation of E-cadherin-α-catenin complexes via colocalization of Ec-GFP-Halo and SNAP-mCherry-α(280-906). The dimerizer induced AJs mature into linear structures between cells that are immediately gone after exposure to UV light (λ=350/50 nm). E-cadherin rich membrane tethers remain transiently after dissociation of the AJs. The line plots below show fluorescence intensity values for E-cadherin (GFP) and α-catenin (mCherry) along the white dashed line between the arrow heads in the fluorescence images shown above. b) Same setup as in a) but cells are incubated with the non-cleavable dimerizer Ha-BG. AJs are stable for several hours after the same exposure to UV light as used in a). Scale bars 20 µm.

and β-catenin relocalized from the plasma membrane to the perinuclear region and the nucleus. E-cadherin stayed mainly at the plasma membrane e.g. in the elongated tether structures, but was also found inside the cells in vesicular structures. Although F-actin was also fond in the tethered connections between cells, its localization did not correlate with accumulations of Ec-GFP-Halo or SNAP-mCherry-α(280-906). If Ha-BG was used to induce E-cadherin-α-catenin dimer formation, the same UV intensity could not destroy the dimers and the cell clusters stayed closely connected with linearly arranged cell-cell contacts.

Following the process in living cells (figure 12.10), shows that Dual1 transfected A431 α-catenin KO cells did not form overlapping membrane extrusions as found in A431D cells. Instead, Ec-GFP-Halo formed transient aggregates in the plasma membrane, but SNAP-mCherry-α(280-906) did not colocalize with these clusters in absence of the dimerizer. However, as reported for A431D cells, when the dimerizer was added SNAP-mCherry-α(280-906) was recruited to the plasma membrane, thereby stabilizing the Ec-GFP-Halo aggregates. The E-cadherin-α-catenin dimers accumulated at cell-cell interfaces and expanded the contact areas increasingly into defined linear arrangements. Similar to the results presented for fixed samples, the cells treated with Ha-pl-BG (figure 12.10a) retracted from each other under formation of elongated membrane tethers when cleaving the dimerizer with a short pulse of UV light. SNAP-mCherry-α(280-906) was immediately released to the cytosol and did not translocate back to the membrane during the time course of this experiment. Most of the membrane tethers disassembled briefly after the light pulse, but some were maintained for several hours. Ec-GFP-Halo was accumulated in these tethers but also formed temporary aggregates in the plasma membrane and was intensively internalized. In contrast, Ha-BG treated cells (figure12.10b) were not affected by the same UV light exposure.

Another difference between Dual1 expressing A431D cells and A431 α-catenin KO cells was discovered during the live cell experiments. When imaged with phase contrast microscopy, without dimerizer both KO cell lines form highly diffractive monolayers i.e. they they appear with a bright halo ring around their cell body (see figure 12.11). While A431D cells did not change their appearance during incubation with the dimerizer, A431 α-catenin KO cells lost the halo effect. This means the monolayer became less diffractive which could be explained by a more homogeneously flattened cell layer in contrast to a cobblestone like arrangement without dimerizer. The appearance of the cells after incubation with the dimerizer widely resembles the morphology of A431 WT cells. Furthermore, cleaving the dimerizer indeed reversed the morphologic changes completely (please refer to section 12.2.2). This means that the formation of dimerizer induced

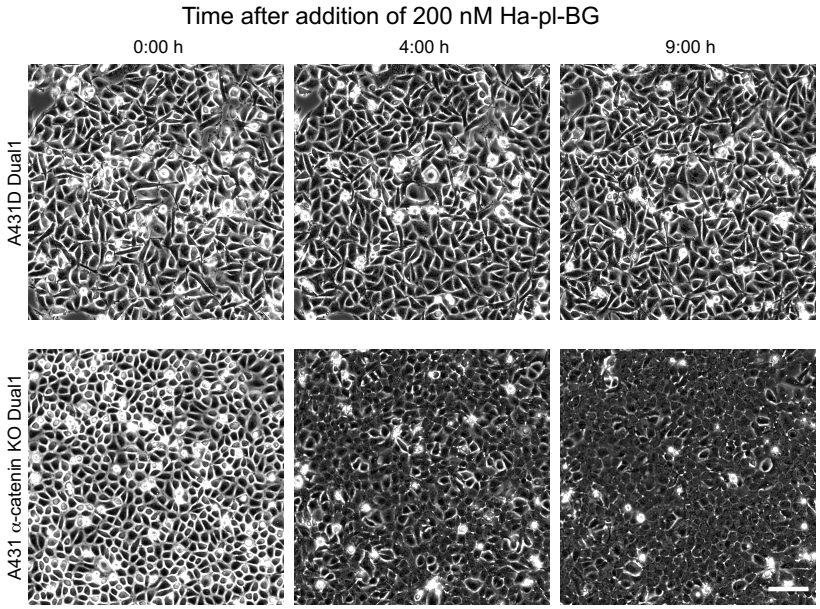

Figure 12.11: **Dimerizer induced E-cadherin-α-catenin complex formation initializes strong morphologic changes in confluent A431 α-catenin KO Dual1 cell layers, but not between A431D Dual1 cells.**
Phase contrast time lapse recordings of confluent monolayers of A431D Dual1 and A431 α-catenin KO Dual1 cells after addition of Ha-pl-BG. A431 α-catenin KO Dual1 cells show a strong reduction of diffracted light (bright "halo" around rounded cells), but A431D Dual1 cells stay morphologically unchanged during the formation of E-cadherin-α-catenin complex. Scale bar 100 µm.

E-cadherin-α-catenin complexes could rescue A431 α-catenin KO, but not A431D cells in terms of monolayer morphology. To summarize, dimerization of Ec-GFP-Halo and SNAP-mCherry-α(280-906) could be proven to occur in both Dual1 transfected cell lines and depended on the administration of the small molecules Ha-pl-BG or Ha-BG. If the dimers were formed using Ha-pl-BG they could be dissociated via exposure to UV light, while the Ha-BG formed dimers were stable under UV light exposure. In A431 α-catenin KO cells formation of the E-cadherin-α-catenin dimers led to recruitment of β-catenin to the cell-cell contact sites, while β-catenin was not affected in A431D cells. As discussed in section 12.1.2 for the fusion construct Ec-GFP-α(280-906), β-catenin might be indirectly recruited via lateral clustering of actomyosin connected E-cadherin-α-catenin dimers with endogenous E-cadherin. In A431 α-catenin KO cells treatment with dimerizer induced a morphological switch towards the phenotype of A431 WT cells, while A431D cells did not change their morphology. The dimerizer mediated complexes in A431 α-catenin KO cells were considered to be functional AJs as they built a connection between neighboring cells via E-cadherin, β-catenin and α-catenin connected with the acto-

myosin network. Since the protein complexes that formed in A431D cells after dimerizer administration did not contain β-catenin and could not rescue the A431 WT phenotype, they were not considered to be functional AJs and will be called AJ like complexes hereafter.

While in A431 α-catenin KO cells cleaving Ha-pl-BG directly led to a full relocation of SNAP-mCherry-α(280-906) to the cytosol and an immediate retraction of the cells from each other under formation of extended membrane tethers, in A431D cells a significant amount of SNAP-mCherry-α(280-906) transiently remained at the cell-cell contact sites. Furthermore, A431D cells did not retract from each other and did not form membrane tethers upon light induced dissociation of the AJ like structures. A possible explanation for this difference could be that the AJ like structures in A431D cells are connected to the actomyosin network as shown in the immunofluorescence stainings, but the connection is under much lower tension than in A431 α-catenin KO cells. When releasing the α-catenin construct that is interacting with a network under low tension, α-catenin might be retained at the actin rich cell outline, while in cases of high tension, the actomyosin network contracts immediately and thereby withdraws α-catenin from the plasma membrane. A higher stress load on dimerizer mediated AJs in A431 α-catenin KO cells would also explain the immediate retraction of cells after light induced dissociation of AJs. The tether structures that form during this retraction are unlikely to arise from clusters of incompletely dissociated AJs, since no accumulation of SNAP-mCherry-α(280-906) were found in the immunostainings and the western blot analysis of samples treated with the same light intensity showed the complete disruption of the dimers. Possibly, the reconstituted AJs triggered the formation of other cell-cell contact structures like desmosomes or tight junctions. When the AJs were dissociated, these structures would stay intact and would have to maintain the stress load that what was built up between the cells without support from the AJs and would therefore stretch the membrane on tubular structures to transiently maintain the cell-cell connections, while the cell body is retracting. To proof this concept immunostainings for desmosomal or tight junction markers should be done.

The intracellular vesicular structure containing Ec-GFP-Halo found in A431 α-catenin KO cells indicate an increased internalization of E-cadherins after light induced dissociation of the AJ complexes. Since these E-cadherin loaded vesicles did not occur after exposure to UV light in cells incubated with Ha-BG, they are unlikely to arise from a an unspecific stress reaction to the UV light. They might rather be explained by an increased uptake of E-cadherin that is destabilized in its plasma membrane localization due to missing connection to the actomyosin network as discussed in 2.2.1or reviewed in Delva et al. [153].

12.2 LIGHT INDUCED DISSOCIATION OF ADHERENS JUNCTIONS WITH HIGH SPATIAL PRECISION

Having shown the formation of dimerizer induced AJs in A431 α-catenin KO cells and the possibility to dissociate them with light, the next aim was to test the applicability and flexibility of this tool to manipulate epithelial cells at different length and time scales. Using light as a trigger offers the ability to dissociate dimerizer mediated AJs not only at defined timepoints as demonstrated in the previous section, but should also allows to target defined regions within an epithelial monolayer or when using higher magnification also subcellular regions of cell-cell contacts. To do so a 405 nm laser in a laser scanner unit was mounted on the microscope. Using a 405 nm laser instead of wide field near UV light exposure had multiple advantages. Despite the low light doses necessary to cleave the Ha-pl-BG dimerizer, using visible light instead of near UV light reduced potential DNA damage caused by irradiation with high energetic wave lengths. Furthermore, the spot size of the laser could be set to sub-micrometer size to achieve high spatial precision and the scanner unit allowed to target subregions with various shape and size in the field of view.

12.2.1 *Adherens junctions can be dissociated with subcellular precision*

As shown in figure 12.12 A431 α-catenin KO Dual1 cells were treated with Ha-pl-BG and formed defined AJ outlining the cell-cell contact areas. For dissociation of AJs in subcellular regions, AJs at the interface of two adjacent cells (area outlined in white dashes) were targeted with the 405 nm laser. By measuring the fluorescence intensity profiles (figure 12.12b+c) across the targeted AJs (line 1) in comparison with non-targeted AJs (line 2) showed that before cleaving Ha-pl-BG the α-catenin construct (red) colocalized with the E-cadherin construct (timepoint -01:00 min). Directly after laser irradiation (timepoint 00:00 min), the α-catenin peak disappeared at the targeted AJ, and AJ dissociation led to detachment of the cells from each other (timepoint 05:00 min). Cell-cell attachment and colocalization of E-cadherin and α-catenin at the non-targeted AJs were not affected. Kymograph analysis (figure 12.12 b) showed that the E-cadherin intensity stayed stable until the cells start to detach from each other ca. 60 seconds after irradiation. This indicated that even without connection to the actomyosin network E-cadherin at least transiently remained clustered, but could not build enough adhesive strength to maintain the connection between the cells. Herewith it was proven that dimerizer mediated adherens junctions could be dissociated with subcellular precision. The frame rate in these experiments was on a scale of seconds, but could be reduced to subsecond resolution if necessary.

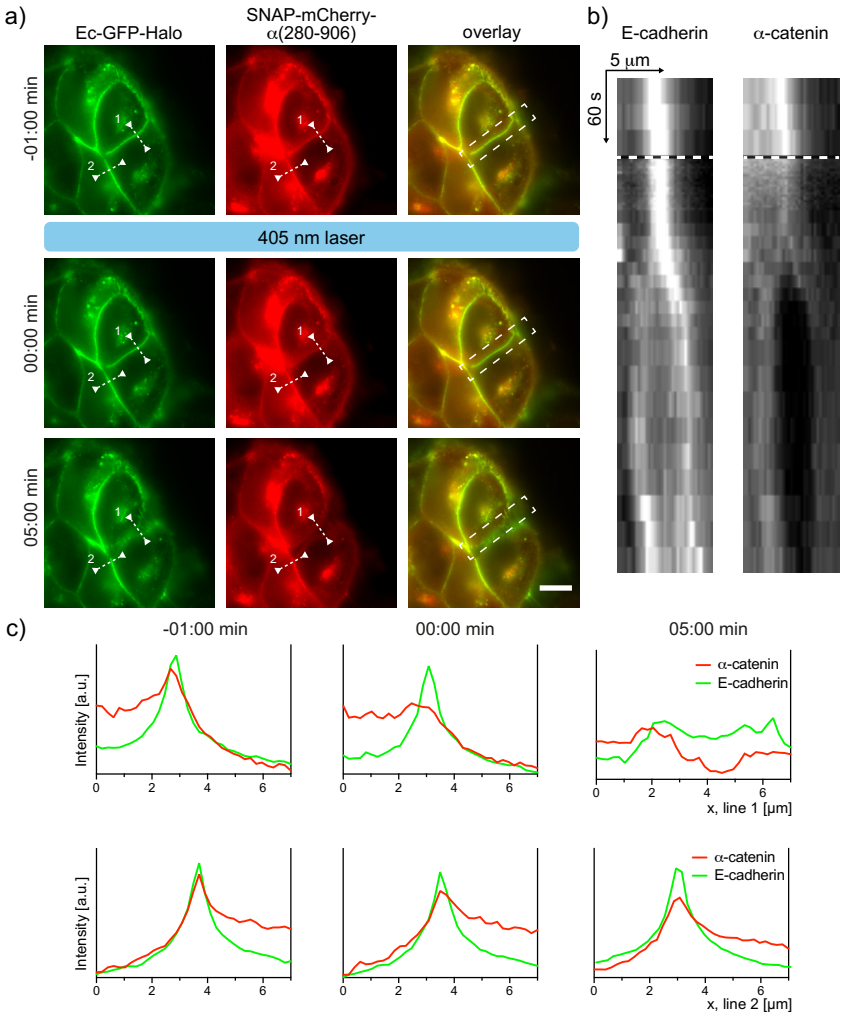

Figure 12.12: **Dimerizer mediated adherens junctions can be dissociated with subcellular precision using a 405 nm laser.**
a) Detaching of cells at targeted AJs is followed in a fluorescence time lapse recording. Irradiation of AJs of two adjacent Ha-pl-BG treated A431 α-catenin KO Dual1 cells with a 405 nm laser (area outlined in white dashes) directly before timepoint 00:00 min dissociates targeted AJ between two adjacent cells without affecting untargeted AJs. b) Kymograph of the targeted AJ along line 1 (white dashed line between arrowheads in a)) for E-cadherin (GFP fluorescence) and α-catenin (mCherry fluorescence) signal shows the immediate dispersal of α-catenin after laser irradiation (black and white dashed line), while E-cadherin dissociates only after 60 seconds. Note that the kymograph is displayed corrected for different frame rates used in this recording. The frame rate was adopted dynamically to the occuring process to reduce bleaching effects. c) Line plots for E-cadherin (GFP) and α-catenin (mCherry) intensities of the cross sections of targeted (line 1) or untargeted (line 2) AJs indicated by white dashed lines between arrowheads in a). Scale bar 10 µm.

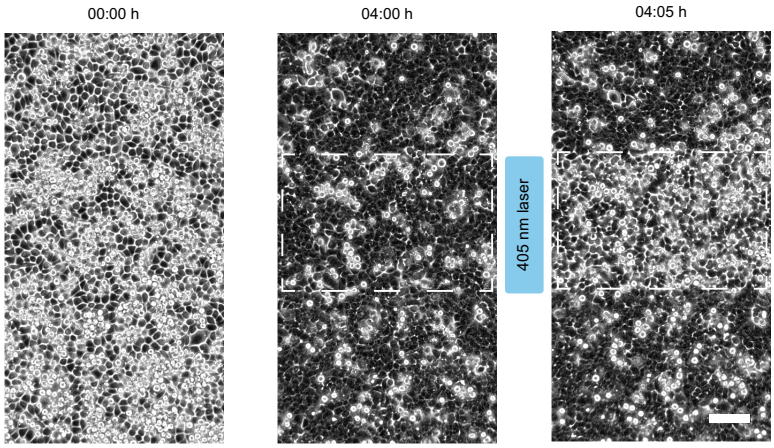

Figure 12.13: **Dimerizer mediated compaction of adherent monolayer can be reversed in confined areas.**
Highly diffractive round cells laying loosely attached on top of an overconfluent surface attached layer of A431 α-catenin KO Dual1 cells. Incubation with Ha-pl-BG induces the formation of dimerizer mediated AJs within 4 h that leads to a less diffractive morphology. During this process the round cells integrate into the cell layer and increase the compaction of surface attached cells. A 405 nm laser is used to cleave the dimerizer in the area marked by the white dashed outline between two frames of the phase contrast time lapse recording (one frame every 5 min). Dissociation of dimerizer mediated AJs causes the compacted cell layer to disseminate by cells detaching from the surface only in the targeted area. Scale bar 200 µm.

12.2.2 *Dimerizer induced compaction of epithelial monolayers and disintegration in defined patterns*

A431 α-catenin KO cells did not stop to proliferate when reaching full confluence, although when undergoing cytokinesis the dividing cells could not reintegrate into the monolayer. Instead, the newly formed cells stayed loosely attached in a spherical shape on top of the adherent cell layer. As shown in figure 12.13 (00:00 h) the round cells were highly diffractive and appeared as bright spheres in phase contrast images. After addition of Ha-pl-BG, the cells started to form AJs and the round cells integrated into the monolayer. This compaction was characterized by reduced scattering of light around the cell body in the phase contrast images (04:00 h). The 405 nm laser was used to cleave the dimerizer and thereby trigger AJs dissociation in the area marked by the dashed outline in figure12.13 (04:05 h). In the targeted area the compacted cell layer immediately disseminated and pushed out cells that had been integrated during the compaction, whereas the monolayer in the non-targeted area maintained the compacted, low diffractive morphology. Note that from the time lapse recording it could be seen that the few highly diffractive cells in the non-targeted are either cells that were in the process of cytokinesis and reintegrated into the cell layer after cell fission or were not re-

sponding to the dimerizer treatment over the full time course of the experiment. The later were mainly cells that did not express sufficient levels of Ec-GFP-Halo or SNAP-mCherry-α(280-906) as could be seen in fluorescent imaging (data not shown).

These experiments showed that the induction of dimerizer mediated AJs is not only passively changing the appearance of a adherent cell layer, but the monolayer underwent an active compaction by reintegrating previously expelled cells. Furthermore, the process could be reversed completely by cleaving the dimerizer that maintained the AJs.

12.3 COLLECTIVE CELL MIGRATION AND CONTRACTION

To proof whether the dimerizer mediated AJs were functional in terms of force transmission, the cells were analyzed for their collective behavior. If the AJs were mechanically connecting cells they should not only influence their direct neighbors but be able to transmit the exerted forces across the surrounding cells as described in section 2.2.1. Thereby, they should be able to coordinate the direction of their movement and pulling forces over distances of several cell diameters (see section 2.3 and **??**).

12.3.1 *Dimerizer mediated cell adhesion increases coordination in the migrating cell layer*

Despite being a well established model to study adherens junctions A431 cells (and therefrom derived KO cells) are known to have very low migratory activity without external stimuli[154]. However it was possible to stimulate cell migration in a modified wound healing assay. Cells were cultured in a confined area to form a confluent cell monolayer. When the confinement was removed, the cells migrated into the open space (see figure 12.14). Unlike in a standard wound healing assay, where two opposing cell fronts are investigated for the time they need to close the gap between them, only a single front of migrating cells was studied. The migration was analyzed by calculating the correlation length in a velocity field that was derived from consecutive phase contrast images via particle image velocimetry (PIV). Since the cells were prone to migrate into the open space (defined as axial direction) due to the experimental setup, only the lateral components of the velocity vectors were considered for the calculation of the correlation length. Therefore, the lateral correlation length or correlation diameter is a measure of how far cells could align their motions[123, 124]. As shown in figure 12.14 the lateral correlation diameter calculated for Ha-pl-BG treated Dual1 expressing A431 α-catenin KO cells was 258.0 +/- 4.9 µm while for the same cells without the dimerizer it was 165.5 +/- 1.4 µm. Thus, the lat-

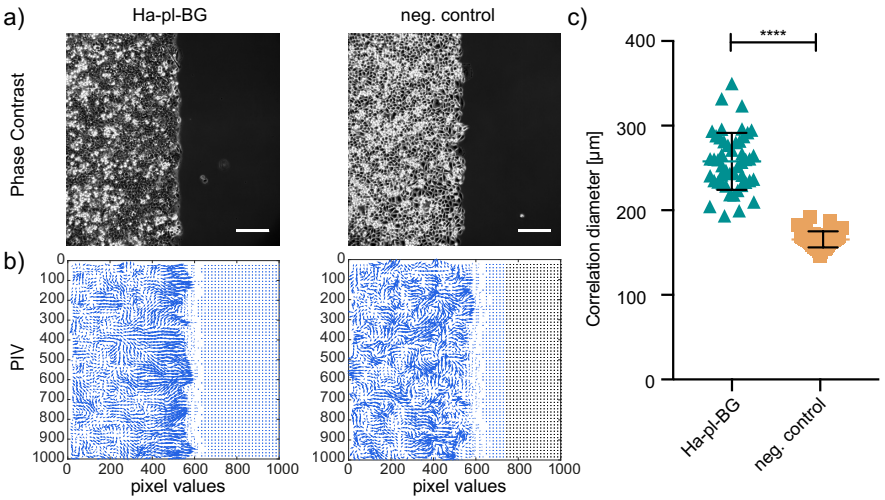

Figure 12.14: **Cells with dimerizer induced adherens junctions show higher degree of collectivity.**
a) Time lapse phase contrast recordings of a migration front of A431 α-catenin KO Dual1 cells with Ha-pl-BG and a negative control control layer of the cells without dimerizer in a rupture free wound healing assay 2 h after removal of the confinement. b) PIV analysis of collective cell migration of two consecutive frames (Δt: 5 min) show higher turbulances in the velocity vector field calculated for the monolayer of cells without dimerizer. c) Analysis of the lateral component of the velocity vectors shows a significantly higher correlation diameter for Ha-pl-BG treated cells (258.0 +/- 4.9 µm) then for the negative control without dimerizer (165.5 +/- 1.4 µm). ****p<0.0001 Scale bar 200 µm.

eral correlation diameter was significantly higher (p<0.0001) for cells with dimerizer mediated AJs. In a second approach presented in figure 12.15Ha-pl-BG treated cells were irradiated with the 405 nm laser in the middle of the experimental time course, to test if the higher correlation diameter was directly dependent on the presence of AJs. When analyzing the collective migration behavior for cells in the targeted area a significantly different (p<0.0001) average correlation diameter that was calculated with 184.1 +/- 5.5 µm before and 136.1 +/- 2.7 µm after light induced dissociation of the AJs. The experiments showed a dimerizer dependent increase of collectivity in the migrating cell layer and that the collectivity could be immediately reduced by disrupting the AJs. This indicated that the cells are mechanically linked via the dimerizer mediated AJs. The differences for the correlation diameters of Ha-pl-BG treated cells between the two experiments could have been caused by various interdependent parameters. Although the cells were always freshly sorted before and seeded in the same number for each experiment, differences in the cell number and resulting cell density within the confined monolayer could have occurred from variations in the sorting performance due to recurrent technical problems and therefrom resulting reductions in cell viability and incubation times. Nevertheless, the relative shifts

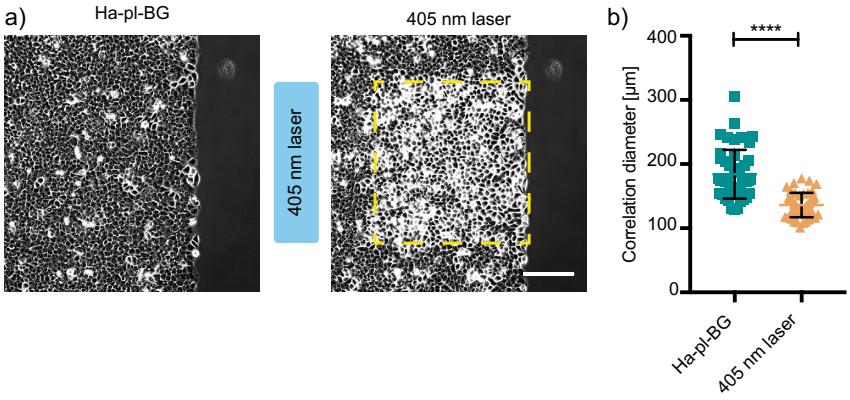

Figure 12.15: **Light induced dissociation of adherence junctions shortens the coordination of cell motions.**
a) Time lapse phase contrast recordings of a migration front of A431 α-catenin KO Dual1 cells preincubated with Ha-pl-BG in a rupture free wound healing assay before and after 405 nm laser irradiation of the area marked with dashed yellow outline. b) The correlation diameter of the lateral component of the velocity vectors is significantly higher before laser irradiation for the cells in the targeted area (before (Ha-pl-BG): 184.1 +/- 5.5 µm; after (405 nm laser): 136.1 +/- 2.7 µm) directly after light induced dissociation of dimerizer mediated AJs. PIV analysis was done from timelapse recordings (Δt: 5 min) 2 h before and after laser irradiation. ****p<0.0001 Scale bar 200 µm.

in the correlation diameter between cells with or without dimerizer mediated AJs is consistent throughout the different experiments.

12.3.2 *Light induced dissociation of adherence junctions discontinues collective contractility*

Since the coordinated migration suggested a mechanical coupling between cells with dimerizer mediated AJs the next aim was to investigate if this was also reflected by the forces exerted on the underlying substrate. Therefore, the wound healing assay was combined with traction force microscopy measurements as shown in figure 12.16. The cells were grown in the confinement on a collagen coated PAA gel with a Young's modulus of 200 Pa. When the cells with reconstituted AJs were released from the confinement traction forces were highest along the migration front and increased over one hour before reaching a steady state. Traction forces at the migration front exert stresses of 7-10 Pa on the gel, while the stresses measured under the cell monolayer were much lower (maximum 4 Pa). When cleaving the dimerizer, large numbers of cells were immediately extruded from the cell layer and the tractions at the migration front gradually decreased and spread throughout the cell layer in irregular patterns. After 1-2 h the traction forces at the migration front became as low and disorganized as under the migrating cell layer. Therefore,

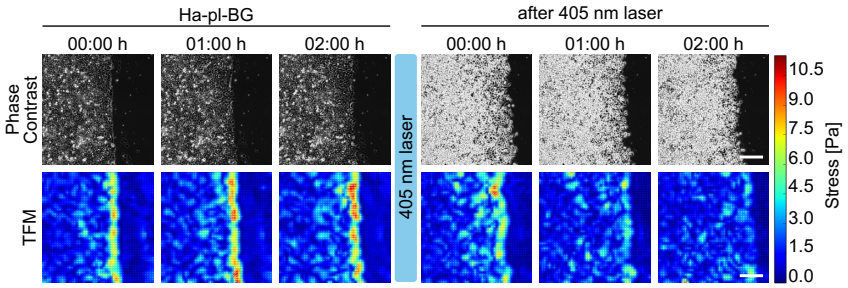

Figure 12.16: **High traction forces at the migration edge dissolve after light induced dissociation of adherence junctions.**
Combination of the rupture free wound healing assay and traction force microscopy (TFM) reveals high traction forces at the migration front of a confluent layer of Ha-pl-BG treated A431 α-catenin KO Dual1 cells. The cell layer becomes highly diffractive immediately after irradiation of the whole field of view with a 405 nm laser and the traction forces at the migration front decrease gradually. Scale bar 200 µm.

it could be shown that dimerizer mediated AJs maintained a mechanical connection between the cells in the monolayer, that allowed them to couple contractile forces. By pulling collectively, the cells could exert much higher forces at the migration front before the dissociation of their AJs. If the gradual decrease of traction forces at the migration front is solely caused by the disruption of AJs or pushing forces of the extruded cells also contribute to this process could not be conclusively clarified. However, it was observed, that cells that were extruded directly after dissociation of AJs reattached to the surface while the migrating cell layer spread out.

Part IV

CONCLUSION AND OUTLOOK

13 CONCLUSION

In this work I developed the first optochemical tool to control the formation of mechanically active adhesion protein complexes inside living cells. The method is based on chemically induced dimerization of proteins or protein domains via photocleavable dimerizers. It is bioorthogonal, because it does not interfere with signaling pathways or proteins others then the ones targeted. The dimerizers I applied are bifunctional small molecules that combine the ligands of two self-labelling tags via a photocleavable linker and therefore can mediate the binding between these protein tags in a light reversible manner. These self-labelling tags can be fused to any protein of interest. The modularity of this dimerizer binding cassette offered me an easy way to test multiple combinations of target proteins and finally led to the herein presented method to control the activity of intracellular proteins with unprecedented spatiotemporal precision.

I synthesized a Halo and SNAP tag binding dimerizer and used this to achieve covalent-covalent binding between the targeted proteins to ensure mechanical stability of the dimerizer induced protein complexes. Furthermore, I solved the stoichiometric problem of the tripartite binding complex. I controlled the expression levels of target proteins via bicistronic expression vectors and optimized the conditions for dimerizer administration to avoid the formation of monoreacted species. Additionally, I showed the possibility to combine the Halo and SNAP tag binding dimerizer with Halo and DHFR tag binding dimerizer for multiplexed dimerization and light induced release in a mitochondrial sequestration setup. By combining photocleavable and photostable dimerizers this system offers a great combinatorial flexibility and thus has great potential for applications in synthetic biology to create e.g. signaling circuits by sequential binding of effector proteins.

I tested three different concepts, retention, recruitment and complementation to apply the dimerizers in the context of adhesion complex formation. I induced sequestration of the FA proteins vinculin and paxillin at the outer mitochondrial membrane. Although further optimizations will be necessary, I could show that it is possible to retain these proteins from integration into FAs by translocation to a cellular compartment where they are functionally inactivated but structurally intact and can be released by cleaving the dimerizer with light. The recruitment concept I applied to control the binding between AJ proteins. I replaced the binding sites of E-cadherin for their intracellular adaptor proteins (e.g. β-catenin and p120-catenin) with a Halo tag and proofed that these proteins are expressed and local-

ized in the plasma membrane, but cannot form stable AJs or bind β-catenin. However, when coexpressed with SNAP tagged α-catenin or β-catenin the protein-protein interaction could be restored via chemically induced dimerization. I could obtain similar results for the intracellular complementation of E-cadherin by recruiting the cytosolic domain to a tailless E-cadherin. The complementation of the extracellular domain of E-cadherin however was technically challenging. I proofed the extracellular presentation and ligand binding capabilities of an E-cadherin where the EC12 domain was replaced with a SNAP tag in living cells. Furthermore, I established a protocol for bacterial expression and proteolytic N-terminal processing of a Halo tagged EC12 domain that could be successfully bound to the extracellularly truncated E-cadherin.

I characterized the different effects of the formation of AJs after chemically induced E-cadherin-α-catenin dimerization in E-cadherin deficient A431D cells and A431 α-catenin KO cells in comparison to A431 wt cells. Thereby I found that the reconstitution of AJs could restore the tightly packed wt phenotype in A431 α-catenin KO cells, but not in A431D cells. I could relate this to the fact that the chemically induced E-cadherin-α-catenin dimers as well as the control E-cadherin-α-catenin fusion protein failed to recruit β-catenin to the E-cadherin-α-catenin dimers in A431D cells. By uncoupling β-catenin recrution from direct binding to α-catenin, I could show that β-catenin is essential for the formation of AJs but unlike vinculin or α-catenin it does not need to be under tension to be fully activated.

For A431 α-catenin KO cells however, I could show that the dimerizer mediated AJs contained also β-catenin and induced a morphological transition from KO to wt phenotype. Using low doses of a blue light 405 nm laser to cut the dimerizer, I could dissociate the reconstituted AJs with subcellular precision and trace the detachment of cells. On a monolayer scale, laser scanning could be used to disseminate tightly packed dimerizer treated cells in defined patterns and follow the rearrangements of the monolayer. Moreover, in a collective monolayer migration experiment, I could increase the correlation of cell motion via dimerizer induced AJ formation and cancel the correlation via cleaving the dimerizer with light. Finally, I could proof that the dimerizer induced AJs also facilitate collective contraction as in TFM measurements they did build up strong traction forces at the migration front that vanished after light induced dissociation of the AJs.

The use of photocleavable dimerizers to control the formation of adherens junction complexes offers two binary switches: a systemic "ON switch" via addition of the dimerizer to induce reconstitution of AJ and a spatiotemporally precise "OFF switch" by cutting the dimerizer with 405 nm or near UV light to disseminate the AJ complex. The possibility of patterned deactivation and combination with

specialized imaging techniques like TFM makes it a powerful tool to study the mechanobiology of AJs and its contribution to collective migration and stress propagation in epithelial cell layers. I am confident that this will help to understand the mechanical aspects of dynamic regulation of AJs and their biological effects in the context of EMT as it is essential for embryonal development, wound healing or cancer metastasis.

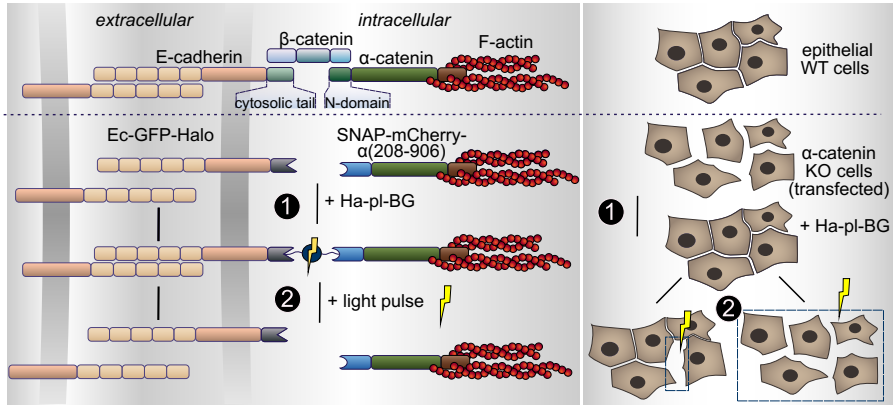

Figure 13.1: **Summary sketch.**
Light induced dissociation of dimerizer mediated adherens junction complexes allows to abort actomyosin coupled cell-cell adhesions with high spatiotemporal precision on subcellular, single cell or tissue lenght scale.

14 OUTLOOK

14.1 E-CADHERIN-α-CATENIN DIMERS INITIATE FORMATION OF DESMOSOMES IN A431 α-CATENIN KO CELLS

One of the open questions about the presented tool of light induced dissociation of AJs in A431 α-catenin KO cells is the origin of the tether structures that arise directly after cleaving the dimerizer. The hypothesys was that the reconstitution of AJs enables cell-cell contacts, that are further manifested by the formation of other cell adhesion structures like desmosomes, tight junctions and gap junctions. Cleaving the dimerizer however, affects AJ dissociation only, while other adhesion complexes stay intact.

Indeed, immunofluorescent staining of A431 α-catenin KO Dual1 cells for the desmosomal marker desmoplakin (see section2.2) showed that without dimerizer the cells are not able to connect their intermediate filaments (figure 14.1 a) while in presence of the dimerizer intracellular cables of cytokeratin are linked via desmosomal plaques (figure 14.1 b). After exposure to UV light, cytokeratine was found to stretch through the tethered structures that form after light induced dissociation of AJs and the desmosomal plaques were situated right in the middle of the tethers.

Apparently, the tethers arise from the desmosomal connections of cytokeratin, that are at least transiently resistent to the ripping apart of cells. Whether also other adhesive structures contribute to the formation of these tethers is under current investigation.

The observation that desmosomes are involved in the dimerizer induced transition from KO to WT phenotype in A431 α-catenin KO cells could also explain why A431D cells fail to undergo this transition. Lewis et al. reported that A431D cells fail to form desmosomes after E-cadherin rescue transfection due to low level of plakoglobin[85]. While plakoglobine alone is not sufficient either, double transfection with E-cadherin and plakoglobin on the other side does regain the ability to reorganize desmosomal structure in their experiments. Therefore, it should be possible to induce the switch from KO to wt phenotype in A431D Dual1 cells that are cotransfected with plakoglobin.

14.2 INTRACELLULAR E-CADHERIN COMPLEMENTATION - APPLICATION AND PHYSIOLOGICAL RELEVANCE

As demonstrated in this work, dimerizer induced E-cadherin-α-catenin complexes are able to restore mechanical connection in α-catenin KO

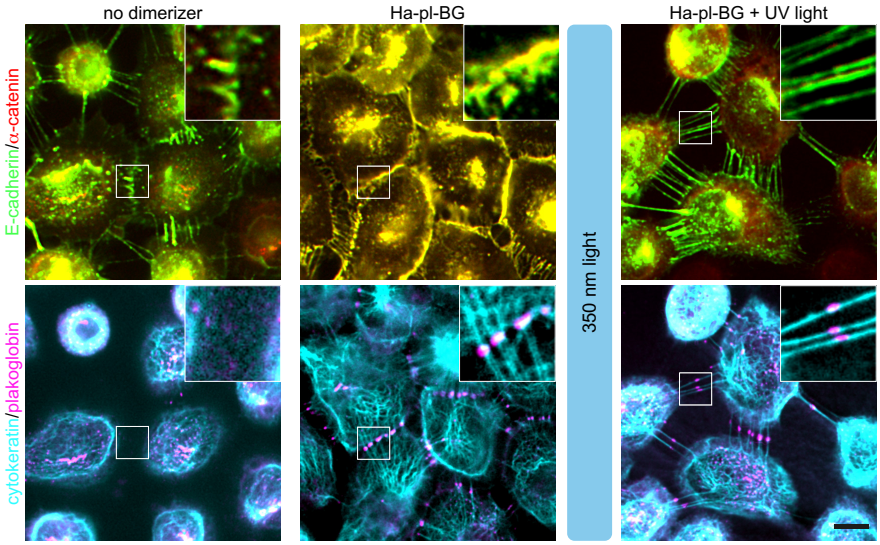

Figure 14.1: **Desmosomes transiently persist adherens junction dissociation.**

cells. The design of the construc made it possible to show that AJs can be functionally restored without incorporating β-catenin in the mechanically stressed protein complex. However, this is not reflecting the physiological situation and might lack important mechanisms that regulate AJ dynamics. As presented in section 11.3 it was also possible to recruit the cytosolic domain of E-cadherin to a tailless E-cadherin in REF52 fibroblasts. As discussed, fibroblast are an inadequat model for the reconstitution of AJs via E-cadherin complementation, because they express only very little amounts of β-catenin and α-catenin. Meanwhile, a MDCK E-cadherin KO cell line was generated in the Ladoux-Mège lab that is still forming AJs via cadherin-6, but these AJs are weaker in terms of stresses that can be build up between the cells [118].

A bicistronic vector that combines a Halo tagged tailless E-cadherin (E-cadherin-Δ-cyto-Halo) and the DHFR-EGFP tagged cytosolic E-cadherin domain (DHFR-EGFP-cytotail) was transfected into the MDCK E-cadherin KO cells. While DHFR-EGFP-cytotail is strictly cytosolic on the absence of dimerizer (data not shown) it is efficiently recruited to the plasma membrane presumably via binding to E-cadherin-Δ-cyto-Halo upon addition of Ha-pl-TMP (figure 14.2). The effects of E-cadherin complementation on cell adhesion strength, collective migration behaviour and contraction of MDCK monolayers is currently under investigation in collaboration with the Ladoux-Mège lab.

It should be mentioned that the DHFR-EGFP-cytotail construc used here contains the full cytosolic domain and should therefore enable interaction with all endogenous binding partners (e.g p120-catenin and β-catenein) and full regulation via phosphorylation [89]. Furthermore, the release of this domain via photocleaving the Ha-pl-TMP

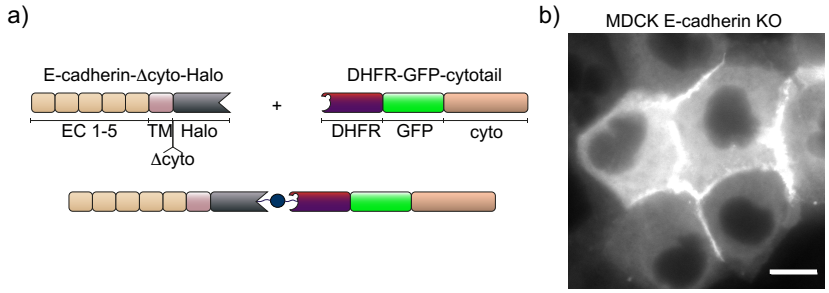

Figure 14.2: **The DHFR tagged cytosolic domain of E-cadherin is recruited to a Halo tagged tailless E-cadherin via the dimerizer Ha-pl-TMP.**
a) Sketch illustrating the intracellular complementation setup. b) DHFR-GFP-cytotail is recruited to E-cadherin-Δ-cyto-Halo after addition of Ha-pl-TMP. Scale bar 10 µm. Sketches not to scale.

dimerizer reflects the cleaving of endogenous E-cadherin between the aa577 and aa588 by γ-secretase[155] . The fragment is associated with Alzheimer´s disease[155] and might be involved in pathways regulating proliferation and apoptosis[88, 148][88, 148], but the excact mechanisms are still elusive. By offering high spatiotemporal control for the release of this fragment dimerizer mediated complementation of E-cadherin will be a powerfull tool to invastigate on these pathways.

14.3 NEURAL CREST CELLS ON THE MOVE - AN APPLICATIONS FOR SPATIOTEMPORAL CONTROL OF ADHERENS JUNCTION

Neural crest cells are specifc group of cells that arise transiently during embyonal development in all vertebrates and give rise to various tissues and organs like the skull bone and cartilage, neurons and glia cells in the peripheral nervous system and the aortic outflow tract of the heart[103, 156]. They originate from the neuroepithelium that forms the neural tube and accumulate at the boarder to the ectoderm (figure 14.3 a). During a process called delamination they undergo EMT, which makes them more motile and allows them to spread across the embryo before differentiating into the desired cell type [76] (figure 14.3 b,c). As a hallmark of EMT they downregulate E-cadherin and upregulate N-cadherin and integrin β, which allows them to become migratory and crawl in between the sourrounding tissue.

The group of Roberto Mayor established a model system of neural crest explants from *Xenopus* embryos to analyze the migration behavior during this process[157, 158]. They could show that the E- to N-cadherin switch control a behaviour that is known as "contact inhibition of locomotion" (CIL). During CIL forces are redistributed from cell-cell to cell-matrix contacts and E-cadherin represses CIL[156, 157].

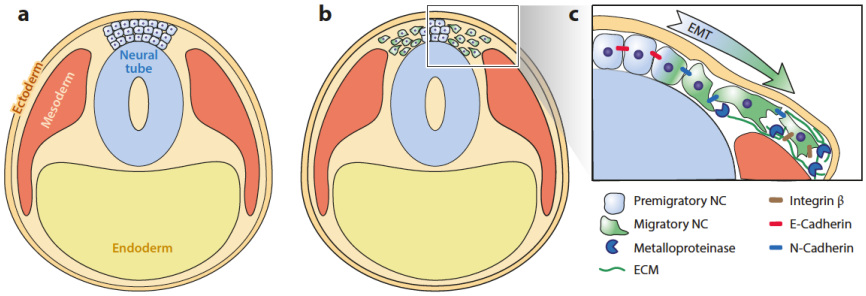

Figure 14.3: **Neural crest cells are undergoing EMT to spread in the developing embryo before differentiating into various tissues.**
Figure originally from Szabó et al.[156].

Currently it is tested if the dimerizer mediated reconstitution of adherens junctions can help to control the onset of migration of explanted neural crest cells and thereby help to understand this fundamental process.

14.4 TALIN COMPLEMENTATION - A TOOL TO CONTROL FOCAL ADHESION COMPLEX FORMATION

To extend the dimerizer mediated control of cell adhesion from cell-cell adhesion to cell-matrix adhesion complexes the complementation of split protein approach is currently tested for talin (see also section 2.2.3). The group of Carsten Grashoff generated a mouse fibroblast cell line that is deficient of both isoforms talin-1 and talin-2, which led to strongly impaired cell-matrix adhesion (figure 14.4a). Transfection with a C-terminally tagged talin-1 or a talin-1 with a FRET based tension sensor (TS) could restore the typical fibroblast spreading behaviour and formation of defined FA complexes (see figure 14.4b). The incorporation of the TS module between the head and the rod domain (figure 14.4c) did not perturb the function of talin, which makes it an ideal position for incorporation of a dimerizer binding cassette. It is planned to replace the TS module with the EGFP-Halo-IRES-SNAP-mCherry sequence from the Dual1 construct, which will create a split talin where the head domain carries the EGFP-Halo tag and the rod doamin is fused to the SNAP-mCherry tag coexpressed from a bicistronic vector due to the IRES sequence. If coexpressed in the talin double deficient cells, the dimerization of TalinHead-EGFP-Halo and SNAP-mCherry-TalinRod can be induced with Ha-pl-BG and reversed with light, analogue to the Dual1 construct presented in this thesis. Cloning of the split talin is currently in progress.

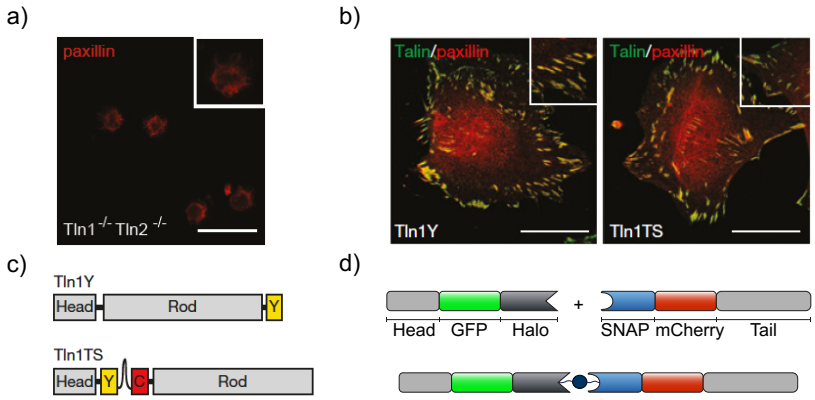

Figure 14.4: **Talin as a target for dimerizer controlled cell-matrix adhesion.** a) Cell adhesion and spreading is impaired in double knock out cells for talin1 and talin 2, but b, c) can be rescue transfected with C-terminally YFP tagged talin1(Tln1Y) or tension sensor talin Talin1TS. d) The tension sensor module will be replaced by a dimerizer binding cassette, which generates a split talin protein, that can be reconstituted with Ha-pl-TMP dimerizer. Figure adapted from [107]. Scale bars: 20 µm. Sketches not to scale.

Part V

APPENDIX

A

SUPPLEMENTARY FIGURES

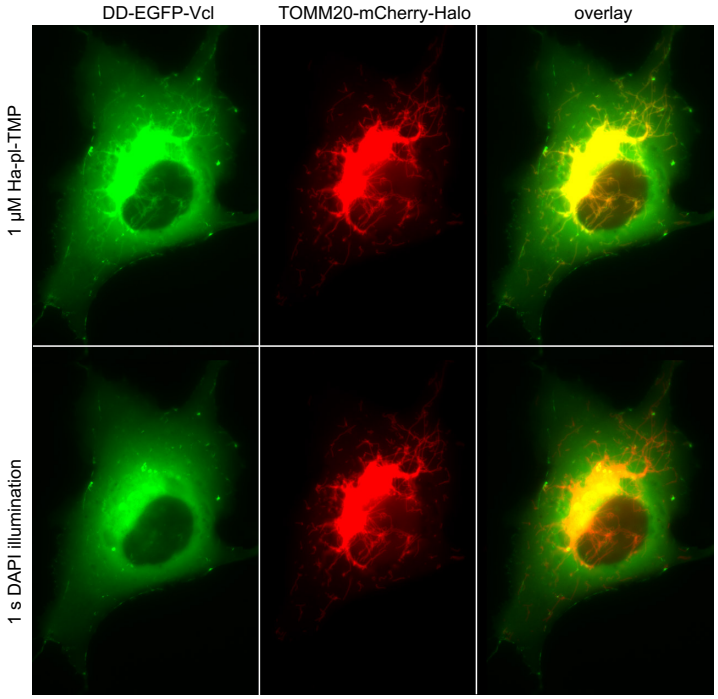

Figure A.1: Mitochondrial retention of DD-EGFP-Vcl.

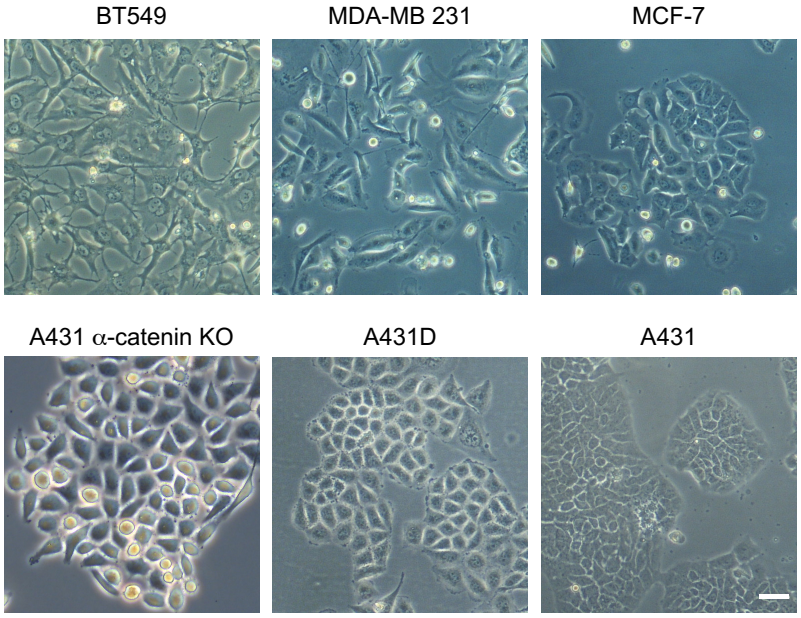

Figure A.2: Phenotypic variations of epithelial cancer cell lines.

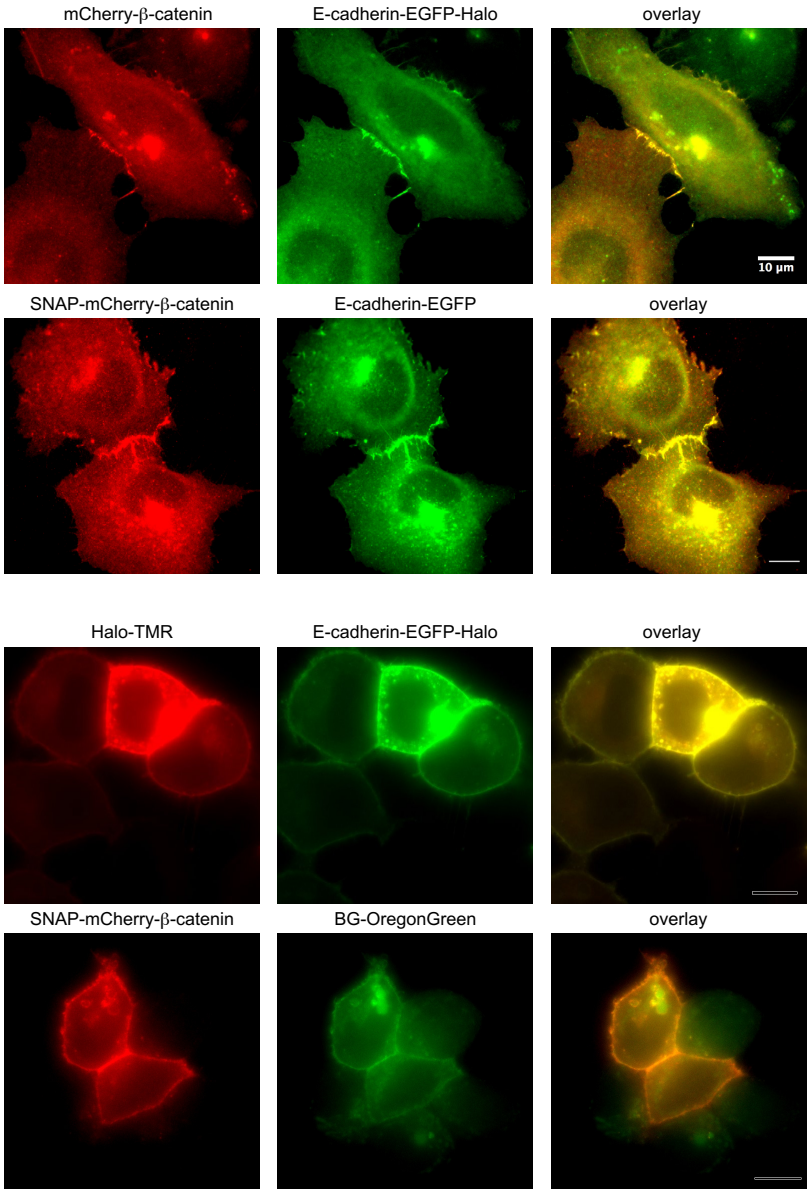

Figure A.3: Labelling and localization of SNAP-mCherry-β-catenin and E-cadherin-EGFP-Halo in living cells.

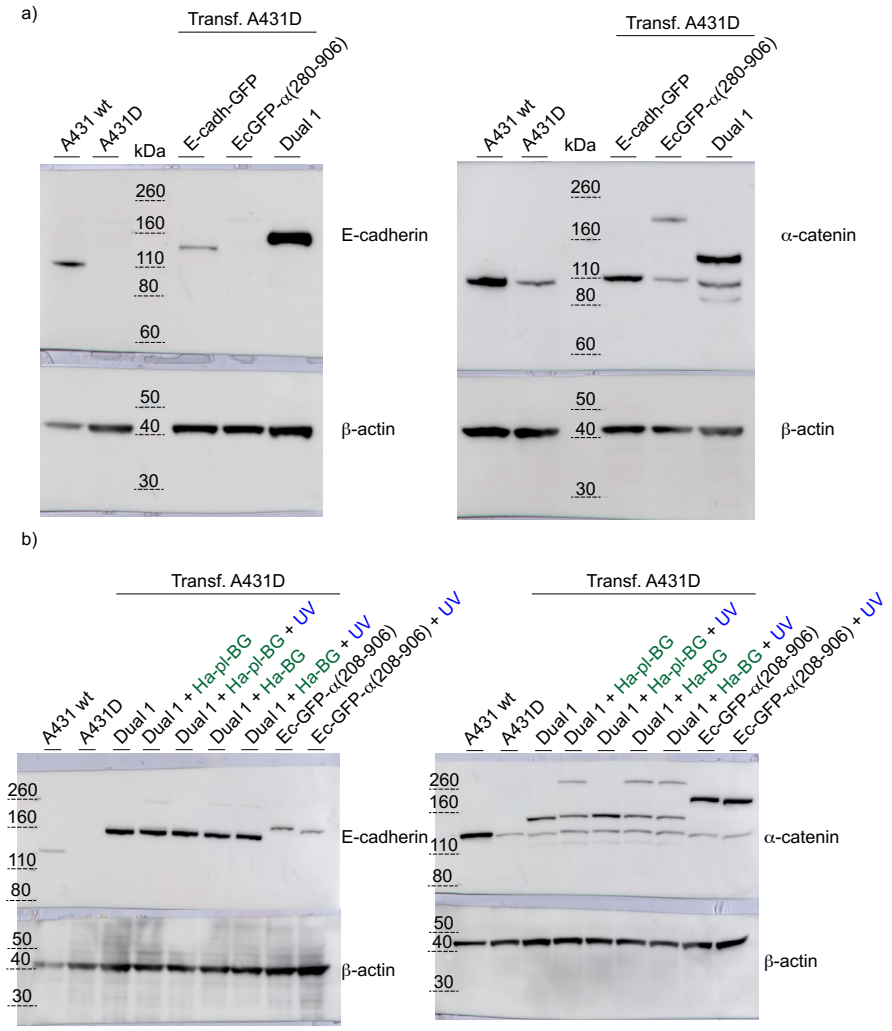

Figure A.4: Complete Western blots for A431D cell lines.

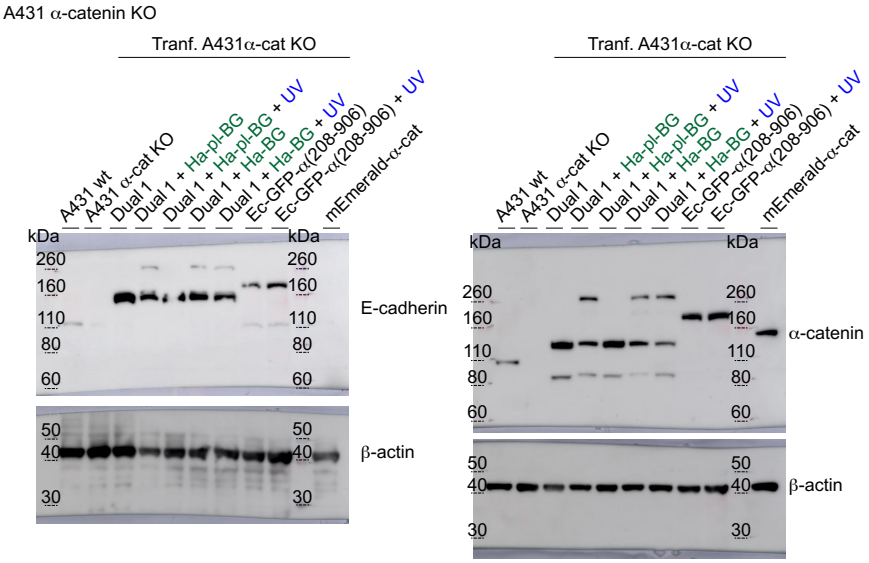

Figure A.5: Complete Western blots for A431 α-catenin KO cell lines.

B

DNA OLIGOS AND PLASMIDS

B.1 PRIMER LISTS

B.1.1 *List of cloning primers*

Int. Ref. No.	Name	Sequence	Tm [° C]	Length [bp]
1	SNAP_N-term-Fw	ATG GAC AAA GAC TGC GAA ATG	53.6	21
2	SLIC-rev-primer	CTC GCC CTT GCT CAC CAT ACT TCC TCC TCC TCC ACT TCC TCC TCC TCC ATT AAC CTC GAG TTT AAA CG	71.2	68
3	SNAP-N-term-Rev	CAT TTC GCA GTC TTT GTC CAT	53.6	21
4	mCherry-Fw	ATG GTG AGC AAG GGC GAG	57.9	18
37	GFP-mCherry-ex_Nterm Fw	GTG AGC AAG GGC GAG GAG	58.5	18
38	GFP-mCherry-ex_Nterm Rev	CTC CTC GCC CTT GCT CAC	58.5	18
39	GFP-mCherry-ex_Cterm Fw	CGG CAT GGA CGA GCT GTA CAA G	60.3	22
40	GFP-mCherry-ex_Cterm Rev	CTT GTA CAG CTC GTC CAT GCC G	60.3	22
51	GA_bCatenin-Cterm-Rev	CTT TGT TAG CAG CCG GAT CAG CTT TTA CAG GTC AGT ATC AAA CCA GGC CAG C	69.4	52
52	Flexi_3′-Fw	GCT GAT CCG GCT GCT AAC AAA GC	60.9	23
53	GA_paxillinC-term Rev	CTT TGT TAG CAG CCG GAT CAG CGA GCC TAG CAG AAG AGC TTG AGG	69.8	45

Int. Ref. No.	Name	Sequence	Tm [° C]	Length [bp]
56	eDHFR-Cterm-FW_neu	GCT ATT GCT TTG AGA TTC TGG AGC GGC GGG CGG ATC C	69.9	37
57	eDHFR-Nterm-Rev_neu	ATC TAC CGC TAA CGC CGC AAT CAG ACT GAT CAT CTC G	66.3	37
67	GA_hECad-EGFP-Fw	ATG TAC GGA GGC GGC GAG GAC GAC CCG CGG GTG AGC AAG GGC GAG GAG CTG TTC ACC	77	57
68	GA_hECad-EGFP-Halo-Rev	TTA GGT GAC ACT ATA GAA TAG GGC CCT CTA GAA TTC TAT TAA CCG GAA ATC TCC	65.2	54
69	GA_hECad-EGFP-Rev	AAC AGC TCC TCG CCC TTG CTC ACC CGC GGG TCG TCC TCG CCG CCT CC	77.9	47
70	GA-hECad-EGFP-Halo-Fw	ATT TCC GGT TAA TAG AAT TCT AGA GGG CCC TAT TCT ATA GTG TCA CCT AAA TGC	65	54
77	E-Cad-[bCat]_Fw	GGA GGA GGA GGA AGT GTG AGC AAG GGC GAG GAG CTG TTC ACC G	72.2	43
78	E-Cad-[bCat]_Rev	ACT TCC TCC TCC TCC GGA GCT CAG ACT AGC AGC TTC GGA ACC G	71.4	43
85	GA_hECad-cytosol-Fw	GCA TGG ACG AGC TGT ACA AGG GAG GAG GAG GAA GTA AAG AGC CCT TAC TGC CCC CAG AGG	72.6	60
86	GA-hECad-cytosol-Rev	GCT GAT TAT GAT CTA GAG TCG CGG CCT TAG TCG TCC TCG CCG CCT CCG TAC ATG TCA GC	72	59
87	GA-hECad-[cyt]-Rev	TTG CTC ACA CTT CCT CCT CCT CCG ACC ACC GCT CTC CTC CGA AGA AAC AGC	72.6	51
88	CMV_GA_Fw	CCA TTG ACG CAA ATG GGC GGT AGG CGT GTA CGG TGG	70.4	36
89	CMV_GA_Rev	CCA CCG TAC ACG CCT ACC GCC CAT TTG CGT CAA TGG	70.4	36
109	ECad12-Halo_Fw	ACA CTA TAG AAT AAG GAG CGA TAT GCA CCA CCA CCA CCA CCA CGA AAA CC	68.5	50

Int. Ref. No.	Name	Sequence	Tm [° C]	Length [bp]
110	ECad12-Halo-Rev	AAA GCC AGT ACC GAT TTC GGA TCT GTC GTT CAG ACC GCC ACC AGG AGC	71,4	48
111	ECad12-EGFP-Halo Fwd	AAT GAC AAC GCT CCT GGT GGC GGT TCT TCT GTG AGC AAG GGC GAG G	72.6	46
113	prohECad_vector Fw	GAA TTC TAG AGG GCC CTA TTC TAT AGT GTC ACC TAA ATG CTA GAG CTC GC	66.1	50
114	prohECad_vector Rev	TCT CTT CTG TCT TCT GAG GCC AGG AGA GGA GTT GGG AAA TGT GAG C	68.9	46
115	SNAP-hECad3 Fw	TGG CCT CAG AAG ACA GAA GAG AGA CAA AGA CTG CGA AAT GAA GC	67.2	44
116	SNAP-hECad3 Rev	CC TTG TAC GTG GTG GGA TTA TTA ACC TCG AGT TTA AAC GC	64.2	40
117	hECad3 Fw	ATC CGC GTT TAA ACT CGA GGT TAA TAA TCC CAC CAC GTA CAA GGG TCA GG	68.4	50
118	hECad3 Rev	CCT TGC TCA CCA TAC TTC CTC CTC CTC CGT CGT CCT CGC CGC CTC CG	73.8	47
119	hECad-mCherry Fw	CGG AGG CGG CGA GGA CGA CGG AGG AGG AGG AAG TAT GGT GAG CAA GG	73.8	47
120	hECad-mCherry Rev	TGA CAC TAT AGA ATA GGG CCC TCT AGA ATT CTT ACT TGT ACA GCT CGT CCA TGC C	67.4	55
121	ECad12-EGFP_Rev	TCG CCC TTG CTC ACA GAA GAA CCG CCA CCA GGA GCG TTG TCA TTA ATA TCC	70.8	51
122	ECad12-EGFP-Halo Rev2	CCA GTA CCG ATT TCG GAT CCC TCG ATC CCC TTG TAC AGC TCG	69.1	42
138	GA_Halo-IRES-Fw	GGA GAT TTC CGG TTA ATA GAA TTC TAG ACA ATT GCT TAA GGA TCC GCC CCT CTC C	67.3	55
139	GA_Halo-IRES-Rev	GGA GAG GGG CGG ATC CTT AAG CAA TTG TCT AGA ATT CTA TTA ACC GGA AAT CTC C	67.3	55

Int. Ref. No.	Name	Sequence	Tm [° C]	Length [bp]
140	GA_IRES-SNAP-Fw	GGT TTT CCT TTG AAA AAC ACG ATG ATA ATA TGG ACA AAG ACT GCG AAA TGA AGC GCA CC	67.6	59
141	GA_IRES-SNAP-Rev	GGT GCG CTT CAT TTC GCA GTC TTT GTC CAT ATT ATC ATC GTG TTT TTC AAA GGA AAA CC	67.6	59
142	GA_mCh-a(280)-Rev	GTC AAA GTT ATT GAG TGC ATA CCG CGG TGC AGA ATT CGA AGC TTG AGC TCG	68.9	51
157	GA_IRES-DHFR_fw	GGT TTT CCT TTG AAA AAC ACG ATG ATA ATA TGA TCA GTC TGA TTG CGG CGT TAG CG	66.8	56
158	GA_IRES-DHFR_rev	CGC TAA CGC CGC AAT CAG ACT GAT CAT ATT ATC ATC GTG TTT TTC AAA GGA AAA CC	66.8	56
159	GA_exSNAP wDHFR_rev	TTC CTC CTC CTC CAT TAA CCT CGA GTT TCC GCC GCT CCA GAA TCT CAA AGC	70.4	51
161	GA_mCh-SNAP_rev	AGG CGG CCG CCT CGA GCG CTT AAT TAA CCT CGA GTT TAA ACG CGG ATC C	72.2	49
163	GA_mCh-SNAP_fw2	ATG GAC GAG CTG TAT AAG GCC GGC CAC ATG GAC AAA GAC TGC GAA ATG AAG C	70.8	52
180	ECad[cyto]-Halo_Fw	CCA GAG GAT GAC ACC CGG GCT AGC GAT AAC GAT GGA TCC GAA ATC GGT ACT GG	71	53
181	cytoECad_ XbaI_Rev	TGA CAC TAT AGA ATA GGG CCC TCT AGA GTC GCG GCC TTA GTC GTC CTC G	69,7	49

B.1.2 *List of sequencing primers*

Int. Ref. No.	Name	Sequence	Tm [° C]	Length [bp]
29	EGFP-C-term_Fw	CAA CGA GAA GCG CGA TCA CAT GG	60.6	23
30	EGFP-N-term_Rev	CTG AAC TTG TGG CCG TTT ACG TCG	60.3	24

Int. Ref. No.	Name	Sequence	Tm [° C]	Length [bp]
31	SNAPf-mCherry-C-term_Fw	TGA AAG AGT GGC TGC TGG	55.2	18
32	SNAPf-mCherry-N-term_Rev	TGT TCG CAC CCA GAC AGT TCC	59.8	21
41	mCherry-C-term Fw	TGG ACA TCA CCT CCC ACA ACG	59.4	21
42	mCherry-N-term Rev	CAC CCT TGG TCA CCT TCA GCT TGG	62	24
58	Bcat-Rev	GAA GGG TCC CAG CAG TAC AAC GAG C	63.2	25
59	Pax_Rev	TGC GTG TCT GCT GTT GGG TGG AG	63.9	23
123	Halo_Nterm_Rev	TCT GGA GCA ATG CAG CGA TGG	60.3	21
136	h_aCat(295)-Fw	CCT TGA GCT TCA GCG AGG AG	57.8	20
137	h_aCat(310)-Rev	CAC TAA TGA TGC TTT CCA GAC G	53.8	22
143	CMV-for	CGC AAA TGG GCG GTA GGC GTG	63.9	21
144	BGH-rev	TAG AAG GCA CAG TCG AGG	53.6	18
151	aCat_Cterm_fw	GCA GAC AGT GAA GGC ATC CTA CG	59.7	23
152	T7	TAA TAC GAC TCA CTA TAG G	44.5	19
153	T7term	TGC TAG TTA TTG CTC AGC GG	55.2	20
162	IRES_fw	CAA ACA ACG TCT GTA GCG ACC	56.3	21

B.2 PLASMID LIST

Int. Ref. No	Name
pDO13	SNAPf-mCherry
pDO25	TOMM20-EGFP-Halo
pDO30	DD-EGFP-Vcl
pDO31	SNAPf-mCherry-paxillin
pDO32	SNAPf-mCherry-betaCatenin
pDO33	hE-Cadherin-EGFP-Halo
pDO34	hE-Cadherin-β-EGFP-Halo
pDO35	hE-Cadherin[cyto]-EGFP-Halo
pDO36	hE-Cadherin[cyto]-mCherry-Halo
pDO37	eDHFR-EGFP-cytoECad
pDO38	eDHFR-mEmerald-α1-Catenin-C18
pDO56	EcGFP-Halo_IRES_SNAP-mCherry-α(280-906)
pDO60	Halo-GFP-Mito+mCherry-SNAPf
pDO61	EcGFP-Halo_IRES_DHFR-mCherry-α(280-906)
pDO68	E-cadherin-Δ-cyto-Halo_IRES_DHFR-EGFP-cytotail
pNB01	ECad12-Halo
pNB02	ECad12-GFP-Halo
pNB03	SNAP-ECad345-mCherry
pFC20A	HaloTag T7 SP6 FlexiVector

B.3 SYNTHETIC DS-DNA

DHFR degron sequence ordere das gBlocks Gene Fragment from IDT

```
ATG ATC AGT CTG ATT GCG GCG TTA GCG GTA GAT TAC GTT ATC GGC ATG
GAA AAC GCC ATG CCG TGG AAC CTG CCT GCC GAT CTC GCC TGG TTT AAA
CGC AAC ACC TTA AAT AAA CCC GTG ATT ATG GGC CGC CAT ACC TGG GAA
TCA ATC GGT CGT CCG TTG CCA GGA CGC AAA AAT ATT ATC CTC AGC AGT
CAA CCG AGT ACG GAC GAT CGC GTA ACG TGG GTG AAG TCG GTG GAT GAA
GCC ATC GCG GCG TGT GGT GAC GTA CCA GAA ATC ATG GTG ATT GGC GGC
GGT CGC GTT ATT GAA CAG TTC TTG CC AAA AGC GCA AAA ACT GTA TCT
GAC GCA TAT CGA CGC AGA AGT GGA AGG CGA CAC CCA TTT CCC GGA TTA
CGA GCC GGA TGA CTG GGA ATC GGT ATT CAG CGA ATT CCA CGA TGC TGA
TGC GCA GAA CTC TCA CAG CTA TTG CTT TGA GAT TCT GGA GCG GCG A
```

B.4 CLONING TABLES

pDO13	**SNAPf-mCherry**						
		Fw Primer			Rev Primer		
linearized Backbone	Template	#	Name	Sequence	#	Name	Sequence
	hAGT-mCherry (pDO08)	4	mCherry-Fw	ATG GTG AGC AAG GGC GAG	3	SNAP-N-term-Rev	CAT TTC GCA GTC TTT GTC CAT
Inserts	Template	#	Name	Sequence	#	Name	Sequence
SNAPf	Lck-ECFP-SNAP (pDO12)	1	SNAP-N-term-Fw	ATG GAC AAA GAC TGC GAA ATG	2	SLIC-rev-primer	CTC GCC CTT GCT CAC CAT ACT TCC TCC TCC TCC ACT TCC TCC TCC TCC ATT AAC CTC GAG TTT AAA CG

pDO25	**TOMM20-EGFP-Halo**						
		Fw Primer			Rev Primer		
linearized Backbone	Template	#	Name	Sequence	#	Name	Sequence
	TOMM20-mCherry-Halo (pDO04)	39	GFP-mCherry-ex-Cterm Fw	CGG CAT GGA CGA GCT GTA CAA G	38	GFP-mCherry-ex-Nterm Rev	CTC CTC GCC CTT GCT CAC
Inserts	Template	#	Name	Sequence	#	Name	Sequence
EGFP	EGFP-DHFR (pDO07)	37	GFP-mCherry-ex-Nterm Fw	GTG AGC AAG GGC GAG GAG	40	GFP-mCherry-ex-Cterm Rev	CTT GTA CAG CTC GTC CAT GCC G

pDO30	**DD-EGFP-Vcl**						
		Fw Primer			Rev Primer		
linearized Backbone	Template	#	Name	Sequence	#	Name	Sequence
	DHFR-EGFP-Vcl (pDO05)	56	eDHFR-Cterm-FW-neu	GCT ATT GCT TTG AGA TTC TGG AGC GGC GGG CGG ATC C	57	eDHFR-Nterm-Rev-neu	ATC TAC CGC TAA CGC CGC AAT CAG ACT GAT CAT CTC G
Inserts	Template	#	Name	Sequence	#	Name	Sequence
DHFR-degron	gBlock fragment ordered from IDT						

pDO31	**SNAP-mCherry-paxillin**						
		Fw Primer			Rev Primer		
linearized Backbone	Template	#	Name	Sequence	#	Name	Sequence
	SNAPf-mCherry (pDO13)	52	Flexi-3′-Fw	GCT GAT CCG GCT GCT AAC AAA GC	40	GFP-mCherry-ex-Cterm Rev	CTT GTA CAG CTC GTC CAT GCC G
Inserts	Template	#	Name	Sequence	#	Name	Sequence
paxillin	GFP-Pax (pDO62)	39	GFP-mCherry-ex-Cterm Fw	CGG CAT GGA CGA GCT GTA CAA G	53	GA-paxillinC-term Rev	CTT TGT TAG CAG CCG GAT CAG CGA GCC TAG CAG AAG AGC TTG AGG

pDO32	**SNAP-mCherry-β-catenin**						
		Fw Primer			Rev Primer		
linearized Backbone	Template	#	Name	Sequence	#	Name	Sequence
	SNAPf-mCherry (pDO13)	52	Flexi-3′-Fw	GCT GAT CCG GCT GCT AAC AAA GC	40	GFP-mCherry-ex-Cterm Rev	CTT GTA CAG CTC GTC CAT GCC G
Inserts	Template	#	Name	Sequence	#	Name	Sequence
ß-catenin	mCherry-ß-Catenin20 (pDO20)	39	GFP-mCherry-ex-Cterm Fw	CGG CAT GGA CGA GCT GTA CAA G	51	GA-bCatenin-Cterm-Rev	CTT TGT TAG CAG CCG GAT CAG CTT TTA CAG GTC AGT ATC AAA CCA GGC CAG C

pDO33	**E-cadherin-EGFP-Halo**						
		Fw Primer			Rev Primer		
linearized Backbone	Template	#	Name	Sequence	#	Name	Sequence
	E-cadherin-GFP (pDO48)	70	GA-hECad-EGFP-Halo-Fw	ATT TCC GGT TAA TAG AAT TCT AGA GGG CCC TAT TCT ATA GTG TCA CCT AAA TGC	69	GA-hECad-EGFP-Rev	AAC AGC TCC TCG CCC TTG CTC ACC CGC GGG TCG TCC TCG CCG CCT CC
Inserts	Template	#	Name	Sequence	#	Name	Sequence
EGFP-Halo	TOMM20-EGFP-Halo (pDO25)	67	GA-hECad-EGFP-Fw	ATG TAC GGA GGC GGC GAG GAC GAC CCG CGG GTG AGC AAG GGC GAG GAG CTG TTC ACC	68	GA-hECad-EGFP-Halo-Rev	TTA GGT GAC ACT ATA GAA TAG GGC CCT CTA GAA TTC TAT TAA CCG GAA ATC TCC

pDO34	**E-cadherin-Δβ-ctnBS-EGFP-Halo**						
		Fw Primer			Rev Primer		
linearized Backbone	Template	#	Name	Sequence	#	Name	Sequence
	E-cadherin-GFP (pDO48)	70	GA-hECad-EGFP-Halo-Fw	ATT TCC GGT TAA TAG AAT TCT AGA GGG CCC TAT TCT ATA GTG TCA CCT AAA TGC	89	CMV-GA-Rev	CCA CCG TAC ACG CCT ACC GCC CAT TTG CGT CAA TGG
Inserts	Template	#	Name	Sequence	#	Name	Sequence
E-cadherin-[ß-Cat]	E-cadherin-GFP (pDO48)	88	CMV-GA-Fw	CCA TTG ACG CAA ATG GGC GGT AGG CGT GTA CGG TGG	78	E-Cad-[bCat]-Rev	ACT TCC TCC TCC TCC GGA GCT CAG ACT AGC AGC TTC GGA ACC G
EGFP-Halo2	TOMM20-EGFP-Halo (pDO25)	77	E-Cad-[bCat]-Fw	GGA GGA GGA GGA AGT GTG AGC AAG GGC GAG GAG CTG TTC ACC G	68	GA-hECad-EGFP-Halo-Rev	TTA GGT GAC ACT ATA GAA TAG GGC CCT CTA GAA TTC TAT TAA CCG GAA ATC TCC

pDO35	**E-cadherin-Δcyto-EGFP-Halo**						
		Fw Primer			Rev Primer		
linearized Backbone	Template	#	Name	Sequence	#	Name	Sequence
	E-cadherin-GFP (pDO48)	70	GA-hECad-EGFP-Halo-Fw	ATT TCC GGT TAA TAG AAT TCT AGA GGG CCC TAT TCT ATA GTG TCA CCT AAA TGC	89	CMV-GA-Rev	CCA CCG TAC ACG CCT ACC GCC CAT TTG CGT CAA TGG
Inserts	Template	#	Name	Sequence	#	Name	Sequence
E-cadherin-Δcyto	E-cadherin-GFP (pDO48)	88	CMV-GA-Fw	CCA TTG ACG CAA ATG GGC GGT AGG CGT GTA CGG TGG	87	GA-hECad-[cyt]-Rev	TTG CTC ACA CTT CCT CCT CCT CCG ACC ACC GCT CTC CTC CGA AGA AAC AGC
EGFP-Halo2	TOMM20-EGFP-Halo (pDO25)	77	E-Cad-[bCat]-Fw	GGA GGA GGA GGA AGT GTG AGC AAG GGC GAG GAG CTG TTC ACC G	68	GA-hECad-EGFP-Halo-Rev	TTA GGT GAC ACT ATA GAA TAG GGC CCT CTA GAA TTC TAT TAA CCG GAA ATC TCC

pDO36	**E-cadherin-Δcyto-mCherry-Halo**						
		Fw Primer			Rev Primer		
linearized Backbone	Template	#	Name	Sequence	#	Name	Sequence
	E-cadherin-GFP (pDO48)	70	GA-hECad-EGFP-Halo-Fw	ATT TCC GGT TAA TAG AAT TCT AGA GGG CCC TAT TCT ATA GTG TCA CCT AAA TGC	89	CMV-GA-Rev	CCA CCG TAC ACG CCT ACC GCC CAT TTG CGT CAA TGG
Inserts	Template	#	Name	Sequence	#	Name	Sequence
E-cadherin-Δcyto	E-cadherin-GFP (pDO48)	88	CMV-GA-Fw	CCA TTG ACG CAA ATG GGC GGT AGG CGT GTA CGG TGG	38	GFP-mCherry-ex-Nterm Rev	CTC CTC GCC CTT GCT CAC
mCherry	SNAPf-mCherry (pDO13)	37	GFP-mCherry-ex-Nterm Fw	GTG AGC AAG GGC GAG GAG	40	GFP-mCherry-ex-Cterm Rev	CTT GTA CAG CTC GTC CAT GCC G
Halo	E-cadherin-Δcyto-EGFP-Halo (pDO35)	39	GFP-mCherry-ex-Cterm Fw	CGG CAT GGA CGA GCT GTA CAA G	68	GA-hECad-EGFP-Halo-Rev	TTA GGT GAC ACT ATA GAA TAG GGC CCT CTA GAA TTC TAT TAA CCG GAA ATC TCC

pDO37	**DHFR-EGFP-cytotail**						
		5' cut			3' cut		
linearized Backbone	Source Plasmid	#	Name	Sequence	#	Name	Sequence
	DHFR-EGFP (pDO28)		BsrGI	T/GTACA		NotI	GC/GGCCGC
		Fw Primer			Rev Primer		
Inserts	Template	#	Name	Sequence	#	Name	Sequence
cytotail	E-cadherin-GFP (pDO48)	85	GA-hECad-cytosol-Fw	GCA TGG ACG AGC TGT ACA AGG GAG GAG GAG GAA GTA AAG AGC CCT TAC TGC CCC CAG AGG	86	GA-hECad-cytosol-Rev	GCT GAT TAT GAT CTA GAG TCG CGG CCT TAG TCG TCC TCG CCG CCT CCG TAC ATG TCA GC

pDO38	**DHFR-mEmerald-α-catenin**						
		5' cut			3' cut		
linearized Backbone	Source Plasmid	#	Name	Sequence	#	Name	Sequence
	mEmerald-α-catenin (pDO23)		BmtI	GCTAG/C		AgeI	A/CCGGT
		Fw Primer			Rev Primer		
Inserts	Template	#	Name	Sequence	#	Name	Sequence
DHFR	DHFR-EGFP (pDO28)	88	CMV-GA-Fw	CCA TTG ACG CAA ATG GGC GGT AGG CGT GTA CGG TGG	38	GFP-mCherry-ex-Nterm Rev	CTC CTC GCC CTT GCT CAC

pDO56	**Ec-GFP-Halo-IRES-SNAP-mCherry-α(280-906)**						
		5' cut			3' cut		
linearized Backbone	Source Plasmid	#	Name	Sequence	#	Name	Sequence
	EcGFP-α(280-906) (pDO52)		BrsGI	T/GTACA		SacII	CCGC/GG
		Fw Primer			Rev Primer		
Inserts	Template	#	Name	Sequence	#	Name	Sequence
Halo2	E-cadherin-EGFP-Halo (pDO33)	39	GFP-mCherry-ex-Cterm Fw	CGG CAT GGA CGA GCT GTA CAA G	139	GA-Halo-IRES-Rev	GGA GAG GGG CGG ATC CTT AAG CAA TTG TCT AGA ATT CTA TTA ACC GGA AAT CTC C
IRES	Halo-GFP-Mito+mCherry-DHFR (pDO47)	138	GA-Halo-IRES-Fw	GGA GAT TTC CGG TTA ATA GAA TTC TAG ACA ATT GCT TAA GGA TCC GCC CCT CTC C	141	GA-IRES-SNAP-Rev	GGT GCG CTT CAT TTC GCA GTC TTT GTC CAT ATT ATC ATC GTG TTT TTC AAA GGA AAA CC
SNAP-mCherry	SNAP-mCherry-β-catenin (pDO32)	140	GA-IRES-SNAP-Fw	GGT TTT CCT TTG AAA AAC ACG ATG ATA ATA TGG ACA AAG ACT GCG AAA TGA AGC GCA CC	142	GA-mCh-a(280)-Rev	GTC AAA GTT ATT GAG TGC ATA CCG CGG TGC AGA ATT CGA AGC TTG AGC TCG

pDO60	**Halo-GFP-Mito+mCherry-SNAPf**						
		5' cut			3' cut		
linearized Backbone	Source Plasmid	#	Name	Sequence	#	Name	Sequence
	Halo-GFP-Mito+mCherry-DHFR (pDO47)		FseI	GGCCGG/CC		PacI	TTAAT/TAA
		Fw Primer			Rev Primer		
Inserts	Template	#	Name	Sequence	#	Name	Sequence
SNAP2	SNAPf-mCherry (pDO13)	163	GA-mCh-SNAP-fw2	ATG GAC GAG CTG TAT AAG GCC GGC CAC ATG GAC AAA GAC TGC GAA ATG AAG C	161	GA-mCh-SNAP-rev	AGG CGG CCG CCT CGA GCG CTT AAT TAA CCT CGA GTT TAA ACG CGG ATC C

pDO61	**EcGFP-Halo-IRES-DHFR-mCherry-α(280-906)**						
		5' cut			3' cut		
linearized Backbone	Source Plasmid	#	Name	Sequence	#	Name	Sequence
	EcGFP-Halo-IRES-SNAP-mCherry-α(280-906) (pDO56)		AflII	C/TTAAG		PmeI	GTTT/AAAC
		Fw Primer			Rev Primer		
Inserts	Template	#	Name	Sequence	#	Name	Sequence
DHFR-EGFP-cytotail	eDHFR-EGFP (pDO28)	157	GA-IRES-DHFR-fw	GGT TTT CCT TTG AAA AAC ACG ATG ATA ATA TGA TCA GTC TGA TTG CGG CGT TAG CG	159	GA-exSNAPwDHFR-rev	TTC CTC CTC CTC CAT TAA CCT CGA GTT TCC GCC GCT CCA GAA TCT CAA AGC
IRES2	Halo-GFP-Mito+mCherry-DHFR (pDO47)	138	GA-Halo-IRES-Fw	GGA GAT TTC CGG TTA ATA GAA TTC TAG ACA ATT GCT TAA GGA TCC GCC CCT CTC C	158	GA-IRES-DHFR-rev	CGC TAA CGC CGC AAT CAG ACT GAT CAT ATT ATC ATC GTG TTT TTC AAA GGA AAA CC

pDO68	**E-cadherin-Δ-cyto-Halo_IRES_DHFR-EGFP-cytotail**						
		5′ cut			3′ cut		
linearized Backbone	Source Plasmid	#	Name	Sequence	#	Name	Sequence
	EcGFP-α(280-906) (pDO68)		BmtI	GCTAG/C		XbaI	T/CTAGA
		Fw Primer			Rev Primer		
Inserts	Template	#	Name	Sequence	#	Name	Sequence
Halo-IRES	EcGFP-Halo_IRES_DHFR-mCherry-α280-906 (pDO61)	180	ECad[cyto]-Halo_Fw	CCA GAG GAT GAC ACC CGG GCT AGC GAT AAC GAT GGA TCC GAA ATC GGT ACT GG	158	GA_IRES-DHFR_rev	CGC TAA CGC CGC AAT CAG ACT GAT CAT ATT ATC ATC GTG TTT TTC AAA GGA AAA CC
DHFR-EGFP-cytotail	eDHFR-EGFP-cytoECad (pDO37)	157	GA-IRES-DHFR-fw	GGT TTT CCT TTG AAA AAC ACG ATG ATA ATA TGA TCA GTC TGA TTG CGG CGT TAG CG	181	cytoECad_XbaI_Rev	TGA CAC TAT AGA ATA GGG CCC TCT AGA GTC GCG GCC TTA GTC GTC CTC G

pNB01	**EC12-Halo**						
		5' cut			3' cut		
linearized Backbone	Source Plasmid	#	Name	Sequence	#	Name	Sequence
	pFC20A HaloTag T7 SP6 FlexiVector		BamHI	G/GATCC		AsiSI	GCGAT/CGC
		Fw Primer			Rev Primer		
Inserts	Template	#	Name	Sequence	#	Name	Sequence
ECad12	ECad12-Avi (pDO40)	109	ECad12-Halo-Fw	ACA CTA TAG AAT AAG GAG CGA TAT GCA CCA CCA CCA CCA CCA CGA AAA CC	110	ECad12-Halo-Rev	AAA GCC AGT ACC GAT TTC GGA TCT GTC GTT CAG ACC GCC ACC AGG AGC

pNB02	**EC12-EGFP-Halo**						
		5' cut			3' cut		
linearized Backbone	Source Plasmid	#	Name	Sequence	#	Name	Sequence
	pFC20A HaloTag T7 SP6 FlexiVector		BamHI	G/GATCC		AsiSI	GCGAT/CGC
Inserts	Template	Fw Primer			Rev Primer		
		#	Name	Sequence	#	Name	Sequence
ECad12-2	ECad12-Avi (pDO40)	109	ECad12-Halo-Fw	ACA CTA TAG AAT AAG GAG CGA TAT GCA CCA CCA CCA CCA CCA CGA AAA CC	121	ECad12-EGFP-Rev	TCG CCC TTG CTC ACA GAA GAA CCG CCA CCA GGA GCG TTG TCA TTA ATA TCC
GFP	pET-His6-GFP (pDO46)	111	ECad12-EGFP-Halo Fwd	AAT GAC AAC GCT CCT GGT GGC GGT TCT TCT GTG AGC AAG GGC GAG G	122	ECad12-EGFP-Halo Rev2	CCA GTA CCG ATT TCG GAT CCC TCG ATC CCC TTG TAC AGC TCG

pNB03	**SNAP-E-cadherin345-mCherry**						
		Fw Primer			Rev Primer		
linearized Backbone	Template	#	Name	Sequence	#	Name	Sequence
	E-cadherin-EGFP-Halo (pDO33)	113	prohECad-vector Fw	GAA TTC TAG AGG GCC CTA TTC TAT AGT GTC ACC TAA ATG CTA GAG CTC GC	114	prohECad-vector Rev	TCT CTT CTG TCT TCT GAG GCC AGG AGA GGA GTT GGG AAA TGT GAG C
Inserts	Template	#	Name	Sequence	#	Name	Sequence
SNAP3	SNAPf-mCherry (pDO13)	115	SNAP-hECad3 Fw	TGG CCT CAG AAG ACA GAA GAG AGA CAA AGA CTG CGA AAT GAA GC	116	SNAP-hECad3 Rev	CC TTG TAC GTG GTG GGA TTA TTA ACC TCG AGT TTA AAC GC
[EC12]-E-cadherin	E-cadherin-EGFP-Halo (pDO33)	117	hECad3 Fw	ATC CGC GTT TAA ACT CGA GGT TAA TAA TCC CAC CAC GTA CAA GGG TCA GG	118	hECad3 Rev	CCT TGC TCA CCA TAC TTC CTC CTC CTC CGT CGT CCT CGC CGC CTC CG
mCherry2	SNAPf-mCherry (pDO13)	119	hECad-mCherry Fw	CGG AGG CGG CGA GGA CGA CGG AGG AGG AGG AAG TAT GGT GAG CAA GG	120	hECad-mCherry Rev	TGA CAC TAT AGA ATA GGG CCC TCT AGA ATT CTT ACT TGT ACA GCT CGT CCA TGC C
SNAP-mCherry	SNAP-mCherry-β-catenin (pDO32)	140	GA-IRES-SNAP-Fw	GGT TTT CCT TTG AAA AAC ACG ATG ATA ATA TGG ACA AAG ACT GCG AAA TGA AGC GCA CC	142	GA-mCh-a(280)-Rev	GTC AAA GTT ATT GAG TGC ATA CCG CGG TGC AGA ATT CGA AGC TTG AGC TCG

C

SUPPLEMENTARY FIGURES

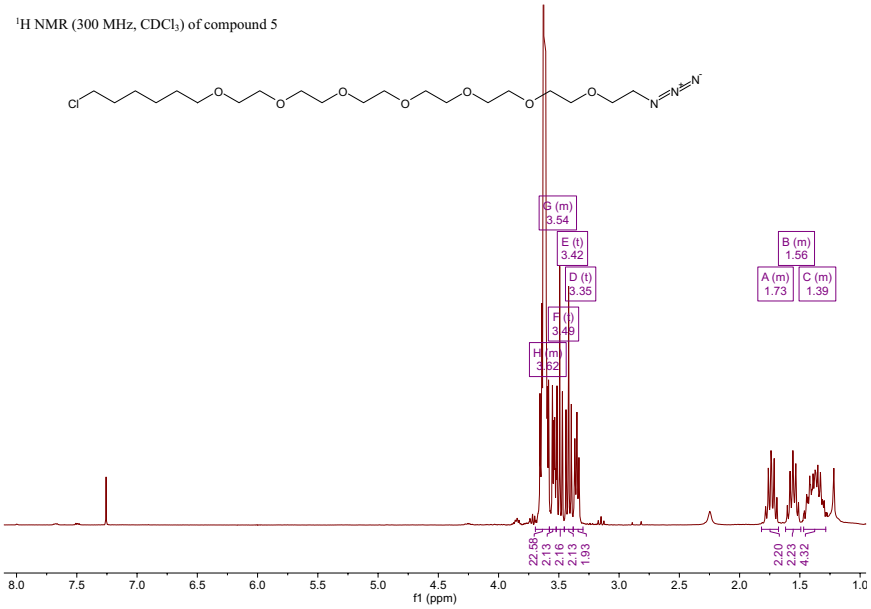

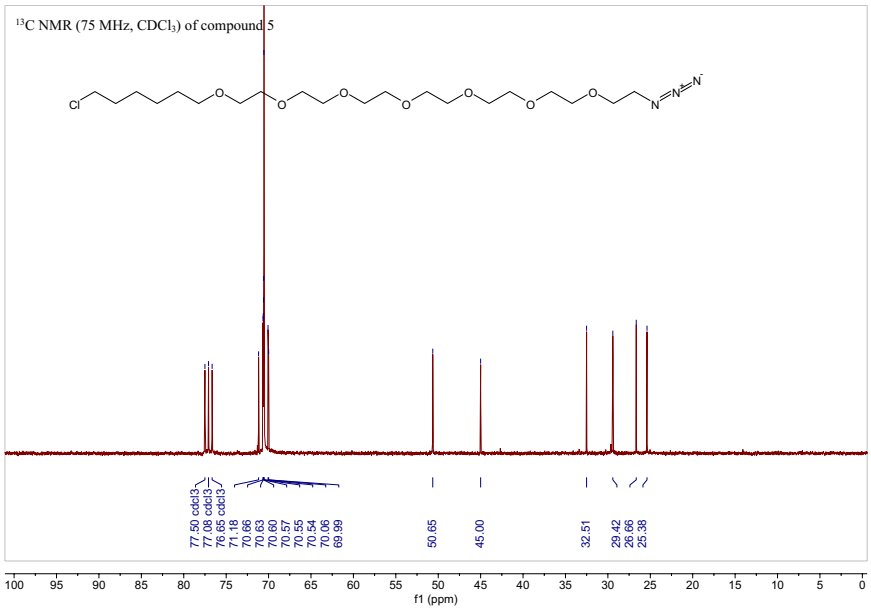

^{1}H NMR (300 MHz, $CDCl_3$) of compound 6

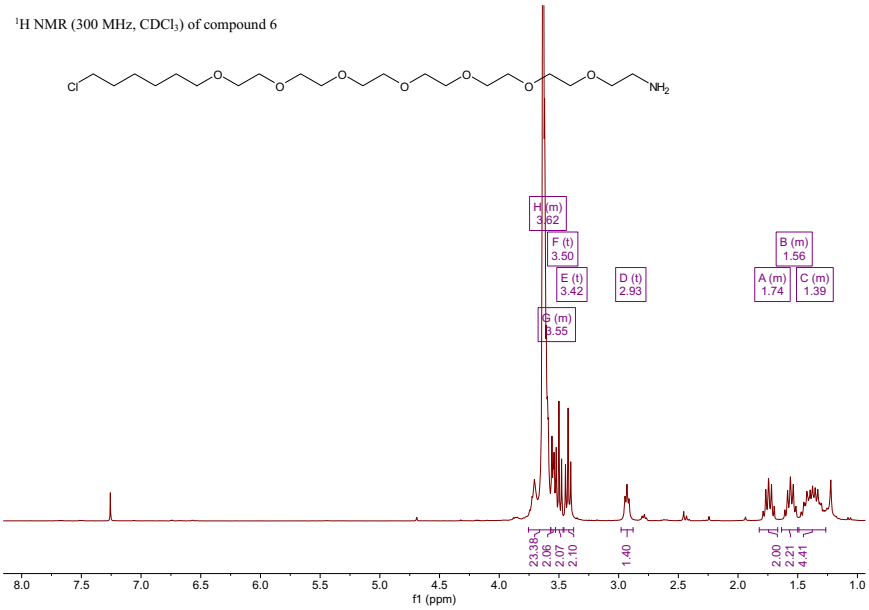

^{13}C NMR (75 MHz, $CDCl_3$) of compound 6

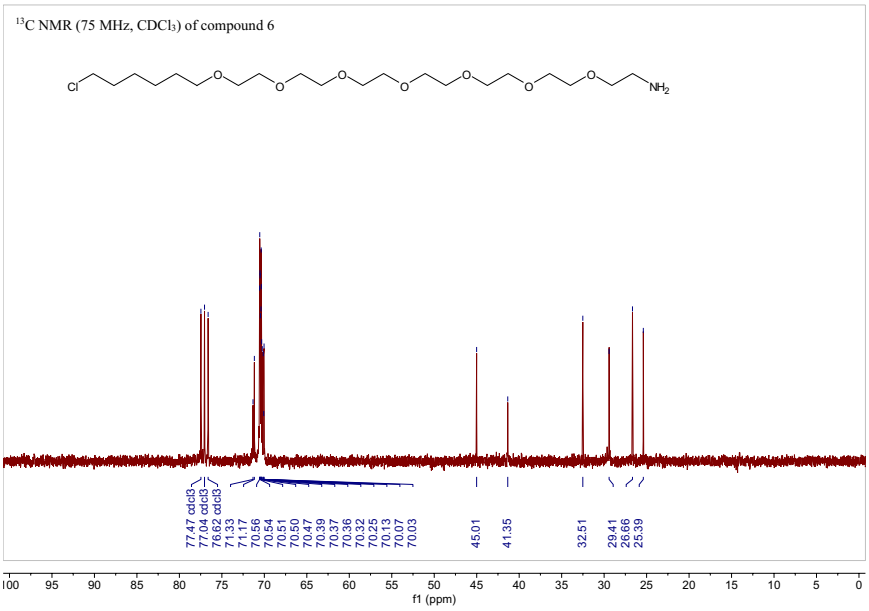

^{1}H NMR (300 MHz, CD_3OD) of compound 7

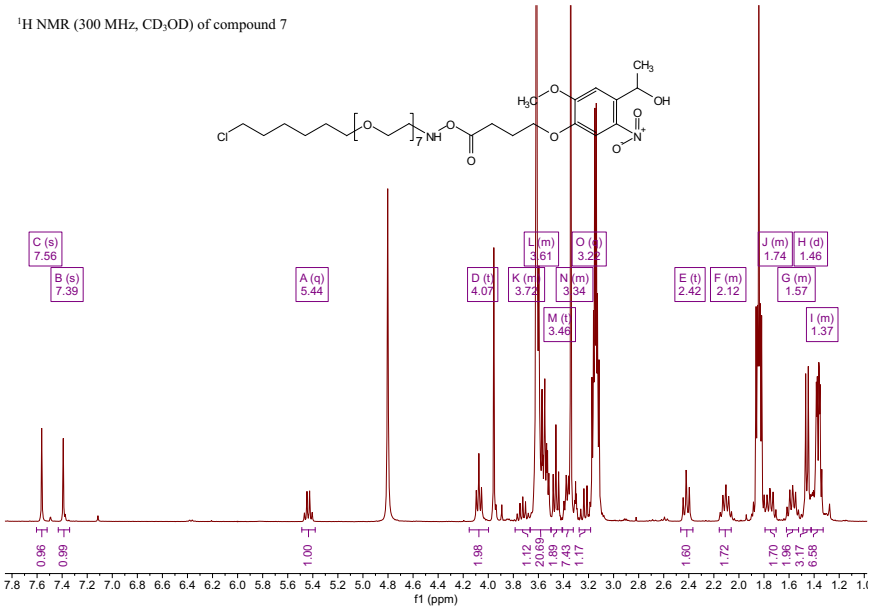

^{13}C NMR (75 MHz, CD_3OD) of compound 7

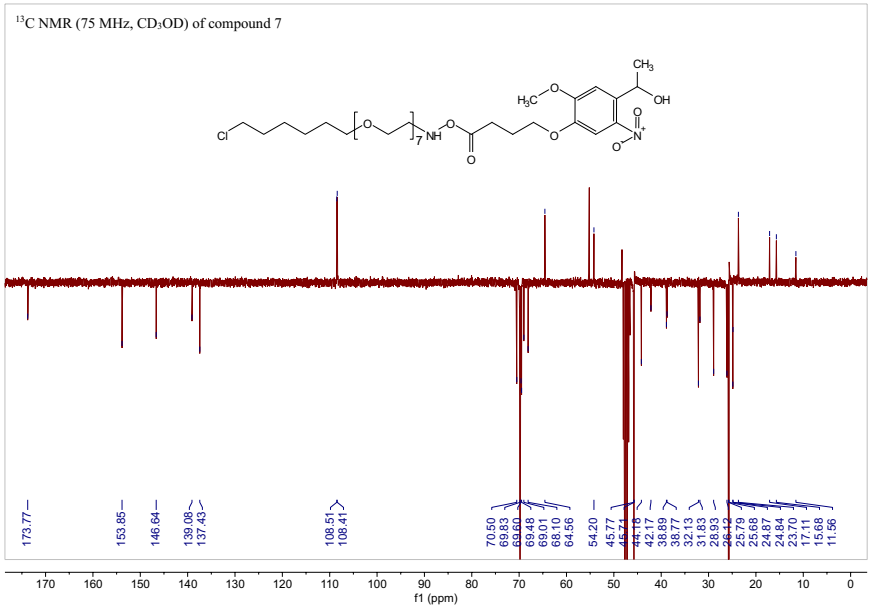

^{1}H NMR (300 MHz, CD_3OD) of compound 8

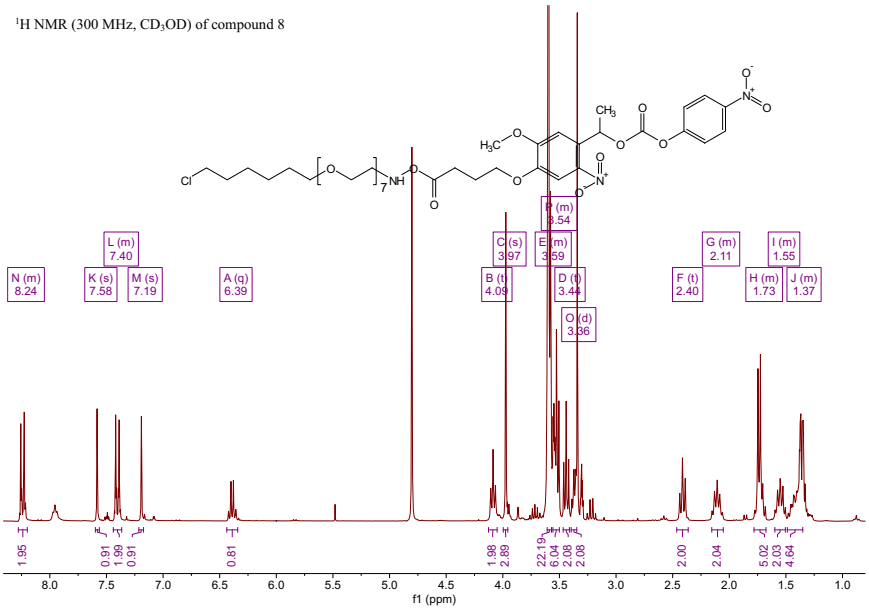

^{13}C NMR (75 MHz, CD_3OD) of compound 8

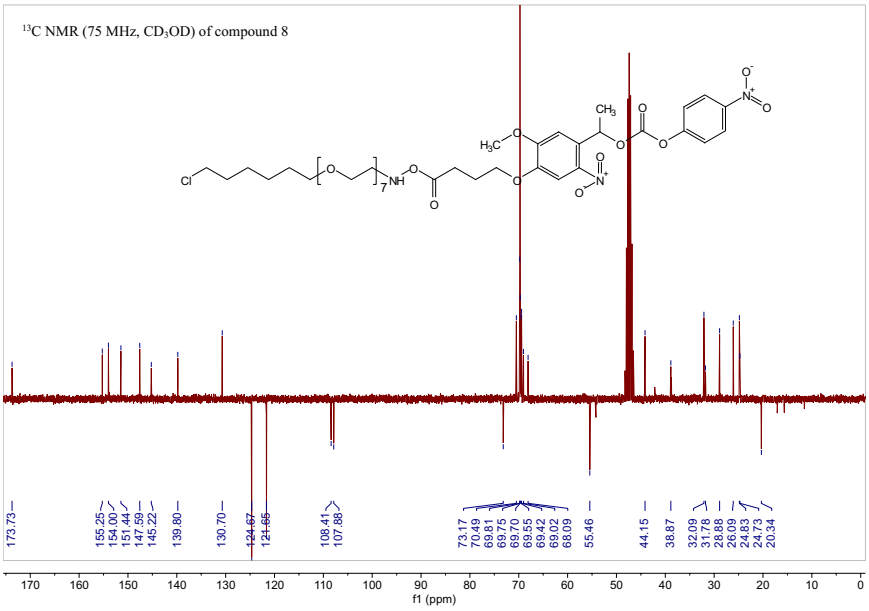

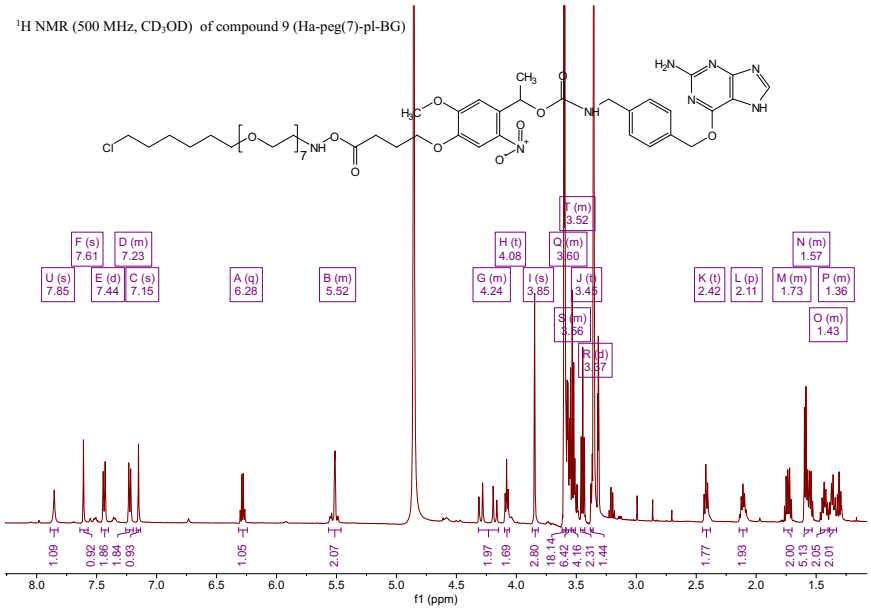
1H NMR (500 MHz, CD3OD) of compound 9 (Ha-peg(7)-pl-BG)
F (s) 7.61
D (m) 7.23
U (s) 7.85
E (d) 7.44
C (s) 7.15
A (q) 6.28
B (m) 5.52
H (t) 4.08
G (m) 4.24
I (s) 3.85
Q (m) 3.60
J (t) 3.45
F (m) 3.52
R (d) 3.37
K (t) 2.42
L (p) 2.11
N (m) 1.57
M (m) 1.73
P (m) 1.36
O (m) 1.43
1.09
0.92
1.86
1.84
0.93
1.05
2.07
1.97
1.69
2.80
18.14
6.42
4.16
2.31
1.44
1.77
1.93
2.00
5.13
2.05
2.01
f1 (ppm)

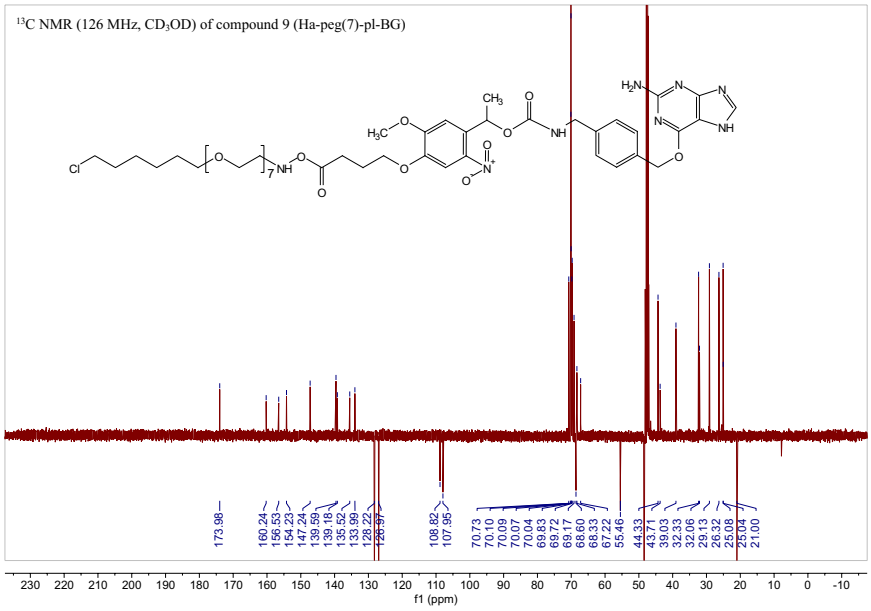
13C NMR (126 MHz, CD3OD) of compound 9 (Ha-peg(7)-pl-BG)
173.98
160.24
156.53
154.23
147.24
139.59
139.18
135.52
133.99
128.22
126.97
108.82
107.95
70.73
70.10
70.09
70.07
70.04
69.83
69.72
69.17
68.60
68.33
67.22
55.46
44.33
43.71
39.03
32.33
32.06
29.13
26.32
25.08
25.04
21.00
f1 (ppm)

BIBLIOGRAPHY

[1] Lin Xue, Iuliia A Karpenko, Julien Hiblot, and Kai Johnsson. "Imaging and manipulating proteins in live cells through covalent labeling." In: *Nat. Chem. Biol.* (2015) (cit. on p. 3).

[2] Antje Keppler, Susanne Gendreizig, Thomas Gronemeyer, Horst Pick, Horst Vogel, and Kai Johnsson. "A general method for the covalent labeling of fusion proteins with small molecules in vivo." In: *Nat Biotechnol* (2002) (cit. on pp. 3, 10).

[3] Georgyi V Los et al. "HaloTag: A Novel Protein Labeling Technology for Cell Imaging and Protein Analysis." In: *ACS Chem. Biol.* (2008) (cit. on pp. 3, 10).

[4] Boglarka H Varkuti, Miklos Kepiro, Istvan Adam Horvath, Laszlo Vegner, Szilvia Rati, Aron Zsigmond, Gyoergy Hegyi, Zsolt Lenkei, Mate Varga, and Andras Malnasi-Csizmadia. "A highly soluble, non-phototoxic, non-fluorescent blebbistatin derivative." In: *Sci Rep* (2016) (cit. on pp. 3, 28).

[5] Anna Rutkowska and Carsten Schultz. "Protein Tango: The Toolbox to Capture Interacting Partners." In: *Angew. Chem. Int. Ed. Engl.* (2012) (cit. on pp. 3, 7).

[6] Clara Brieke, Falk Rohrbach, Alexander Gottschalk, Günter Mayer, and Alexander Heckel. "Light-controlled tools." In: *Angew. Chem. Int. Ed. Engl.* (2012) (cit. on pp. 3, 5, 12).

[7] Joachim Engels and Ernst Juergen Schlaeger. "Synthesis, structure, and reactivity of adenosine cyclic 3',5'-phosphate-benzyltriesters." In: *Journal of Medicinal Chemistry* (1977) (cit. on p. 3).

[8] J H Kaplan, B Forbush, and J F Hoffman. "Rapid photolytic release of adenosine 5'-triphosphate from a protected analogue: utilization by the Na:K pump of human red blood cell ghosts." In: *Biochemistry* (1978) (cit. on p. 3).

[9] Graham C R Ellis-Davies. "Caged compounds: photorelease technology for control of cellular chemistry and physiology." In: *Nat Meth* (2007) (cit. on pp. 3, 4).

[10] Arnaud Gautier, Duy P Nguyen, Hrvoje Lusic, Wenlin An, Alexander Deiters, and Jason W Chin. "Genetically Encoded Photocontrol of Protein Localization in Mammalian Cells." In: *J. Am. Chem. Soc.* (2010) (cit. on p. 4).

[11] Gerard Marriott. "Caged Protein Conjugates and Light-Directed Generation of Protein Activity: Preparation, Photoactivation, and Spectroscopic Characterization of Caged G-Actin Conjugates." In: *Biochemistry* (2002) (cit. on p. 4).

[12] Mousumi Ghosh, Xiaoyan Song, Ghassan Mouneimne, Mazen Sidani, David S Lawrence, and John S Condeelis. "Cofilin promotes actin polymerization and defines the direction of cell motility." In: *Science* (2004) (cit. on p. 4).

[13] Michael E Hahn and Tom W Muir. "Photocontrol of Smad2, a Multiphosphorylated Cell-Signaling Protein, through Caging of Activating Phosphoserines." In: *Angewandte Chemie International Edition* (2004) (cit. on p. 5).

[14] David Mendel, Jonathan A Ellman, and Peter G Schultz. "Construction of a light-activated protein by unnatural amino acid mutagenesis." In: *J. Am. Chem. Soc.* (1991) (cit. on p. 5).

[15] Nicholas Ankenbruck, Taylor Courtney, Yuta Naro, and Alexander Deiters. "Optochemical Control of Biological Processes in Cells and Animals." In: *Angew. Chem. Int. Ed. Engl.* (2018) (cit. on p. 5).

[16] R Serfling and I Coin. "Incorporation of Unnatural Amino Acids into Proteins Expressed in Mammalian Cells." In: *Meth. Enzymol.* (2016) (cit. on p. 5).

[17] Johannes Broichhagen, James Allen Frank, and Dirk Trauner. "A roadmap to success in photopharmacology." In: *Acc. Chem. Res.* (2015) (cit. on pp. 5, 6).

[18] Andreas Reiner and Ehud Y Isacoff. "Photoswitching of Cell Surface Receptors Using Tethered Ligands." In: *Photoswitching Proteins*. 2014 (cit. on p. 6).

[19] Johannes Broichhagen, Arunas Damijonaitis, Joshua Levitz, Kevin R Sokol, Philipp Leippe, David Konrad, Ehud Y Isacoff, and Dirk Trauner. "Orthogonal Optical Control of a G Protein-Coupled Receptor with a SNAP-Tethered Photochromic Ligand." In: *ACS Central Science* (2015) (cit. on p. 6).

[20] Yu-Hsuan Tsai, Sebastian Essig, John R James, Kathrin Lang, and Jason W Chin. "Selective, rapid and optically switchable regulation of protein function in live mammalian cells." In: *Nature Chemistry* (2015) (cit. on p. 6).

[21] Timothy W Corson, Nicholas Aberle, and Craig M Crews. "Design and Applications of Bifunctional Small Molecules: Why Two Heads Are Better Than One." In: *ACS Chem. Biol.* (2008) (cit. on p. 7).

[22] Mateusz Putyrski and Carsten Schultz. "Protein translocation as a tool: The current rapamycin story." In: *FEBS Lett.* (2012) (cit. on pp. 7–9).

[23] Benjamin Z Stanton, Emma J Chory, and Gerald R Crabtree. "Chemically induced proximity in biology and medicine." In: *Science* (2018) (cit. on p. 7).

[24] Devin Strickland, Yuan Lin, Elizabeth Wagner, C Matthew Hope, Josiah Zayner, Chloe Antoniou, Tobin R Sosnick, Eric L Weiss, and Michael Glotzer. "TULIPs: tunable, light-controlled interacting protein tags for cell biology." In: *Nat Meth* (2012) (cit. on pp. 7, 12, 13).

[25] Stephanie Voß, Laura Klewer, and Yao-Wen Wu. "Chemically induced dimerization: reversible and spatiotemporal control of protein function in cells." In: *Curr Opin Chem Biol* (2015) (cit. on p. 7).

[26] Brian Ross, Sohum Mehta, and Jin Zhang. "Molecular tools for acute spatiotemporal manipulation of signal transduction." In: *Curr Opin Chem Biol* (2016) (cit. on p. 7).

[27] D Spencer, T Wandless, S Schreiber, and G Crabtree. "Controlling signal transduction with synthetic ligands." In: *Science* (1993) (cit. on p. 7).

[28] A Borchardt, S D Liberles, S R Biggar, G R Crabtree, and S L Schreiber. "Small molecule-dependent genetic selection in stochastic nanodroplets as a means of detecting protein-ligand interactions on a large scale." In: *Chem. Biol.* (1997) (cit. on p. 7).

[29] Stephen L Hussey, Smita S Muddana, and Blake R Peterson. "Synthesis of a beta-estradiol-biotin chimera that potently heterodimerizes estrogen receptor and streptavidin proteins in a yeast three-hybrid system." In: *J. Am. Chem. Soc.* (2003) (cit. on p. 7).

[30] K Baker, C Bleczinski, H Lin, G Salazar-Jimenez, D Sengupta, S Krane, and V W Cornish. "Chemical complementation: A reaction-independent genetic assay for enzyme catalysis." In: *Proceedings of the National Academy of Sciences* (2002) (cit. on p. 7).

[31] Andrei V Karginov, Feng Ding, Pradeep Kota, Nikolay V Dokholyan, and Klaus M Hahn. "Engineered allosteric activation of kinases in living cells." In: *Nat Biotechnol* (2010) (cit. on p. 7).

[32] Martin N Pruschy, David M Spencer, Tarun M Kapoor, Hiroshi Miyake, Gerald R Crabtree, and Stuart L Schreiber. "Mechanistic studies of a signaling pathway activated by the organic dimerizer FK1012." In: *Chem. Biol.* (1994) (cit. on p. 7).

[33] John S Schneekloth, Fabiana N Fonseca, Michael Koldobskiy, Amit Mandal, Raymond Deshaies, Kathleen Sakamoto, and Craig M Crews. "Chemical Genetic Control of Protein Levels: Selective in Vivo Targeted Degradation." In: *J. Am. Chem. Soc.* (2004) (cit. on p. 7).

[34] John S Schneekloth Jr. and Craig M Crews. "Chemical Approaches to Controlling Intracellular Protein Degradation." In: *Chembiochem* (2004) (cit. on p. 7).

[35] Daniel M Janse, Bernat Crosas, Daniel Finley, and George M Church. "Localization to the Proteasome Is Sufficient for Degradation." In: *Journal of Biological Chemistry* (2004) (cit. on p. 7).

[36] N Fili, V Calleja, R Woscholski, P J Parker, and B Larijani. "Compartmental signal modulation: Endosomal phosphatidylinositol 3-phosphate controls endosome morphology and selective cargo sorting." In: *Proceedings of the National Academy of Sciences* (2006) (cit. on p. 7).

[37] D Varma, A Dawn, A Ghosh-Roy, S J Weil, K M Ori-McKenney, Y Zhao, J Keen, R B Vallee, and J C Williams. "Development and application of in vivo molecular traps reveals that dynein light chain occupancy differentially affects dynein-mediated processes." In: *Proceedings of the National Academy of Sciences* (2010) (cit. on p. 7).

[38] Flavia Castellano, Philippe Montcourrier, Jean-Claude Guillemot, Edith Gouin, Laura Machesky, Pascale Cossart, and Philippe Chavrier. "Inducible recruitment of Cdc42 or WASP to a cell-surface receptor triggers actin polymerization and filopodium formation." In: *Current Biology* (1999) (cit. on p. 7).

[39] Takanari Inoue, Won Do Heo, Joshua S Grimley, Thomas J Wandless, and Tobias Meyer. "An inducible translocation strategy to rapidly activate and inhibit small GTPase signaling pathways." In: *Nat Meth* (2005) (cit. on p. 7).

[40] Dries J H De Clercq, Jan Tavernier, Sam Lievens, and Serge Van Calenbergh. "Chemical Dimerizers in Three-Hybrid Systems for Small Molecule–Target Protein Profiling." In: *ACS Chem. Biol.* (2016) (cit. on p. 7).

[41] Joachim Goedhart and Jakobus van Unen. "Molecular perturbation strategies to examine spatiotemporal features of Rho GEF and Rho GTPase activity in living cells." In: *Small GTPases* (2017) (cit. on p. 7).

[42] David A Fruman, Michael A Wood, Carl K Gjertson, Howard R Katz, Steven J Burakoff, and Barbara E Bierer. "FK506 binding protein 12 mediates sensitivity to both FK506 and rapamycin in murine mast cells." In: *European Journal of Immunology* (1995) (cit. on p. 8).

[43] Nobuhiro Umeda, Tasuku Ueno, Christopher Pohlmeyer, Tetsuo Nagano, and Takanari Inoue. "A Photocleavable Rapamycin Conjugate for Spatiotemporal Control of Small GTPase Activity." In: *J. Am. Chem. Soc.* (2011) (cit. on p. 8).

[44] Andrei V Karginov, Yan Zou, David Shirvanyants, Pradeep Kota, Nikolay V Dokholyan, Douglas D Young, Klaus M Hahn, and Alexander Deiters. "Light regulation of protein dimerization and kinase activity in living cells using photocaged rapamycin and engineered FKBP." In: *J. Am. Chem. Soc.* (2011) (cit. on pp. 8, 9).

[45] Kalyn A Brown, Yan Zou, David Shirvanyants, Jie Zhang, Subhas Samanta, Pavan K Mantravadi, Nikolay V Dokholyan, and Alexander Deiters. "Light-cleavable rapamycin dimer as an optical trigger for protein dimerization." In: *Chem. Commun.* (2015) (cit. on p. 8).

[46] Shubbir Ahmed, Jun Xie, David Horne, and John C Williams. "Photocleavable dimerizer for the rapid reversal of molecular trap antagonists." In: *J. Biol. Chem.* (2014) (cit. on p. 8).

[47] Shile Huang, Mary-Ann Bjornsti, and Peter J Houghton. "Rapamycins: Mechanisms of Action and Cellular Resistance." In: *Cancer Biology & Therapy* (2003) (cit. on p. 8).

[48] Catherine W Wright, Zhi-Fo Guo, and Fu-Sen Liang. "Light control of cellular processes by using photocaged abscisic acid." In: *Chembiochem* (2015) (cit. on p. 9).

[49] Korwin M Schelkle, Tristan Griesbaum, Dirk Ollech, Steffy Becht, Tiago Buckup, Manuel Hamburger, and Richard Wombacher. "Light-induced protein dimerization by one- and two-photon activation of gibberellic acid derivatives in living cells." In: *Angew. Chem. Int. Ed. Engl.* (2015) (cit. on p. 9).

[50] Fu-Sen Liang, Wen Qi Ho, and Gerald R Crabtree. "Engineering the ABA Plant Stress Pathway for Regulation of Induced Proximity." In: *Sci. Signal.* (2011) (cit. on p. 9).

[51] Takafumi Miyamoto, Robert DeRose, Allison Suarez, Tasuku Ueno, Melinda Chen, Tai-ping Sun, Michael J Wolfgang, Chandrani Mukherjee, David J Meyers, and Takanari Inoue. "Rapid and orthogonal logic gating with a gibberellin-induced dimerization system." In: *Nat. Chem. Biol.* (2012) (cit. on pp. 9, 76).

[52] Alexandre Juillerat, Thomas Gronemeyer, Antje Keppler, Susanne Gendreizig, Horst Pick, Horst Vogel, and Kai Johnsson. "Directed Evolution of O6-Alkylguanine-DNA Alkyltransferase for Efficient Labeling of Fusion Proteins with Small Molecules In Vivo." In: *Chem. Biol.* (2003) (cit. on p. 10).

[53] Lawrence W Miller, Yunfei Cai, Michael P Sheetz, and Virginia W Cornish. "In vivo protein labeling with trimethoprim conjugates: a flexible chemical tag." In: *Nat Meth* (2005) (cit. on p. 10).

[54] David P Baccanari, Susan Daluge, and R W King. "Inhibition of dihydrofolate reductase: effect of NADPH on the selectivity and affinity of diaminobenzylpyrimidines." In: *Biochemistry* (2002) (cit. on p. 10).

[55] Dominik Erhart, Mirjam Zimmermann, Olivier Jacques, Matthias B Wittwer, Beat Ernst, Edwin Constable, Marketa Zvelebil, Florent Beaufils, and Matthias P Wymann. "Chemical Development of Intracellular Protein Heterodimerizers." In: *Chem. Biol.* (2013) (cit. on pp. 10, 73).

[56] Mirjam Zimmermann, Ruben Cal, Elia Janett, Viktor Hoffmann, Christian G Bochet, Edwin Constable, Florent Beaufils, and Matthias P Wymann. "Cell-permeant and photocleavable chemical inducer of dimerization." In: *Angew. Chem. Int. Ed. Engl.* (2014) (cit. on pp. 11, 73).

[57] Edward R Ballister, Chanat Aonbangkhen, Alyssa M Mayo, Michael A Lampson, and David M Chenoweth. "Localized light-induced protein dimerization in living cells using a photocaged dimerizer." In: *Nat Commun* (2014) (cit. on pp. 11, 77).

[58] Huaiying Zhang, Chanat Aonbangkhen, Ekaterina V Tarasovetc, Edward R Ballister, David M Chenoweth, and Michael A Lampson. "Optogenetic control of kinetochore function." In: *Nat. Chem. Biol.* (2017) (cit. on p. 11).

[59] Xi Chen and Yao-Wen Wu. "Tunable and Photoswitchable Chemically Induced Dimerization for Chemo-optogenetic Control of Protein and Organelle Positioning." In: *Angew. Chem. Int. Ed. Engl.* (2018) (cit. on p. 11).

[60] Chanat Aonbangkhen, Huaiying Zhang, Daniel Z Wu, Michael A Lampson, and David M Chenoweth. "Reversible Control of Protein Localization in Living Cells Using a Photocaged-Photocleavable Chemical Dimerizer." In: *J. Am. Chem. Soc.* (2018) (cit. on p. 11).

[61] Benjamin R Rost, Franziska Schneider-Warme, Dietmar Schmitz, and Peter Hegemann. "Optogenetic Tools for Subcellular Applications in Neuroscience." In: *Neuron* (2017) (cit. on pp. 12, 13).

[62] Lukasz Kowalik and James K Chen. "Illuminating developmental biology through photochemistry." In: *Nat. Chem. Biol.* (2017) (cit. on pp. 12, 13).

[63] Jacqueline Niu, Manu Ben Johny, Ivy E Dick, and Takanari Inoue. "Following Optogenetic Dimerizers and Quantitative Prospects." In: *Biophys. J.* (2016) (cit. on pp. 12, 13).

[64] Heath E Johnson and Jared E Toettcher. "Illuminating developmental biology with cellular optogenetics." In: *Curr. Opin. Biotechnol.* (2018) (cit. on pp. 12, 14).

[65] Shannon M Harper, John M Christie, and Kevin H Gardner. "Disruption of the LOV-Jalpha helix interaction activates phototropin kinase activity." In: *Biochemistry* (2004) (cit. on p. 12).

[66] Yi I Wu, Daniel Frey, Oana I Lungu, Angelika Jaehrig, Ilme Schlichting, Brian Kuhlman, and Klaus M Hahn. "A genetically encoded photoactivatable Rac controls the motility of living cells." In: *Nature* (2009) (cit. on p. 12).

[67] Oana I Lungu, Ryan A Hallett, Eun Jung Choi, Mary J Aiken, Klaus M Hahn, and Brian Kuhlman. "Designing photoswitchable peptides using the AsLOV2 domain." In: *Chem. Biol.* (2012) (cit. on pp. 12, 13).

[68] Dominik Niopek, Dirk Benzinger, Julia Roensch, Thomas Draebing, Pierre Wehler, Roland Eils, and Barbara Di Ventura. "Engineering light-inducible nuclear localization signals for precise spatiotemporal control of protein dynamics in living cells." In: *Nat Commun* (2014) (cit. on p. 13).

[69] Lukasz J Bugaj, Atri T Choksi, Colin K Mesuda, Ravi S Kane, and David V Schaffer. "Optogenetic protein clustering and signaling activation in mammalian cells." In: *Nat Meth* (2013) (cit. on p. 13).

[70] Giorgia Guglielmi, Joseph D Barry, Wolfgang Huber, and Stefano De Renzis. "An Optogenetic Method to Modulate Cell Contractility during Tissue Morphogenesis." In: *Dev. Cell* (2015) (cit. on p. 13).

[71] Anselm Levskaya, Orion D Weiner, Wendell A Lim, and Christopher A Voigt. "Spatiotemporal control of cell signalling using a light-switchable protein interaction." In: *Nature* (2009) (cit. on p. 13).

[72] Sangkyu Lee, Hyerim Park, Taeyoon Kyung, Na Yeon Kim, Sungsoo Kim, Jihoon Kim, and Won Do Heo. "Reversible protein inactivation by optogenetic trapping in cells." In: *Nat Meth* (2014) (cit. on p. 13).

[73] Léo Valon, Ariadna Marın-Llauradó, Thomas Wyatt, Guillaume Charras, and Xavier Trepat. "Optogenetic control of cellular forces and mechanotransduction." In: *Nat Commun* (2017) (cit. on p. 13).

[74] Matthew Weitzman and Klaus M Hahn. "Optogenetic approaches to cell migration and beyond." In: *Curr. Opin. Cell Biol.* (2014) (cit. on p. 13).

[75] Wei Zhang et al. "Optogenetic control with a photocleavable protein, PhoCl." In: *Nat Meth* (2017) (cit. on pp. 13, 14).

[76] Jean Paul Thiery, Hervé Acloque, Ruby Y J Huang, and M Angela Nieto. "Epithelial-mesenchymal transitions in development and disease." In: *Cell* (2009) (cit. on pp. 15, 20, 27, 133).

[77] Mahmut Yilmaz and Gerhard Christofori. "Mechanisms of motility in metastasizing cells." In: *Mol. Cancer Res.* (2010) (cit. on p. 15).

[78] Michael Zeisberg and Eric G Neilson. "Biomarkers for epithelial-mesenchymal transitions." In: *J. Clin. Invest.* (2009) (cit. on p. 15).

[79] Thomas D Pollard and Robert D Goldman. "Overview of the Cytoskeleton from an Evolutionary Perspective." In: *Cold Spring Harb Perspect Biol* (2018) (cit. on pp. 15, 17).

[80] Michael Murrell, Patrick W Oakes, Martin Lenz, and Margaret L Gardel. "Forcing cells into shape: the mechanics of actomyosin contractility." In: *Nat Rev Mol Cell Biol* (2015) (cit. on pp. 15, 16, 21, 23).

[81] Bruce Alberts, Alexander Johnson, Julian Lewis, Martin Raff, Keith Roberts, and Peter Walter. "The Cytoskeleton and Cell Behavior." In: *Molecular Biology of the Cell. 4th edition*. 2008 (cit. on pp. 15, 17, 18, 22).

[82] Miguel Vicente-Manzanares, Xuefei Ma, Robert S Adelstein, and Alan Rick Horwitz. "Non-muscle myosin II takes centre stage in cell adhesion and migration." In: *Nat Rev Mol Cell Biol* (2009) (cit. on pp. 17, 22–24).

[83] Cécile Leduc and Sandrine Etienne-Manneville. "Intermediate filaments in cell migration and invasion: the unusual suspects." In: *Curr. Opin. Cell Biol.* (2015) (cit. on p. 17).

[84] Bruce Alberts, Alexander Johnson, Julian Lewis, Martin Raff, Keith Roberts, and Peter Walter. "Cell Junctions." In: *Molecular Biology of the Cell. 4th edition*. 2008 (cit. on pp. 18, 20, 21).

[85] J E Lewis, J K Wahl, K M Sass, P J Jensen, K R Johnson, and M J Wheelock. "Cross-talk between adherens junctions and desmosomes depends on plakoglobin." In: *J. Cell Biol.* (1997) (cit. on pp. 18, 131).

[86] Chiara De Pascalis, Carlos Pérez-González, Shailaja Seetharaman, Batiste Boëda, Benoit Vianay, Mithila Burute, Cécile Leduc, Nicolas Borghi, Xavier Trepat, and Sandrine Etienne-Manneville. "Intermediate filaments control collective migration by restricting traction forces and sustaining cell-cell contacts." In: *J. Cell Biol.* (2018) (cit. on p. 18).

[87] Pierre-Olivier Strale et al. "The formation of ordered nanoclusters controls cadherin anchoring to actin and cell-cell contact fluidity." In: *J. Cell Biol.* (2015) (cit. on p. 19).

[88] Mark Yulis, Dennis H M Kusters, and Asma Nusrat. "Cadherins: cellular adhesive molecules serving as signalling mediators." In: *J. Physiol. (Lond.)* (2018) (cit. on pp. 19, 133).

[89] F van Roy and G Berx. "The cell-cell adhesion molecule E-cadherin." In: *Cell. Mol. Life Sci.* (2008) (cit. on pp. 19, 21, 91, 103, 132).

[90] Sabine Pokutta and William I Weis. "Structure and mechanism of cadherins and catenins in cell-cell contacts." In: *Annu. Rev. Cell Dev. Biol.* (2007) (cit. on p. 19).

[91] D E Leckband and J de Rooij. "Cadherin adhesion and mechanotransduction." In: *Annu. Rev. Cell Dev. Biol.* (2014) (cit. on p. 19).

[92] Carien M Niessen, Deborah Leckband, and Alpha S Yap. "Tissue organization by cadherin adhesion molecules: dynamic molecular and cellular mechanisms of morphogenetic regulation." In: *Physiol. Rev.* (2011) (cit. on p. 19).

[93] Lawrence Shapiro and William I Weis. "Structure and Biochemistry of Cadherins and Catenins." In: *Cold Spring Harb Perspect Biol* (2009) (cit. on p. 19).

[94] Brenton D Hoffman and Alpha S Yap. "Towards a Dynamic Understanding of Cadherin-Based Mechanobiology." In: *Trends in Cell Biology* (2015) (cit. on p. 19).

[95] Daniel Häussinger, Thomas Ahrens, Thomas Aberle, Jürgen Engel, Jörg Stetefeld, and Stephan Grzesiek. "Proteolytic E-cadherin activation followed by solution NMR and X-ray crystallography." In: *EMBO J.* (2004) (cit. on pp. 19, 21, 94).

[96] Chi-Shuo Chen, Soonjin Hong, Indrajyoti Indra, Alina P Sergeeva, Regina B Troyanovsky, Lawrence Shapiro, Barry Honig, and Sergey M Troyanovsky. "α-Catenin-mediated cadherin clustering couples cadherin and actin dynamics." In: *J. Cell Biol.* (2015) (cit. on pp. 20, 89).

[97] Sylvie Dufour, René-Marc Mège, and Jean Paul Thiery. "α-catenin, vinculin, and F-actin in strengthening E-cadherin cell–cell adhesions and mechanosensing." In: *Cell Adhesion & Migration* (2013) (cit. on p. 20).

[98] Hee-Jung Choi, Sabine Pokutta, Gregory W Cadwell, Andrey A Bobkov, Laurie A Bankston, Robert C Liddington, and William I Weis. "αE-catenin is an autoinhibited molecule that coactivates vinculin." In: *Proc. Natl. Acad. Sci. U.S.A.* (2012) (cit. on p. 20).

[99] Frauke Drees, Sabine Pokutta, Soichiro Yamada, W James Nelson, and William I Weis. "Alpha-catenin is a molecular switch that binds E-cadherin-beta-catenin and regulates actin-filament assembly." In: *Cell* (2005) (cit. on p. 20).

[100] Craig D Buckley, Jiongyi Tan, Karen L Anderson, Dorit Hanein, Niels Volkmann, William I Weis, W James Nelson, and Alexander R Dunn. "Cell adhesion. The minimal cadherin-catenin complex binds to actin filaments under force." In: *Science* (2014) (cit. on p. 20).

[101] A W Koch, S Pokutta, A Lustig, and J Engel. "Calcium binding and homoassociation of E-cadherin domains." In: *Biochemistry* (1997) (cit. on p. 20).

[102] Ramsey A Foty and Malcolm S Steinberg. "The differential adhesion hypothesis: a direct evaluation." In: *Developmental Biology* (2005) (cit. on pp. 20, 23).

[103] Jean Paul Thiery and Jonathan P Sleeman. "Complex networks orchestrate epithelial-mesenchymal transitions." In: *Nat Rev Mol Cell Biol* (2006) (cit. on pp. 20, 133).

[104] Pakorn Kanchanawong, Gleb Shtengel, Ana M Pasapera, Ericka B Ramko, Michael W Davidson, Harald F Hess, and Clare M Waterman. "Nanoscale architecture of integrin-based cell adhesions." In: *Nature* (2010) (cit. on p. 21).

[105] David R Critchley and Alexandre R Gingras. "Talin at a glance." In: *J Cell Sci* (2008) (cit. on p. 21).

[106] David A Calderwood, Iain D Campbell, and David R Critchley. "Talins and kindlins: partners in integrin-mediated adhesion." In: *Nat Rev Mol Cell Biol* (2013) (cit. on pp. 21, 82).

[107] Katharina Austen, Pia Ringer, Alexander Mehlich, Anna Chrostek-Grashoff, Carleen Kluger, Christoph Klingner, Benedikt Sabass, Roy Zent, Matthias Rief, and Carsten Grashoff. "Extracellular rigidity sensing by talin isoform-specific mechanical linkages." In: *Nat. Cell Biol.* (2015) (cit. on pp. 21, 135).

[108] Xian Hu, Chaoran Jing, Xiaochun Xu, Naotaka Nakazawa, Virginia W Cornish, Felix M Margadant, and Michael P Sheetz. "Cooperative Vinculin Binding to Talin Mapped by Time-Resolved Super Resolution Microscopy." In: *Nano Lett.* (2016) (cit. on p. 21).

[109] Armando del Rio, Raul Perez-Jimenez, Ruchuan Liu, Pere Roca-Cusachs, Julio M Fernandez, and Michael P Sheetz. "Stretching single talin rod molecules activates vinculin binding." In: *Science* (2009) (cit. on p. 21).

[110] Carsten Grashoff et al. "Measuring mechanical tension across vinculin reveals regulation of focal adhesion dynamics." In: *Nature* (2010) (cit. on p. 22).

[111] Donna J Webb, Karen Donais, Leanna A Whitmore, Sheila M Thomas, Christopher E Turner, J Thomas Parsons, and Alan F Horwitz. "FAK–Src signalling through paxillin, ERK and MLCK regulates adhesion disassembly." In: *Nat. Cell Biol.* (2004) (cit. on pp. 22, 82).

[112] Benjamin Geiger, Joachim P Spatz, and Alexander D Bershadsky. "Environmental sensing through focal adhesions." In: *Nat Rev Mol Cell Biol* (2009) (cit. on pp. 23, 24, 82).

[113] Benoit Ladoux and René-Marc Mège. "Mechanobiology of collective cell behaviours." In: *Nat Rev Mol Cell Biol* (2017) (cit. on pp. 23, 25, 29, 30).

[114] Xavier Trepat, Michael R Wasserman, Thomas E Angelini, Emil Millet, David A Weitz, James P Butler, and Jeffrey J Fredberg. "Physical forces during collective cell migration." In: *Nature Physics* (2009) (cit. on pp. 23, 30).

[115] Dhananjay T Tambe et al. "Collective cell guidance by cooperative intercellular forces." In: *Nat Mater* (2011) (cit. on p. 23).

[116] Tsveta S Malinova and Stephan Huveneers. "Sensing of Cytoskeletal Forces by Asymmetric Adherens Junctions." In: *Trends in Cell Biology* (2017) (cit. on p. 27).

[117] Tannishtha Reya, Sean J Morrison, Michael F Clarke, and Irving L Weissman. "Stem cells, cancer, and cancer stem cells." In: *Nature* (2001) (cit. on p. 27).

[118] René-Marc Mège. "Regarding the CRISPR E-CAD cells" (cit. on pp. 27, 132).

[119] Julien Colombelli, Achim Besser, Holger Kress, Emmanuel G Reynaud, Philippe Girard, Emmanuel Caussinus, Uta Haselmann, John V Small, Ulrich S Schwarz, and Ernst H K Stelzer. "Mechanosensing in actin stress fibers revealed by a close correlation between force and protein localization." In: *J Cell Sci* (2009) (cit. on p. 27).

[120] Christopher C DuFort, Matthew J Paszek, and Valerie M Weaver. "Balancing forces: architectural control of mechanotransduction." In: *Nat Rev Mol Cell Biol* (2011) (cit. on p. 27).

[121] Dirk Ollech. "Development of a modular system for rapid control of protein activation in vivo based on translocation via photocleavable dimerizers." PhD thesis. 2014 (cit. on p. 28).

[122] Markus Raffel, Christian E Willert, Steve T Wereley, and Jurgen Kompenhans. *PIV Analysis- a practicle guide*. 2007 (cit. on p. 29).

[123] Tamal Das, Kai Safferling, Sebastian Rausch, Niels Grabe, Heike Boehm, and Joachim P Spatz. "A molecular mechanotransduction pathway regulates collective migration of epithelial cells." In: *Nat. Cell Biol.* (2015) (cit. on pp. 29, 66, 120).

[124] L Petitjean, M Reffay, E Grasland-Mongrain, M Poujade, B Ladoux, A Buguin, and P Silberzan. "Velocity fields in a collectively migrating epithelium." In: *Biophys. J.* (2010) (cit. on pp. 29, 120).

[125] M Dembo, T Oliver, A Ishihara, and K Jacobson. "Imaging the traction stresses exerted by locomoting cells with the elastic substratum method." In: *Biophys. J.* (1996) (cit. on p. 29).

[126] Gregory R Fulmer, Alexander J M Miller, Nathaniel H Sherden, Hugo E Gottlieb, Abraham Nudelman, Brian M Stoltz, John E Bercaw, and Karen I Goldberg. "NMR Chemical Shifts of Trace Impurities: Common Laboratory Solvents, Organics, and Gases in Deuterated Solvents Relevant to the Organometallic Chemist." In: *Organometallics* (2010) (cit. on p. 47).

[127] Daniel G Gibson, Lei Young, Ray-Yuan Chuang, J Craig Venter, Clyde A Hutchison, and Hamilton O Smith. "Enzymatic assembly of DNA molecules up to several hundred kilobases." In: *Nat Meth* (2009) (cit. on p. 52).

[128] Ryan S Ritterson, Kristopher M Kuchenbecker, Michael Michalik, and Tanja Kortemme. "Design of a Photoswitchable Cadherin." In: *J. Am. Chem. Soc.* (2013) (cit. on pp. 54, 94).

[129] Jana Hanke, Dimitri Probst, Assaf Zemel, Ulrich S Schwarz, and Sarah Köster. "Dynamics of force generation by spreading platelets." In: *Soft Matter* (2018) (cit. on p. 66).

[130] Patrick W Oakes, Elizabeth Wagner, Christoph A Brand, Dimitri Probst, Marco Linke, Ulrich S Schwarz, Michael Glotzer, and Margaret L Gardel. "Optogenetic control of RhoA reveals zyxin-mediated elasticity of stress fibres." In: *Nat Commun* (2017) (cit. on p. 66).

[131] Medhavi Vishwakarma, Jacopo Di Russo, Dimitri Probst, Ulrich S Schwarz, Tamal Das, and Joachim P Spatz. "Mechanical interactions among followers determine the emergence of leaders in migrating epithelial cell collectives." In: *Nat Commun* (2018) (cit. on p. 66).

[132] Yvonne Aratyn-Schaus, Patrick W Oakes, Jonathan Stricker, Stephen P Winter, and Margaret L Gardel. "Preparation of complaint matrices for quantifying cellular contraction." In: *J Vis Exp* (2010) (cit. on p. 67).

[133] Carlos Pérez-González, Ricard Alert, Carles Blanch-Mercader, Manuel Gómez-González, Tomasz Kolodziej, Elsa Bazellières, Jaume Casademunt, and Xavier Trepat. "Active wetting of epithelial tissues." In: *Nature Physics* (2018) (cit. on p. 67).

[134] Benedikt Sabass, Margaret L Gardel, Clare M Waterman, and Ulrich S Schwarz. "High resolution traction force microscopy based on experimental and computational advances." In: *Biophys. J.* (2008) (cit. on p. 69).

[135] Gene H Golub, Michael Heath, and Grace Wahba. "Generalized Cross-Validation as a Method for Choosing a Good Ridge Parameter." In: *Technometrics* (1979) (cit. on p. 69).

[136] Thomas Gronemeyer, Christopher Chidley, Alexandre Juillerat, Christian Heinis, and Kai Johnsson. "Directed evolution of O6-alkylguanine-DNA alkyltransferase for applications in protein labeling." In: *Protein Eng. Des. Sel.* (2006) (cit. on p. 73).

[137] Birgit Mollwitz, Elizabeth Brunk, Simone Schmitt, Florence Pojer, Michael Bannwarth, Marc Schiltz, Ursula Rothlisberger, and Kai Johnsson. "Directed evolution of the suicide protein O-alkylguanine-DNA alkyltransferase for increased reactivity results in an alkylated protein with exceptional stability." In: *Biochemistry* (2012) (cit. on p. 73).

[138] Mathew E Berginski, Eric A Vitriol, Klaus M Hahn, and Shawn M Gomez. "High-resolution quantification of focal adhesion spatiotemporal dynamics in living cells." In: *PLoS ONE* (2011) (cit. on p. 82).

[139] Sergey V Plotnikov, Benedikt Sabass, Ulrich S Schwarz, and Clare M Waterman. "High-resolution traction force microscopy." In: *Methods Cell Biol.* (2014) (cit. on p. 82).

[140] Paul Atherton et al. "Vinculin controls talin engagement with the actomyosin machinery." In: *Nat Commun* (2015) (cit. on p. 82).

[141] Kimberly M Bonger, Ling-chun Chen, Corey W Liu, and Thomas J Wandless. "Small-molecule displacement of a cryptic degron causes conditional protein degradation." In: *Nat. Chem. Biol.* (2011) (cit. on p. 82).

[142] Soonjin Hong, Regina B Troyanovsky, and Sergey M Troyanovsky. "Binding to F-actin guides cadherin cluster assembly, stability, and movement." In: *J. Cell Biol.* (2013) (cit. on p. 89).

[143] S Chappuis-Flament, E Wong, L D Hicks, C M Kay, and B M Gumbiner. "Multiple cadherin extracellular repeats mediate homophilic binding and adhesion." In: *J. Cell Biol.* (2001) (cit. on pp. 92, 96, 98).

[144] Dagmar Fichtner, Bärbel Lorenz, Sinem Engin, Christina Deichmann, Marieelen Oelkers, Andreas Janshoff, Andre Menke, Doris Wedlich, and Clemens M Franz. "Covalent and density-controlled surface immobilization of E-cadherin for adhesion force spectroscopy." In: *PLoS ONE* (2014) (cit. on pp. 92, 98).

[145] Cristina Bertocchi et al. "Nanoscale architecture of cadherin-based cell adhesions." In: *Nat. Cell Biol.* (2016) (cit. on p. 92).

[146] Masayuki Ozawa and Wakako Kobayashi. "Cadherin cytoplasmic domains inhibit the cell surface localization of endogenous E-cadherin, blocking desmosome and tight junction formation and inducing cell dissociation." In: *PLoS ONE* (2014) (cit. on p. 92).

[147] Masayuki Ozawa. "E-cadherin cytoplasmic domain inhibits cell surface localization of endogenous cadherins and fusion of C2C12 myoblasts." In: *Biol Open* (2015) (cit. on p. 92).

[148] Emma C Ferber, Mihoko Kajita, Anthony Wadlow, Lara Tobiansky, Carien Niessen, Hiroyoshi Ariga, Juliet Daniel, and Yasuyuki Fujita. "A role for the cleaved cytoplasmic domain of E-cadherin in the nucleus." In: *J. Biol. Chem.* (2008) (cit. on pp. 92, 133).

[149] Jean-Denis Pédelacq, Stéphanie Cabantous, Timothy Tran, Thomas C Terwilliger, and Geoffrey S Waldo. "Engineering and characterization of a superfolder green fluorescent protein." In: *Nat Biotechnol* (2005) (cit. on p. 94).

[150] Yunxiang Zhang, Sanjeevi Sivasankar, W James Nelson, and Steven Chu. "Resolving cadherin interactions and binding cooperativity at the single-molecule level." In: *Proc. Natl. Acad. Sci. U.S.A.* (2009) (cit. on p. 96).

[151] Soonjin Hong, Regina B Troyanovsky, and Sergey M Troyanovsky. "Spontaneous assembly and active disassembly balance adherens junction homeostasis." In: *Proc. Natl. Acad. Sci. U.S.A.* (2010) (cit. on p. 97).

[152] Nivetha Kannan and Vivian W Tang. "Myosin-1c promotes E-cadherin tension and force-dependent recruitment of α-actinin to the epithelial cell junction." In: *J Cell Sci* (2018) (cit. on p. 98).

[153] Emmanuella Delva and Andrew P Kowalczyk. "Regulation of cadherin trafficking." In: *Traffic* (2009) (cit. on p. 116).

[154] Yair Elisha, Vyacheslav Kalchenko, Yuri Kuznetsov, and Benjamin Geiger. "Dual role of E-cadherin in the regulation of invasive collective migration of mammary carcinoma cells." In: *Sci Rep* (2018) (cit. on p. 120).

[155] Philippe Marambaud et al. "A presenilin-1/gamma-secretase cleavage releases the E-cadherin intracellular domain and regulates disassembly of adherens junctions." In: *EMBO J.* (2002) (cit. on p. 133).

[156] András Szabó and Roberto Mayor. "Mechanisms of Neural Crest Migration." In: *Annu. Rev. Genet.* (2018) (cit. on pp. 133, 134).

[157] Elena Scarpa, András Szabó, Anne Bibonne, Eric Theveneau, Maddy Parsons, and Roberto Mayor. "Cadherin Switch during EMT in Neural Crest Cells Leads to Contact Inhibition of Locomotion via Repolarization of Forces." In: *Dev. Cell* (2015) (cit. on p. 133).

[158] Adam Shellard, András Szabó, Xavier Trepat, and Roberto Mayor. "Supracellular contraction at the rear of neural crest cell groups drives collective chemotaxis." In: *Science* (2018) (cit. on p. 133).

LIST OF FIGURES

LIST OF TABLES

PUBLICATIONS

JOURNAL ARTICLES

Aurich, C.; Weber, J.; Nagel, C.; Merkl, M.; Jude, R.; Wostmann, S.; Ollech, D.; Baron, U.; Olek, S.; Jansen, T. (2014). *Low levels of naturally occurring regulatory T lymphocytes in blood of mares with early pregnancy loss.* Reprod. Fertil. Dev., 26 (6), 827.

Schelkle, K. M.; Griesbaum, T.; Ollech, D.; Becht, S.; Buckup, T.; Hamburger, M.; Wombacher, R. (2015). *Light-Induced Protein Dimerization by One- and Two-Photon Activation of Gibberellic Acid Derivatives in Living Cells*. Angew. Chem. Int. Ed. Engl. 54 (9), 2825.

Ollech D., Pflästerer T., Zambarda C., Spatz J., Wombacher R., Cavalcanti-Adam E.A. *"LInDA: An optochemical tool for light induced dissociation of adherens junctions"*. Under submission

Zambarda C., Pérez González C., Schimmer C., Ollech D., Trepat X., Cavalcanti-Adam E. A. *"Force distribution during collective contractility is governed by cell number in epithelial clusters"*. In preparation

CONFERENCE CONTRIBUTIONS

Selected Talks

"Controlling Cadherin mediated Adhesion using Photocleavable Dimerizers" (2016) XII Recontres du Vietnam Mechanobiology from molecules to tissues – theory and application, Quy Nhon, Vietnam, 07/2016.

"Reconstitution of cadherin-catenin complexes with photocleavable dimerizers for light induced dissociation of adherens junctions" (2018) International Meeting of the German Society for Cell Biology (DGZ) "Concepts of Cell Organisation and Dynamics", Leipzig, Germany, September 17 – 19, 2018

Conference organization

Member of the organization team of *"The 5th Heidelberg Forum for Young Life Scientists"*, which took place on June 8th – 9th 2017, at the German Cancer Research Center (DKFZ), Heidelberg, Germany.

EIDESSTATTLICHE VERSICHERUNG GEMÄSS § 8 DER PROMOTIONSORDNUNG DER NATURWISSENSCHAFTLICH-MATHEMATISCHEN GESAMTFAKULTÄT DER UNIVERSITÄT HEIDELBERG

---

1. Bei der eingereichten Dissertation zu dem Thema *Optochemical control of adhesion protein complexes in living cells* handelt es sich um meine eigenständig erbrachte Leistung.

2. Ich habe nur die angegebenen Quellen und Hilfsmittel benutzt und mich keiner unzulässigen Hilfe Dritter bedient. Insbesondere habe ich wörtlich oder sinngemäß aus anderen Werken übernommene Inhalte als solche kenntlich gemacht.

3. Die Arbeit oder Teile davon habe ich bislang nicht an einer Hochschule des In- oder Auslands als Bestandteil einer Prüfungs- oder Qualifikationsleistung vorgelegt.

4. Die Richtigkeit der vorstehenden Erklärungen bestätige ich.

5. Die Bedeutung der eidesstattlichen Versicherung und die strafrechtlichen Folgen einer unrichtigen oder unvollständigen eidesstattlichen Versicherung sind mir bekannt. Ich versichere an Eides statt, dass ich nach bestem Wissen die reine Wahrheit erklärt und nichts verschwiegen habe.

Heidelberg, 05. Februar 2019

Dirk Ollech